

# **Dendritic inhibition: local coordination by excitation**



# **Dendritic inhibition: local coordination by excitation**

**Dendritische inhibitie: lokale coördinatie door excitatie**  
(met een samenvatting in het Nederlands)

## **Proefschrift**

ter verkrijging van de graad van doctor aan de  
Universiteit Utrecht  
op gezag van de  
rector magnificus, prof.dr. H.R.B.M. Kummeling,  
ingevolge het besluit van het college voor promoties  
in het openbaar te verdedigen op

woensdag 17 april 2019 des middags te 12.45 uur

door

**Hai Yin Hu**

geboren op 18 augustus 1986  
te Helmond

**Promotoren:**

Prof. dr. C.C. Hoogenraad

Prof. dr. A.S. Akhmanova

**Copromotor:**

Dr. C.J. Wierenga

*The science of today is the technology of tomorrow*

Edward Teller

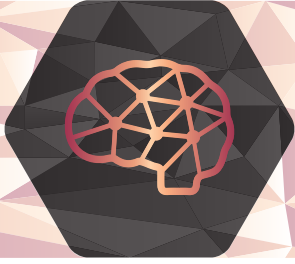


# Table of contents

<b>Chapter 1</b>	General Introduction	9
<b>Chapter 2</b>	Endocannabinoid signaling mediates local dendritic coordination between excitatory and inhibitory synapses	35
<b>Chapter 3</b>	Intuitive and semi-automated analysis tool for axonal bouton dynamics	65
<b>Chapter 4</b>	Semaphorin4D induces inhibitory synapse formation by rapid stabilization of presynaptic boutons via MET co-activation	76
<b>Chapter 5</b>	General Discussion	109
<b>Addendum</b>		131
	Nederlandse samenvatting	
	Curriculum vitae	
	Dankwoord samenvatting	







# General Introduction

---



Life is unpredictable. To cope with the unknown, we rely on our ability to learn and adapt. Often taken for granted, this essential ability is powered by the most complex organ in our body, the brain. The complexity lies in the extensive neural networks that make the human brain, shaped by the billions of neurons that each form thousands of synaptic connections. These synapses form the basis of neuronal communication, allowing us to store information inside the neural networks. Synaptic connections are dynamic and can change in strength and number, and by doing so reshape the neural network and changing the information it holds. It is thus vital that these synaptic changes are tightly regulated as their consequences can be large.

Inhibitory synapses may adhere to even stricter rules as they are tasked with keeping neuronal activity in check, despite being far less numerous than their excitatory counterparts. My interest is drawn to understanding how plasticity of inhibitory synapses is regulated and I focus in this thesis on dendritic inhibitory synapses. In this introduction, I first describe synaptic plasticity in general and inhibitory synapse formation before discussing the role of dendritic inhibitory synapses in information processing by neurons.

## Synapses

Neurons communicate by transmitting signals that initiate and terminate at specialized structures, the synapses. The signaling efficacy of individual synapses varies greatly and the amplitude of the synaptic signal is determined by both pre- and postsynaptic factors. At the presynaptic terminal, the amount of neurotransmitter packaged inside a single vesicle influences synaptic strength, as neurotransmitter release from a single vesicle does not saturate the postsynaptic receptors (Edwards 2007). The size of the presynaptic terminals correlates with the number of neurotransmitter vesicles (Schikorski and Stevens 1997). In turn, the number of docked vesicles correlates with the neurotransmitter release probability for both excitatory and inhibitory synapses, indicating a direct link between presynaptic terminal size and strength (Holderith *et al.* 2012, Pulido *et al.* 2015, Grillo *et al.* 2018). Furthermore, the probability of neurotransmitter release differs between synapses, even along presynaptic terminals of the same axon. This release probability is anti-correlated with the number of synapses the axon makes on the same dendritic branch, implying a homeostatic regulation (Branco *et al.* 2008).

At the postsynaptic side, signal strength is determined by the number of neurotransmitter receptors as well as their subunit composition (Nusser *et al.* 1997, Luscher *et al.* 2011, Vithlani *et al.* 2011, Ferando and Mody 2014). Furthermore, their density and location affect signal strength as it is dependent on the receptor clustering (MacGillavry *et al.* 2013, Pennacchietti *et al.* 2017). Postsynaptic strength and size are also correlated. The number of glutamatergic AMPA (α-amino-3-hydroxy-5-methyl-4-isoxazole propionic acid) receptors correlates with the morphological size of the spine head at excitatory synapses. Interestingly, the other major class of ionotropic glutamatergic receptors, the NMDA (N-methyl-D-aspartate) receptors, does not follow this relationship (Liao *et al.* 1995, Takumi *et al.* 1999). Small synapses may be devoid of AMPA receptors yet still express NMDA receptors, which

are known as silent synapses. The postsynaptic density often matches in size with that of the presynaptic active zone, despite the considerable variation in size (Lisman and Harris 1993), implying strict coordination of the strength of pre- and post-synapse at excitatory synapses (Kay *et al.* 2011). For inhibitory synapses, the number of postsynaptic GABA ( $\gamma$ -aminobutyric acid) receptors is also likely correlated with the size of the postsynaptic gephyrin scaffold (Specht *et al.* 2013, Petrini and Barberis 2014, Tyagarajan and Fritschy 2014). However, as inhibitory synapses form directly on the dendritic shaft and not on protrusions, no morphological correlate exists between postsynaptic size and strength for inhibition.

### Synapse plasticity: LTP and LTD

Synapses are plastic and their strength, size, and number vary over time in an activity-dependent manner. By potentiating synapses that contribute to the firing of a neuron, the link between input and output is strengthened. The synaptic changes that follow this activity-dependent plasticity, called long-term potentiation (LTP), can last several months or longer. Together with its activity-dependent counter-part long-term depression (LTD), LTP is believed to be the basis of learning and memory formation.

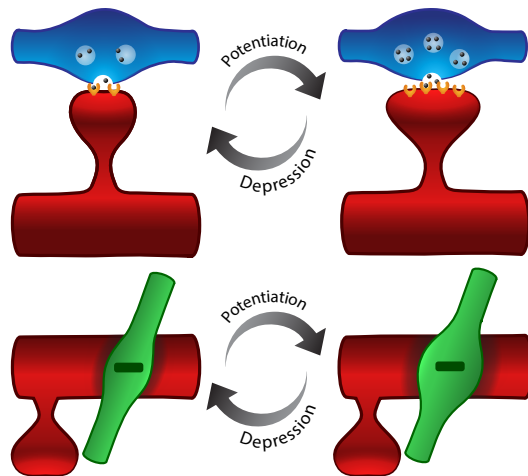


**Figure 1.** Excitatory and inhibitory synaptic plasticity

LTP is often mediated by NMDA receptors, a primary source for synaptic calcium. NMDA receptors bind glutamate with high affinity but remain inactive through a voltage-sensitive magnesium block (Patneau and Mayer 1990). This block is released during strong depolarization, for instance when an action potential propagates back into the dendritic tree. In this way, postsynaptic NMDA receptors act as coincidence detectors by coupling pre- and postsynaptic activity. Calcium flux through activated NMDA receptors leads to increased intracellular calcium levels. As a result, calcium/calmodulin-dependent protein kinase II (CaMKII) is activated and facilitates potentiation of the synapse by modulating or inserting AMPA receptors that increases the excitatory synaptic strength (Malinow and Malenka

2002). The increase in calcium only lasts for less than a second, but CaMKII can prolong its enzymatic activity for several minutes through autophosphorylation (Lengyel et al. 2004). Activated CaMKII binds to NMDA receptors, positioning itself close to AMPA receptors and its regulatory protein stargazin. CaMKII activity increases AMPA receptor conductance by phosphorylating the GluR1 subunit of the receptor (Derkach et al. 1999). In parallel, CaMKII phosphorylates stargazin, which anchors and stabilizes AMPA receptors by reducing surface diffusion (Bats et al. 2007).

Synapses that rarely contribute to the cell output are prone for depression. LTD is mediated by calcineurin, a calcium sensitive phosphatase. The dephosphorylation of AMPA receptors by calcineurin is an important component of LTD, which lowers AMPA receptor conductance and triggers its internalization (Man et al. 2007). In addition, calcineurin dephosphorylates inhibitors of protein phosphatase 1 (PP1, Halpain et al. 1990). In turn, PP1 can also dephosphorylate AMPA receptors as well as CaMKII, terminating its autophosphorylated state (Bradshaw et al. 2003).

Both CaMKII and calcineurin have high affinity for calcium binding, yet interestingly it seems that in excitatory synapses calcineurin is activated by relatively small calcium influxes, while CaMKII activation follows larger calcium influxes (Cummings et al. 1996, Li et al. 2012). The positioning of calcineurin and CaMKII is believed to be a key factor (Penny and Gold 2018). In naïve, non-stimulated spines calcineurin is anchored to the postsynaptic density (PSD), while CaMKII is located deeper, more towards the spine neck (Wyszynski et al. 1998). Weak activation of NMDA receptors is expected release calcium in a restricted microdomain, sensed only by calcineurin. A larger calcium influx activates the CaMKII, which then repositions and anchors to the NMDA receptors, while concurrently disrupts synaptic calcineurin anchoring (Strack and Colbran 1998, Sanderson et al. 2012).

LTP and LTD also occur at inhibitory synapses and the number of postsynaptic GABAA receptors is tightly regulated (Muir et al. 2010, Luscher et al. 2011, Petrini et al. 2014, Lamsa and Lau 2019). However, as inhibitory synapses do not contain NMDA receptors, GABAergic plasticity is often heterosynaptic and many different plasticity mechanisms have been described for inhibitory synapses (Kullmann and Lamsa 2011, Wenner 2011, Maffei et al. 2017).

### **Homeostatic plasticity**

The activity-dependent plasticity of synapses described above (LTP and LTD) has the potential to destabilize neuronal activity. In the absence of constraints, activity would potentiate synapses indefinitely, resulting in strong synchronization and unstable signal transmission (Turrigiano 1999). This theoretical situation is prevented as the growth of synapses is weight dependent and inversely correlated with its size. This means that potentiation of weaker synapses is favored, but potentiation of synapses that are already strong is limited (Hardingham *et al.* 2007). In addition, synaptic strength is normalized over time through a process called synaptic scaling. This form of homeostatic plasticity serves to maintain relative strength differences among synapses, while restoring the capacity for further potentiation (Turrigiano and Nelson 2004).

---

When the activity is too low, neurons become incapable of forwarding the signal and when the activity is too high, the signal will be lost amongst the non-synapse driven spontaneous action potentials. Neurons can compensate for a prolonged increase in activity by scaling their excitatory synapses down and their inhibitory synapses up. By scaling all synaptic inputs, the neurons keep their output within a certain physiological range. Homeostatic plasticity was first demonstrated in neuronal cultures (Turrigiano *et al.* 1998, Turrigiano 2008), but has since then been demonstrated *in vivo* in multiple systems (Keck *et al.* 2013, Hengen *et al.* 2016). In another form of homeostatic plasticity, neurons compensate for changes in activity levels by changing their intrinsic excitability, the ability of the neuron to generate spikes (Cudmore and Turrigiano 2004, Grubb and Burrone 2010). When neurons were hyperpolarized by overexpressing an inward-rectifier potassium channel they compensated by increasing their firing threshold (Burrone *et al.* 2003). Interestingly, the same procedure did not influence inhibitory synapses, which suggests that not postsynaptic firing, but rather surrounding presynaptic activity is responsible for scaling inhibitory synapses (Hartman *et al.* 2006).

### **Heterosynaptic plasticity**

Plasticity at activated synapses can spread towards neighboring non-active synapses on same dendrite. For instance, the induction of LTP in a single spine lowers the threshold to induce LTP in neighboring spines (Harvey and Svoboda 2007, Harward *et al.* 2016). Furthermore, induction of LTD also increases the chance of elimination of neighboring non-stimulated spines (Wiegert and Oertner 2013). This often occurs via the exchange of synaptic plasticity proteins along the dendrite (Harvey *et al.* 2008).

Heterosynaptic plasticity can also manifest in an opposite direction of the initial synaptic plasticity. By inducing CaMKII (calmodulin-dependent protein kinase II)-dependent LTP in several spines at the same branch, it was shown that non-stimulated spines on the same branch underwent calcineurin-dependent spine shrinkage, indicating that synapses compete for limited resources (Oh *et al.* 2015). Interestingly, this form of heterosynaptic plasticity involves calcium from two distinct sources, i.e. CaMKII activation occurs through NMDA receptor-dependent calcium, while concurrent calcineurin activates through calcium released from internal stores through the mGluR-IP3R pathway. Heterosynaptic plasticity may affect excitatory and inhibitory synapses differentially as excitatory synapses are compartmentalized through a narrow spine neck, while inhibitory synapses form directly on the dendritic shaft.

### **Inhibitory synapse Formation**

In addition to changes in synaptic strength, the number of synapses also varies over time as synapses are continuously formed or lost. Synapse formation depends on proximity between pre- and postsynaptic membranes. For excitatory synapses, formation is often guided by transient dendritic filopodia, which probe potential axonal partners (Lohmann and Bonhoeffer 2008). Dendritic GABAergic synapses form directly on the dendritic shaft, without the involvement of these protrusions, which makes pre-existing axon-dendritic contact a prerequisite for their formation (Wierenga *et al.* 2008).

In our group, we found that inhibitory synapses are highly dynamic structures (Frias and Wierenga 2013). We performed two-photon microscopy of GFP (green fluorescent protein)-labeled inhibitory axons in hippocampal slices of GAD65 (glutamate decarboxylase 65)-GFP mice to monitor the dynamics of individual inhibitory boutons over time. We observed that inhibitory boutons, the presynaptic parts of inhibitory synapses, can appear, disappear and reappear at the same location along axons over time. Stable inhibitory boutons reflect mature inhibitory synapses, while the transient appearances of boutons reflect locations where inhibitory synapses are being formed and disassembled (Wierenga *et al.* 2008, Schuemann *et al.* 2013). Although at first sight these bouton dynamics may appear stochastic and continuous bouton turnover uneconomical, we actually propose that these dynamics are an essential feature of a flexible, dynamic inhibitory system which serves to quickly adapt to changes in activity levels and/or to molecular signals (Frias and Wierenga 2013). Activity-dependent inhibitory synapse formation may play an important role during circuit adaptation.

These inhibitory bouton dynamics also demonstrate that formation of inhibitory synapses is a protracted process, which contains multiple steps (Wierenga 2017). First, a presynaptic bouton is formed along the axon and presynaptic proteins and synaptic vesicles are recruited (Chi *et al.* 2003, Vasin *et al.* 2014). Transsynaptic signaling is then required to assemble the postsynaptic specialization, which may be achieved by the release of signaling molecules, such as FGF7 (fibroblast growth factor 7) or Neuregulin 1, or the accumulation of cell adhesion molecules. The observed order of inhibitory synapse formation (presynaptic protein recruitment occurs before postsynaptic specialization) is in line with previous reports (Dobie and Craig 2011, Fu *et al.* 2012), although postsynaptic induction of inhibitory synapse formation has also been reported (Flores *et al.* 2015). At this moment, not much is known about the signaling pathways that are involved in inhibitory synapse formation and in chapter 4 of this thesis I present how Sema4D (Semaphorin4D) signaling is involved in a specific, early step in this process.

---

## Information processing by neurons

Neurons receive thousands of synaptic inputs and translate these input signals to a meaningful output signal (a train of action potentials). The vast majority (80-90%) of synaptic signals comes from excitatory inputs, which promote action potential output.

Inhibitory synapses have the important task of regulating this output activity (Bar-Ilan *et al.* 2013, Kepecs and Fishell 2014). GABA, the main inhibitory neurotransmitter, activates ionotropic GABA<sub>A</sub> receptors, which are chloride channels. The inhibitory action of GABA<sub>A</sub> receptors is two-fold. First the chloride influx through the receptors hyperpolarizes the membrane, which lowers the likelihood of activating voltage gated channels. The amplitude of this inhibition depends on the chloride gradient across the membrane (Kaila *et al.* 2014). Second, the opening of GABA<sub>A</sub> receptors affects excitation through electrical shunting, independent of hyperpolarization. The opening of ion channels increases the local membrane conductance, which reduces the effect of the ionic currents on the membrane potential (Koch *et al.* 1983).

The response of neurons to changes in membrane potential is shaped by the opening voltage gated channels. For instance, voltage gated sodium and calcium channels in the membrane open upon depolarization and can therefore strongly enhance the depolarization (a 'spike'), while opening of potassium channels leads to hyperpolarization (Johnston and Narayanan 2008, Tran-Van-Minh *et al.* 2015). Neuronal inhibition regulates spike generation through hyperpolarization and shunting, by either gating or preventing spike generation (Larkum *et al.* 1999, Gidon and Segev 2012, Lovett-Barron *et al.* 2012).

The largest spike formed by a neuron is the action potential, which is generated at the axon initial segment (AIS) by the rapid opening of sodium and potassium channels. The action potential is responsible for forwarding the signal onto the next neuron and propagates through the axon, where it induces neurotransmitter release. The action potential also propagates back into the dendrites (Larkum *et al.* 1999). This back-propagating action potential serves as a coincidence signal by boosting the calcium signal at active synapses.

### Dendritic computation

The first step of neuronal computation takes place in dendrites, where the majority of incoming signals arrive (Magee 2000, London and Häusser 2005, Spruston 2008, Fletcher and Williams 2018). Ion channels along the dendrite shape the incoming signals before they arrive at the AIS. By locally enhancing ('boosting') excitatory synaptic inputs, dendritic voltage gated channels and NMDA receptors can generate local spikes (Schiller *et al.* 1997, Antic *et al.* 2010). This so-called non-linear integration of synaptic signals can facilitate transmission over large distances and counter signal attenuation (Larkum *et al.* 2009, Branco *et al.* 2010). It has been shown that NMDA receptor driven dendritic spikes are important for behavior, as blocking NMDA receptors *in vivo* decreased input selectivity in the visual cortex (Smith *et al.* 2013, Palmer *et al.* 2014, Ranganathan *et al.* 2018).

The ability to perform local computations makes the dendritic branch an independent

processing and signaling unit (Branco *et al.* 2010, Kaifosh and Losonczy 2016, Beaulieu-Laroche *et al.* 2018). Inputs with similar properties are often clustered in dendrites (Wilson *et al.* 2016, Iacaruso *et al.* 2017, Bloss *et al.* 2018), enhancing the computational capacity of neurons (Poirazi *et al.* 2003). The efficacy of clustered inputs can be different between branches and this efficacy can change in an activity-dependent manner (Losonczy *et al.* 2008). Furthermore, through heterosynaptic plasticity, activity-dependent changes in one synapse can influence neighboring synapses on the same dendrite (Harvey and Svoboda 2007, Oh *et al.* 2015).

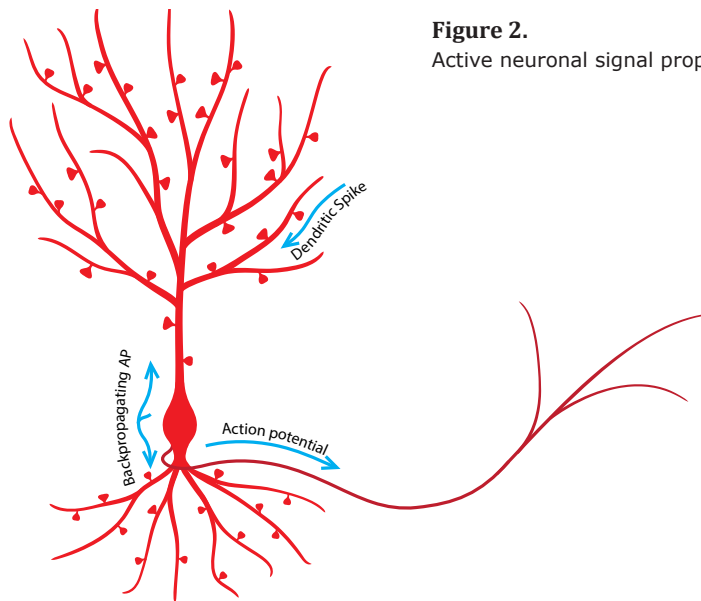


**Figure 2.**

Active neuronal signal propagation.

## Dendritic inhibition

Dendritic computation is tightly controlled by local inhibition, and dendritic inhibition is shown to be essential for synaptic plasticity (Schulz *et al.* 2018), fear learning (Abs *et al.* 2018) and visual processing (Wilson *et al.* 2018). Inhibitory cells have a highly heterogeneous morphology and can target specific subcellular compartments (Kepecs and Fishell 2014, Tremblay *et al.* 2016). Inhibitory synapses can regulate non-linear dendritic integration in the dendrite, by exerting local control over opening of ion channels (Jadi *et al.* 2012, Lovett-Barron *et al.* 2012, Müllner *et al.* 2015). For instance, dendritic inhibition can determine the spread and magnitude of non-linear integration by controlling whether dendritic or somatic burst spiking is generated (Lovett-Barron *et al.* 2012). It was also found that the activation of a single inhibitory synapse is capable of attenuating a back-propagating action potential from travelling further into the dendrite (Müllner *et al.* 2015). While most inhibitory synapses form directly on the shaft, dendritic inhibition can also target and regulate the activity at individual spines (Chiu *et al.* 2013), and these inhibitory synapses may even be more dynamic than those on the shaft (Chen *et al.* 2012, van Versendaal *et al.* 2012).



---

Dendritic inhibition is most potent at silencing excitation when both excitatory and inhibitory inputs arrive close in space and time on the same branch (Liu 2004). Depending on their relative location, dendritic inhibitory synapses mostly impact somatic or dendritic membrane potential. When measured at the soma, dendritic inhibition is most potent when it is on-the-path of excitation (Figure 3). Computational models show that the shunting component of inhibition is most effective if inhibition either colocalizes with excitation or is on-the-path of more distal excitation (Hao *et al.* 2009).

For the local impact on the membrane potential at the dendrite, the opposite is true and off-the-path inhibition is most potent (Gidon and Segev 2012). Off-the-path inhibition becomes more potent towards the distal ends, as the sealed end of the dendritic branch form an electrical resistance. The same electric current will generate a stronger change in membrane potential in high-resistance branches, compared to larger branches. Dendritic inhibitory synapses at these branches effectively enhance the local conductance and block signal propagation via shunting. Off-the-path inhibition is best suited for preventing and regulating spike initiation at distal dendritic sites (Doron *et al.* 2017). However, once a spike has been generated, on-the-path inhibition is best at attenuating it before the signal reaches the soma. These specialized tasks may underly the selective targeting of specific dendritic locations by different types of inhibitory interneurons (Bloss *et al.* 2016, Favuzzi *et al.* 2019).

Together with the relative sparsity of inhibitory synapses, the local action of inhibition suggests that each dendritic inhibitory synapse regulates its own local domain. With only a limited number of inhibitory synapses, a neuron is likely to benefit from strategically placement of these inhibitory synapses (Boivin and Nedivi 2018).

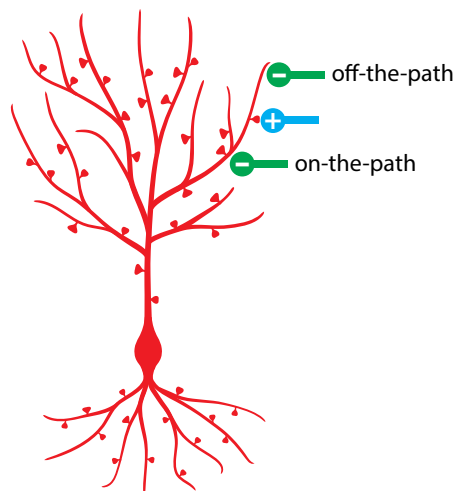


**Figure 3.** Dendritic inhibition, on-the-path and off-the-path.

## Central question of this thesis

The ability of dendrites to independently process synaptic inputs makes local inhibition key to proper regulation of non-linear integration of dendritic signals. However, plasticity of excitatory synapses is ongoing during behavior *in vivo*, and for proper regulation of these changing excitatory inputs, inhibitory synapses would have to change accordingly. This brings us to the **central question of this thesis**: Is plasticity of excitatory and inhibitory synapses coordinated within the functional unit of a single dendritic branch?

## Evidence for coordination between excitation and inhibition

Excitatory and inhibitory synapses are highly plastic, making mechanisms necessary to coordinate their plasticity to prevent excitation and inhibition from diverging, which could otherwise cause neurological disorders (Nelson and Valakh 2015, Schulte *et al.* 2018). Evidence that excitation and inhibition are regulated together comes from both *in vitro* and *in vivo* studies, where inhibition is shown to adapt to changes in activity (Froemke 2015). A piece of evidence stems from the synaptic input variability between neurons, as the input varies with cell morphology together with synapse number, type, and strength. Despite the large variations in signal amplitude of excitatory inputs, pyramidal cells in the visual cortex receive inhibition in similar proportion to their excitatory input (Xue *et al.* 2014). Furthermore, by overexpressing Kir2.1, an inward rectifier potassium channel, it was shown that pyramidal cell activity was instructive. Kir2.1 lowers the firing frequency by hyperpolarizing the membrane potential and the presence of Kir2.1 disrupted the coordination between excitation and inhibition. Onto neurons with lowered activity, inhibition became weaker while excitation remained unchanged (Xue *et al.* 2014). It is unknown if this coordination occurs through a change in inhibitory synapse number or synapse strength.

In the adult visual cortex, it was found that the number of inhibitory synapses onto pyramidal cells is regulated in an activity-dependent manner. After inducing monocular deprivation, which is accompanied by increased responsiveness to the deprived eye, a rapid decline in inhibitory synapses was found (van Versendaal *et al.* 2012). Interestingly, restoration of binocular vision (after the monocular deprivation) was also associated with a reduction in inhibitory synapses, which makes a homeostatic mechanism unlikely. After sensory deprivation by inducing retinal lesions, a region of the visual cortex is left temporarily unresponsive, but it regains responsiveness to visual stimuli through reorganization in the following months (Gilbert and Wiesel 1992). Sensory deprivation causes a reduction in the number of excitatory synapses made onto inhibitory neurons as well as in the number of inhibitory connections that these cells make (Keck *et al.* 2011). These example studies show that reduced neuronal activity due to sensory deprivation leads to a reduction of the number of inhibitory synapses. It is believed that a (temporary) reduction in inhibition facilitates the changes in the excitatory synapses that are necessary to adapt to the new situation (Froemke 2015). Therefore, excitatory and inhibitory plasticity seem to be tightly coordinated at the cellular level.

There is also evidence that coordination between excitation and inhibition occurs on a smaller scale, within dendrites. In a dendrite, the number of excitatory and inhibitory

---

synapses are correlated (Liu 2004), which suggests that inhibitory synapses may not form randomly on the dendrite, but their formation may somehow be coordinated with local excitatory synapses. As mentioned before, inhibitory synapses are very dynamic and often form and later disappear. In an *in vivo* imaging study in which the dynamics of spines and inhibitory synapses were monitored together over several days, it was found that transient inhibitory synapses tend to cluster spatially with changes in dendritic spines (Chen *et al.* 2012). This suggests some kind of local feedback signal between the two types of synaptic inputs. Glutamate may directly influence inhibitory synapses independent from its role in neuron firing. Glutamate has been shown to directly affect inhibitory synapses via NMDA receptor activation, which can induce GABA<sub>A</sub> receptor exocytosis (Marsden *et al.* 2007, Petrini *et al.* 2014). Recently, it was shown that this NMDA receptor-dependent potentiation of inhibitory synapses is specific for synapses made by somatostatin-positive inhibitory cells (Chiu *et al.* 2018).

Furthermore, after LTP induction, the balance between excitation and inhibition seems to be actively regulated as the dendritic spine growth during LTP was counterbalanced by a coordinated growth of inhibitory synapses at the same dendritic stretch (Bourne and Harris 2011), suggesting that a local balance between excitation and inhibition is actively maintained. In our research, we ask if such a local coordination indeed exists and examine the possible signaling mechanism (chapter 2).

## Methodical considerations

Studying neurons and synapses requires specialized techniques in order to prepare and maintain neuron cultures, visualize synaptic plasticity, and record neuronal activity. During experiments we often encounter unforeseen issues, forcing us to learn and revise our approach. Here I describe the techniques I used and some of the lessons I have learned.

### Organotypic hippocampal slice culture

As we were setting out to study a plasticity phenomenon that should not be specific to any brain region, we chose the hippocampus as our model system, a brain region where plasticity has been extensively studied and which is implicated in memory consolidation and spatial cognition. The hippocampus contains clearly defined, and highly characteristic dense layers of neurons of which the overall connectivity is known. In our group, we predominantly use mouse organotypic hippocampal slice cultures (Stoppini *et al.* 1991). A major advantage of these cultures over acutely prepared slices is that they can be kept for several weeks after preparation, reducing the number of animals needed for a study.

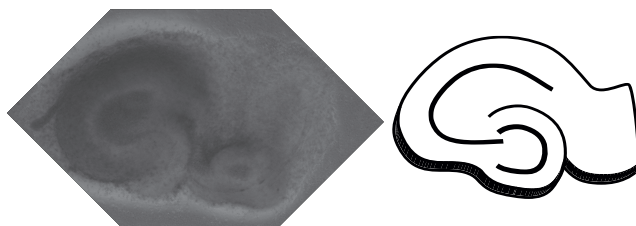


**Figure 4.** Hippocampal slice culture

Extracting the hippocampus from a P6-7 mouse pup is an acquired skill that takes time and practice as the delicate brain tissue is easily damaged. Here I briefly describe the rationale of several crucial steps of the culturing process. Ahead of the culturing process the tools and medium should be prepared sterile to prevent contaminations. After decapitation, the mouse brain is extracted into a cold saline preparation solution (approx. 0 degrees Celsius). The cold temperature slows down metabolism and delays/prevents cell death. Furthermore, kynurenic acid, a glutamate receptor antagonist, is added to our preparation solution to reduce excitotoxicity related cell death. The culture preparation is concluded by washing the slices with a different solution, the culture medium. While the preparation solution is designed to minimize excitotoxicity by lowering neuronal activity, culture medium mimics more closely the physiological conditions, which allows the neurons to continue developing. After the washing step, the hippocampal slices are plated on special inserts and kept in medium at 35 degrees.

The quality of the slices can vary, even within the same preparation. The overall structure and thickness of the slice are in general good indicators of slice health. The characteristic hippocampal structure should be clearly visible in young slices but will fade over several days, as the tissue flattens and attaches to the membrane. In case of fluorescently labeled cells, such as our GAD65-GFP cultures, the amount and location of the fluorescent cells can be used to estimate the culture quality.

---

## Two-photon laser scanning microscopy

To visualize single synapses ( $\sim 1 \mu\text{m}$ ) in living brain slices, conventional light microscopes are not sufficient. Our experiments were performed on a two-photon laser scanning microscope (Denk *et al.* 1990, Zipfel *et al.* 2003). A laser scanning microscope excites only a small part of the sample at a time. Two-photon excitation strongly limits the out-of-focus excitation light as the probability of two photons being absorbed simultaneously is exceedingly low and can only occur when the photon density of the laser is very high (i.e. in the focal point). An added benefit is that out-of-focus bleaching is also reduced. However, bleaching and photo-damage will still occur if the sample is exposed to high power illumination for prolonged periods. As such, it is necessary to find a good trade-off between scanning resolution and dwell time, while keeping in mind the quadratic relationship with resolution and the number of pixels.

Our experiments required imaging two colors with a single excitation source. To do so, we searched for an optimal wavelength at which both fluorophores (red Alexa 596 and green GFP) are approximately equally visible. Fluorescent labeling may vary, meaning that the wavelength at which both fluorophores are comparable for one experiment, may be different for another. While varying the wavelength of the laser between recordings is not ideal, the large variation in fluorescence intensity makes it difficult to avoid. The wavelength of the excitation laser should be chosen so that fluorescence intensity is at its highest for the lowest amount of laser power. As the laser travels through various optical components, how much light reaches the sample is not necessarily correlated with the initial laser power settings.

## Electrophysiology

We used electrophysiology to record electrical signals in neurons, including whole-cell current clamp and voltage clamp. Whole-cell recordings rely on making an electrical connection between the cell and an electrode. In current clamp the membrane potential is directly recorded and current can be injected into the cell to study its firing behavior. In voltage clamp, the membrane potential is held at a preset holding potential, the current needed to do so is the readout and corresponds to the current through the membrane, e.g. via synaptic inputs.

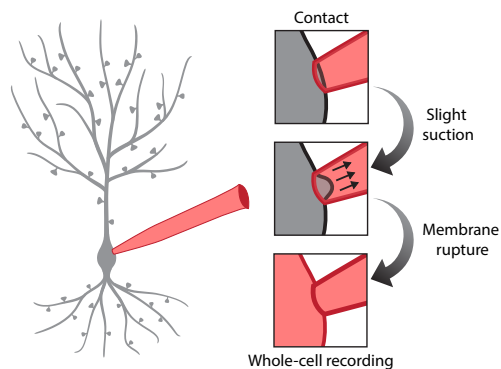


**Figure 5.** Patch clamp procedure

A side effect of whole-cell patch clamp recording is wash out, due to a mixture between the pipette solution and the cytosol. As the volume of pipette solution is many times greater than that of a cell, the native proteins will be strongly diluted over time, which can impact physiological functioning. For instance, it is believed that this wash-out limits the ability of a neuron to undergo LTP. To counter this, ATP (Adenosine triphosphate) and GTP (Guanosine triphosphate) are included to the internal solution, which extends the time window where LTP can be reliably induced to 30 min (Kato *et al.* 1993). Another component that is often added to the internal solution is EGTA (egtazic acid), a calcium chelator. EGTA prevents excitotoxicity by buffering the calcium that may be released from internal stores in response to the membrane rupturing. However, as calcium is important for many aspects of cellular signaling, buffering calcium may affect synaptic plasticity. For this reason, the chelator is only used at low concentrations.

In addition to electrophysiological access, patch clamp also lend themselves for local application by diffusion through the patch pipette. In our experiments, we loaded a pyramidal cell with a red fluorescent dye, which allowed us to visualize the axon-dendritic crossings.

### Two-photon glutamate uncaging

In our experiments we use caged glutamate combined with two-photon excitation which allows us to stimulate single synapses. Caged glutamate molecules consist of glutamate and a caging molecule that keeps the glutamate inert (Ellis-Davies 2019). A laser pulse of the right wavelength induces photolysis of this caged component and releases the glutamate. The high spatial resolution of two-photon glutamate uncaging (Fig. 6) in combination with electrophysiology allows the researcher to map glutamate sensitivity of dendritic spines (Matsuzaki *et al.* 2001). Furthermore, it also enables us to selectively potentiate synapses based on location, making it possible to study synapse plasticity in a highly controlled environment (Matsuzaki *et al.* 2004, Harvey and Svoboda 2007, Govindarajan *et al.* 2011).

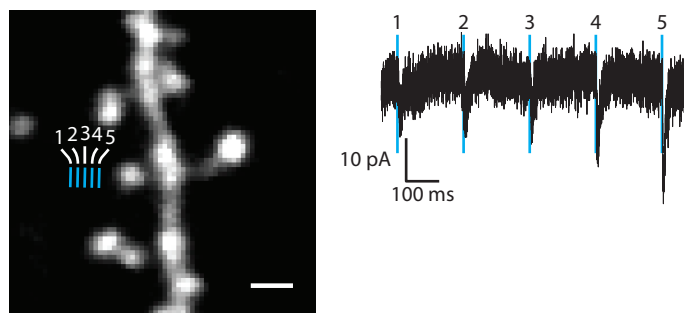


**Figure 6.** Two photon glutamate uncaging locally releases glutamate. Uncaging amplitude increases with decreasing distance. Scalebar 1  $\mu\text{m}$ .

---

Understanding the limitations of this powerful technique allows the researcher to fully utilize its strengths. One aspect of uncaging in general that may pose an issue is unintended uncaging. While several caged compounds are designed specifically for two-photon excitation, they are still easily excited by a one-photon excitation, for instance by background light. The unintended one-photon excitation occurs at roughly half the wavelength of two-photon excitation, making red or yellow light the least likely to cause unwanted uncaging. Thus, we use red light and red filters when preparing our solutions and experiments to minimize exposure to light. However, one cannot completely avoid that caged compounds are contaminated with small amounts of uncaged molecules. In the case of caged glutamate, free glutamate may interfere with the experiment, especially during prolonged exposure. This can be observed during whole-cell recordings, where the application of free glutamate will induce depolarization and may even induce action potentials.

Another concern with caged glutamate compounds, such as MNI-caged glutamate, is that they are agonistic to GABA<sub>A</sub> receptors due to their structural similarity with GABA (Passlick *et al.* 2017, Ellis-Davies 2019). At a high concentration this can become problematic and can lead to epileptic network activity. To prevent this, caged glutamate is often applied in combination with TTX (tetrodotoxin), a voltage gated sodium channel blocker. TTX blocks all action potentials, silencing neuronal activity, which in turn affect both excitatory and inhibitory synapses. In my experiments I therefore used DNI-caged glutamate, a caged compound with a higher quantum yield. With DNI-caged glutamate, I was able to use a lower concentration of caged glutamate, avoiding the problems described above. In addition, during our experiments we apply caged glutamate only briefly before and during the stimulus by local application, further limiting unwanted side effects. However, the disadvantage of local application is that the concentration can only be estimated as the applied solution will mix with the bath medium.

### **Sample drift**

Our experimental setup was designed to keep the sample in a physiological condition by continuously supplying nutrients and oxygen. Any disruption of this continuous supply, however, can cause sample drift that hinders the experiment. In our experiments, we use a peristaltic pump to perfuse the sample, which can only approximately provide a continuous in- and outflow. The outflow of the perfusion occurs at a higher rate than the inflow, to avoid a potential overflow, and therefore must suck up a mixture of air and solution in a continuous flow. I achieved this by carefully shaping the opening of the outflow. A discontinuous outflow can trigger a rapid sample drift of several microns, which is devastating in our experiments.

## Scope of the thesis

Synapses are essential building blocks that connect the neurons in the central and peripheral nervous systems. Through continuous forming and shaping, synapses allow us to learn, adapt, adjust, and grow. This thesis focuses on investigating the local coordination of inhibition and excitation after plasticity of excitatory synapses.

In chapter 2, I show that formation of dendritic inhibitory synapses can be directed by local synaptic activity. We stimulated dendritic spines close to a GABAergic axon crossing by pairing two-photon glutamate uncaging with postsynaptic depolarization in CA1 pyramidal cells. We found that repeated spine stimulation promoted growth of a new GABAergic bouton onto the same dendrite. Our findings reveal a dendritic signaling mechanism to trigger growth of inhibitory boutons at dendritic locations with strong excitatory synaptic activity, which may serve to ensure inhibitory control over clustered excitatory inputs.

The quantification and analysis of bouton growth was one of the challenges I encountered during the studies. With a lack of available tools, I set out to develop my own analysis tool while striving for efficiency, adaptability, and user friendliness. Using this tool, our quantification became straight forward, less time consuming, and easier to reproduce. In chapter 3, I describe the use and benefits of this analysis tool.

In chapter 4, we examined the signaling pathways induced by the postsynaptic signaling molecule Sema4D during inhibitory synapse formation. Sema4D is a well-known axon guidance molecule, which has been shown to be involved in the formation of inhibitory, but not excitatory, synapses. We were able to show that Sema4D signaling does not induce de novo inhibitory synapse formation, but it specifically induces stabilization of non-persistent boutons. I made electrophysiological recordings to show that the boutons that are stabilized by Sema4D signaling, gradually turn into functional, mature inhibitory synapses over time.

In chapter 5, I summarize the experimental findings, further discuss possible underlying mechanisms, and offer future directions.



---

## References

- Abs, E., Poorthuis, R.B., Apelblat, D., Muhammad, K., Pardi, M.B., Enke, L., Kushinsky, D., Pu, D.L., Eizinger, M.F., Conzelmann, K.K., Spiegel, I., and Letzkus, J.J., 2018. Learning-Related Plasticity in Dendrite-Targeting Layer 1 Interneurons. *Neuron*, 100 (3), 684–699.
- Antic, S.D., Zhou, W.-L., Moore, A.R., Short, S.M., and Ikonomu, K.D., 2010. The decade of the dendritic NMDA spike. *Journal of neuroscience research*, 88 (14), 2991–3001.
- Bar-Ilan, L., Gidon, A., and Segev, I., 2013. The role of dendritic inhibition in shaping the plasticity of excitatory synapses. *Frontiers in Neural Circuits*, 6 (April), 1–13.
- Bats, C., Groc, L., and Choquet, D., 2007. The Interaction between Stargazin and PSD-95 Regulates AMPA Receptor Surface Trafficking. *Neuron*, 53 (5), 719–734.
- Beaulieu-Laroche, L., Toloza, E.H.S., van der Goes, M.S., Lafourcade, M., Barnagian, D., Williams, Z.M., Eskandar, E.N., Frosch, M.P., Cash, S.S., and Harnett, M.T., 2018. Enhanced Dendritic Compartmentalization in Human Cortical Neurons. *Cell*, 175 (3), 643–651.e14.
- Bloss, E.B., Cembrowski, M.S., Karsh, B., Colonell, J., Fetter, R.D., and Spruston, N., 2018. Single excitatory axons form clustered synapses onto CA1 pyramidal cell dendrites. *Nature Neuroscience*, 21 (3), 353–363.
- Bloss, E.B., Cembrowski, M.S., Karsh, B., Colonell, J., Fetter, R.D., Spruston, N., Richard, D., Spruston, N., Bloss, E.B., Cembrowski, M.S., Karsh, B., Colonell, J., Fetter, R.D., and Spruston, N., 2016. Structured Dendritic Inhibition Supports Branch-Selective Integration in CA1 Pyramidal Cells. *Neuron*, 89 (5), 1016–1030.
- Boivin, J.R. and Nedivi, E., 2018. Functional implications of inhibitory synapse placement on signal processing in pyramidal neuron dendrites. *Current Opinion in Neurobiology*, 51, 16–22.
- Bourne, J.N. and Harris, K.M., 2011. Coordination of size and number of excitatory and inhibitory synapses results in a balanced structural plasticity along mature hippocampal CA1 dendrites during LTP. *Hippocampus*, 21 (4), 354–73.
- Bradshaw, J.M., Kubota, Y., Meyer, T., and Schulman, H., 2003. An ultrasensitive Ca<sup>2+</sup>/calmodulin-dependent protein kinase II-protein phosphatase 1 switch facilitates specificity in postsynaptic calcium signaling. *Proceedings of the National Academy of Sciences*, 100 (18), 10512–10517.
- Branco, T., Beverley, A.C., and Häusser, M., 2010. Dendritic Discrimination of Temporal Input Sequences in Cortical Neurons. *Science*, (September), 1671–1675.
- Branco, T., Staras, K., Darcy, K.J., and Goda, Y., 2008. Local dendritic activity sets release probability at hippocampal synapses. *Neuron*, 59 (3), 475–85.
- Burrone, J., O’Byrne, M., and Murthy, V., 2003. Multiple forms of synaptic plasticity. *Nature*, 420 (November), 414–418.
- Chen, J.L., Villa, K.L., Cha, J.W., So, P.T.C., Kubota, Y., and Nedivi, E., 2012. Clustered Dynamics of Inhibitory Synapses and Dendritic Spines in the Adult Neocortex. *Neuron*, 74 (2), 361–373.
- Chi, P., Greengard, P., and Ryan, T.A., 2003. Synaptic vesicle mobilization is regulated by distinct synapsin I phosphorylation pathways at different frequencies. *Neuron*, 38 (1), 69–78.

- Chiu, C., Lur, G., and Morse, T., 2013. Compartmentalization of GABAergic inhibition by dendritic spines. *Science*, 340 (May), 759–762.
- Chiu, C.Q., Martenson, J.S., Yamazaki, M., Natsume, R., Sakimura, K., Tomita, S., Tavalin, S.J., and Higley, M.J., 2018. Input-Specific NMDAR-Dependent Potentiation of Dendritic GABAergic Inhibition. *Neuron*, 97 (2), 368–377.e3.
- Cudmore, R.H. and Turrigiano, G.G., 2004. Long-Term Potentiation of Intrinsic Excitability in LV Visual Cortical Neurons. *Journal of Neurophysiology*, 92 (1), 341–348.
- Cummings, J.A., Mulkey, R.M., Nicoll, R.A., and Malenka, R.C., 1996. Ca<sup>2+</sup> Signaling Requirements for Long-Term Depression in the Hippocampus. *Neuron*, 16 (4), 825–833.
- Denk, W., Strickler, J., and Webb, W., 1990. Two-photon laser scanning fluorescence microscopy. *Science*, 248 (4951), 73–76.
- Derkach, V., Barria, A., and Soderling, T.R., 1999. Ca<sup>2+</sup>/calmodulin-kinase II enhances channel conductance of  $\alpha$ -amino-3-hydroxy-5-methyl-4-isoxazolepropionate type glutamate receptors. *Proceedings of the National Academy of Sciences*, 96 (6), 3269–3274.
- Dobie, F.A. and Craig, A.M., 2011. Inhibitory Synapse Dynamics: Coordinated Presynaptic and Postsynaptic Mobility and the Major Contribution of Recycled Vesicles to New Synapse Formation. *Journal of Neuroscience*, 31 (29), 10481–10493.
- Doron, M., Chindemi, G., Muller, E., Markram, H., and Segev, I., 2017. Timed Synaptic Inhibition Shapes NMDA Spikes, Influencing Local Dendritic Processing and Global I/O Properties of Cortical Neurons. *Cell Reports*, 21 (6), 1550–1561.
- Edwards, R.H., 2007. The Neurotransmitter Cycle and Quantal Size. *Neuron*, 55 (6), 835–858.
- Ellis-Davies, G.C.R., 2019. Two-Photon Uncaging of Glutamate. *Frontiers in Synaptic Neuroscience*, 10 (January), 48.
- Favuzzi, E., Deogracias, R., Marques-Smith, A., Maeso, P., Jezequel, J., Exposito-Alonso, D., Balia, M., Kroon, T., Hinojosa, A.J., F. Maraver, E., and Rico, B., 2019. Distinct molecular programs regulate synapse specificity in cortical inhibitory circuits. *Science*, 363 (6425), 413.
- Ferando, I. and Mody, I., 2014. Interneuronal GABA receptors inside and outside of synapses. *Current Opinion in Neurobiology*, 26, 57–63.
- Fletcher, L.N. and Williams, S.R., 2018. Neocortical Topology Governs the Dendritic Integrative Capacity of Layer 5 Pyramidal Neurons. *Neuron*, 101 (1), 76–90.e4.
- Flores, C.E., Nikonenko, I., Mendez, P., Fritschy, J.-M., Tyagarajan, S.K., and Muller, D., 2015. Activity-dependent inhibitory synapse remodeling through gephyrin phosphorylation. *Proceedings of the National Academy of Sciences of the United States of America*, 112 (1), E65-72.
- Frias, C.P. and Wierenga, C.J., 2013. Activity-dependent adaptations in inhibitory axons. *Frontiers in Cellular Neuroscience*, 7 (November), 1–16.
- Froemke, R.C., 2015. Plasticity of Cortical Excitatory-Inhibitory Balance. *Annual Review of Neuroscience*, 38 (1), 195–219.

- 
- Fu, Y., Wu, X., Lu, J., and Huang, Z.J., 2012. Presynaptic GABA(B) Receptor Regulates Activity-Dependent Maturation and Patterning of Inhibitory Synapses through Dynamic Allocation of Synaptic Vesicles. *Frontiers in cellular neuroscience*, 6 (December), 57.
- Gidon, A. and Segev, I., 2012. Principles Governing the Operation of Synaptic Inhibition in Dendrites. *Neuron*, 75 (2), 330–341.
- Gilbert, C.D. and Wiesel, T.N., 1992. Receptive field dynamics in adult primary visual cortex. *Nature*, 356 (6365), 150–152.
- Govindarajan, A., Israely, I., Huang, S.-Y., and Tonegawa, S., 2011. The dendritic branch is the preferred integrative unit for protein synthesis-dependent LTP. *Neuron*, 69 (1), 132–46.
- Grillo, F.W., Neves, G., Walker, A., Vizcay-Barrena, G., Fleck, R.A., Branco, T., and Burrone, J., 2018. A Distance-Dependent Distribution of Presynaptic Boutons Tunes Frequency-Dependent Dendritic Integration. *Neuron*, 99 (2), 275–282.e3.
- Grubb, M.S. and Burrone, J., 2010. Activity-dependent relocation of the axon initial segment fine-tunes neuronal excitability. *Nature*, 465 (7301), 1070–4.
- Halpain, S., Girault, J.-A., and Greengard, P., 1990. Activation of NMDA receptors induces dephosphorylation of DARPP-32 in rat striatal slices. *Nature*, 343 (6256), 369–372.
- Hao, J., Wang, X. -d., Dan, Y., Poo, M. -m., and Zhang, X. -h., 2009. An arithmetic rule for spatial summation of excitatory and inhibitory inputs in pyramidal neurons. *Proceedings of the National Academy of Sciences*, 106 (51), 21906–21911.
- Hardingham, N.R., Hardingham, G.E., Fox, K.D., and Jack, J.J.B., 2007. Presynaptic Efficacy Directs Normalization of Synaptic Strength in Layer 2/3 Rat Neocortex After Paired Activity. *Journal of Neurophysiology*, 97 (4), 2965–2975.
- Hartman, K.N., Pal, S.K., Burrone, J., and Murthy, V.N., 2006. Activity-dependent regulation of inhibitory synaptic transmission in hippocampal neurons. *Nature neuroscience*, 9 (5), 642–9.
- Harvey, C.D. and Svoboda, K., 2007. Locally dynamic synaptic learning rules in pyramidal neuron dendrites. *Nature*, 450 (7173), 1195–1200.
- Harvey, C.D., Yasuda, R., Zhong, H., and Svoboda, K., 2008. The Spread of Ras Activity Triggered by Activation of a Single Dendritic Spine. *Science*, 321 (5885), 136–140.
- Harward, S.C., Hedrick, N.G., Hall, C.E., Parra-Bueno, P., Milner, T.A., Pan, E., Laviv, T., Hempstead, B.L., Yasuda, R., and McNamara, J.O., 2016. Autocrine BDNF–TrkB signalling within a single dendritic spine. *Nature*, 538 (7623), 99–103.
- Hengen, K.B., Torrado Pacheco, A., McGregor, J.N., Van Hooser, S.D., and Turrigiano, G.G., 2016. Neuronal Firing Rate Homeostasis Is Inhibited by Sleep and Promoted by Wake. *Cell*, 165 (1), 180–191.
- Holderith, N., Lorincz, A., Katona, G., Rózsa, B., Kulik, A., Watanabe, M., and Nusser, Z., 2012. Release probability of hippocampal glutamatergic terminals scales with the size of the active zone. *Nature neuroscience*, 15 (7), 988–97.

- Iacaruso, M.F., Gasler, I.T., and Hofer, S.B., 2017. Synaptic organization of visual space in primary visual cortex. *Nature*, 547 (7664), 449–452.
- Jadi, M., Polsky, A., Schiller, J., and Mel, B.W., 2012. Location-dependent effects of inhibition on local spiking in pyramidal neuron dendrites. *PLoS Computational Biology*, 8 (6).
- Johnston, D. and Narayanan, R., 2008. Active dendrites: colorful wings of the mysterious butterflies. *Trends in Neurosciences*, 31 (6), 309–316.
- Kaifosh, P. and Losonczy, A., 2016. Mnemonic Functions for Nonlinear Dendritic Integration in Hippocampal Pyramidal Circuits. *Neuron*, 90 (3), 622–634.
- Kaila, K., Price, T.J., Payne, J.A., Puskarjov, M., and Voipio, J., 2014. Cation-chloride cotransporters in neuronal development, plasticity and disease. *Nature Reviews Neuroscience*, 15 (10), 637–654.
- Kato, K., Clifford, D.B., and Zorumski, C.F., 1993. Long-term potentiation during whole-cell recording in rat hippocampal slices. *Neuroscience*, 53 (1), 39–47.
- Kay, L., Humphreys, L., Eickholt, B.J., and Burrone, J., 2011. Neuronal activity drives matching of pre- and postsynaptic function during synapse maturation. *Nature Neuroscience*, 14 (6), 688–690.
- Keck, T., Keller, G.B., Jacobsen, R.I., Eysel, U.T., Bonhoeffer, T., and Hübener, M., 2013. Synaptic scaling and homeostatic plasticity in the mouse visual cortex in vivo. *Neuron*, 80 (2), 327–334.
- Keck, T., Scheuss, V., Jacobsen, R.I., Wierenga, C.J., Eysel, U.T., Bonhoeffer, T., and Hübener, M., 2011. Loss of sensory input causes rapid structural changes of inhibitory neurons in adult mouse visual cortex. *Neuron*, 71 (5), 869–882.
- Kepecs, A. and Fishell, G., 2014. Interneuron cell types are fit to function. *Nature*, 505 (7483), 318–26.
- Koch, C., Poggio, T., and Torre, V., 1983. Nonlinear interactions in a dendritic tree: localization, timing, and role in information processing. *Proceedings of the National Academy of Sciences of the United States of America*, 80 (9), 2799–802.
- Kullmann, D.M. and Lamsa, K.P., 2011. LTP and LTD in cortical GABAergic interneurons: emerging rules and roles. *Neuropharmacology*, 60 (5), 712–9.
- Kuzirian, M.S., Moore, A.R., Staudenmaier, E.K., Friedel, R.H., and Paradis, S., 2013. The class 4 semaphorin Sema4D promotes the rapid assembly of GABAergic synapses in rodent hippocampus. *The Journal of neuroscience : the official journal of the Society for Neuroscience*, 33 (21), 8961–73.
- Lamsa, K. and Lau, P., 2019. Long-term plasticity of hippocampal interneurons during in vivo memory processes. *Current Opinion in Neurobiology*, 54, 20–27.
- Larkum, M.E., Nevian, T., Sandler, M., Polsky, A., and Schiller, J., 2009. Synaptic integration in tuft dendrites of layer 5 pyramidal neurons: a new unifying principle. *Science (New York, N.Y.)*, 325 (5941), 756–60.
- Larkum, M.E., Zhu, J.J., and Sakmann, B., 1999. A new cellular mechanism for coupling inputs arriving at different cortical layers. *Nature*, 398 (6725), 338–41.

- 
- Lengyel, I., Voss, K., Cammarota, M., Bradshaw, K., Brent, V., Murphy, K.P.S.J., Giese, K.P., Rostas, J.A.P., and Bliss, T.V.P., 2004. Autonomous activity of CaMKII is only transiently increased following the induction of long-term potentiation in the rat hippocampus. *European Journal of Neuroscience*, 20 (11), 3063–3072.
- Li, L., Stefan, M.I., and Le Novère, N., 2012. Calcium Input Frequency, Duration and Amplitude Differentially Modulate the Relative Activation of Calcineurin and CaMKII. *PLoS ONE*, 7 (9).
- Liao, D., Hessler, N.A., and Malinow, R., 1995. Activation of postsynaptically silent synapses during pairing-induced. *Nature*, 375 (6530), 400–404.
- Lisman, J.E. and Harris, K.M., 1993. Quantal analysis and synaptic anatomy — integrating two views of hippocampal plasticity. *Trends in Neurosciences*, 16 (4), 141–147.
- Liu, G., 2004. Local structural balance and functional interaction of excitatory and inhibitory synapses in hippocampal dendrites. *Nature neuroscience*, 7 (4), 373–9.
- Lohmann, C. and Bonhoeffer, T., 2008. A Role for Local Calcium Signaling in Rapid Synaptic Partner Selection by Dendritic Filopodia. *Neuron*, 59 (2), 253–260.
- London, M. and Häusser, M., 2005. Dendritic computation. *Annual review of neuroscience*, 28, 503–32.
- Losonczy, A., Makara, J.K., and Magee, J.C., 2008. Compartmentalized dendritic plasticity and input feature storage in neurons. *Nature*, 452 (7186), 436–41.
- Lovett-Barron, M., Turi, G.F., Kaifosh, P., Lee, P.H., Bolze, F., Sun, X.H., Nicoud, J.F., Zemelman, B. V., Sternson, S.M., and Losonczy, A., 2012. Regulation of neuronal input transformations by tunable dendritic inhibition. *Nature Neuroscience*, 15 (3), 423–430.
- Luscher, B., Fuchs, T., and Kilpatrick, C.L., 2011. GABAAR Receptor Trafficking-Mediated Plasticity of Inhibitory Synapses. *Neuron*, 70 (3), 385–409.
- MacGillavry, H.D., Song, Y., Raghavachari, S., and Blanpied, T.A., 2013. Nanoscale scaffolding domains within the postsynaptic density concentrate synaptic ampa receptors. *Neuron*, 78 (4), 615–622.
- Maffei, A., Charrier, C., Caiati, M.D., Barberis, A., Mahadevan, V., Woodin, M.A., and Tyagarajan, S.K., 2017. Emerging Mechanisms Underlying Dynamics of GABAergic Synapses. *The Journal of Neuroscience*, 37 (45), 10792–10799.
- Magee, J.C., 2000. Dendritic integration of excitatory synaptic input. *Nature Reviews Neuroscience*, 1 (3), 181–190.
- Malinow, R. and Malenka, R.C., 2002. AMPA Receptor Trafficking and Synaptic Plasticity. *Annual Review of Neuroscience*, 25 (1), 103–126.
- Man, H.-Y., Sekine-Aizawa, Y., and Haganir, R.L., 2007. Regulation of  $\alpha$ -amino-3-hydroxy-5-methyl-4-isoxazolepropionic acid receptor trafficking through PKA phosphorylation of the Glu receptor 1 subunit. *Proceedings of the National Academy of Sciences*, 104 (9), 3579–3584.

- Marsden, K.C., Beattie, J.B., Friedenthal, J., and Carroll, R.C., 2007. NMDA Receptor Activation Potentiates Inhibitory Transmission through GABA Receptor-Associated Protein-Dependent Exocytosis of GABAA Receptors. *Journal of Neuroscience*, 27 (52), 14326–14337.
- Matsuzaki, M., Ellis-Davies, G.C.R., Nemoto, T., Miyashita, Y., Iino, M., and Kasai, H., 2001. Dendritic spine geometry is critical for AMPA receptor expression in hippocampal CA1 pyramidal neurons. *Nature neuroscience*, 4 (11), 1086–92.
- Matsuzaki, M., Honkura, N., Ellis-Davies, G.C.R., and Kasai, H., 2004. Structural basis of long-term potentiation in single dendritic spines. *Nature*, 429 (June).
- Muir, J., Arancibia-Carcamo, I.L., MacAskill, A.F., Smith, K.R., Griffin, L.D., and Kittler, J.T., 2010. NMDA receptors regulate GABAA receptor lateral mobility and clustering at inhibitory synapses through serine 327 on the  $\alpha 2$  subunit. *Proceedings of the National Academy of Sciences*, 107 (38), 16679–16684.
- Müllner, F.E., Wierenga, C.J., and Bonhoeffer, T., 2015. Precision of Inhibition: Dendritic Inhibition by Individual GABAergic Synapses on Hippocampal Pyramidal Cells Is Confined in Space and Time. *Neuron*, 87 (3), 576–589.
- Nelson, S.B. and Valakh, V., 2015. Excitatory/Inhibitory Balance and Circuit Homeostasis in Autism Spectrum Disorders. *Neuron*, 87 (4), 684–698.
- Nusser, Z., Cull-Candy, S., and Farrant, M., 1997. Differences in Synaptic GABAA Receptor Number Underlie Variation in GABA Mini Amplitude. *Neuron*, 19 (3), 697–709.
- Oh, W.C., Parajuli, L.K., and Zito, K., 2015. Heterosynaptic Structural Plasticity on Local Dendritic Segments of Hippocampal CA1 Neurons. *Cell Reports*, 10 (2), 162–169.
- Palmer, L.M., Shai, A.S., Reeve, J.E., Anderson, H.L., Paulsen, O., and Larkum, M.E., 2014. NMDA spikes enhance action potential generation during sensory input. *Nature Neuroscience*.
- Paradis, S., Harrar, D.B., Lin, Y., Koon, A.C., Hauser, J.L., Griffith, E.C., Zhu, L., Brass, L.F., Chen, C., and Greenberg, M.E., 2007. An RNAi-based approach identifies molecules required for glutamatergic and GABAergic synapse development. *Neuron*, 53 (2), 217–32.
- Passlick, S., Kramer, P.F., Richers, M.T., Williams, J.T., and Ellis-Davies, G.C.R., 2017. Two-color, one-photon uncaging of glutamate and GABA. *PLoS ONE*, 12 (11), 1–17.
- Patneau, D.K. and Mayer, M.L., 1990. Structure-activity relationships for amino acid transmitter candidates acting at N-methyl-D-aspartate and quisqualate receptors. *The Journal of neuroscience : the official journal of the Society for Neuroscience*, 10 (7), 2385–99.
- Pennacchietti, F., Vascon, S., Nieuws, T., Rosillo, C., Das, S., Tyagarajan, S., Diaspro, A., del Bue, A., Maria Petrini, E., Barberis, A., and Cella Zanacchi, F., 2017. Nanoscale molecular reorganization of the inhibitory postsynaptic density is a determinant of GABAergic synaptic potentiation. *Journal of Neuroscience*, 37 (7), 1747–1756.
- Penny, C.J. and Gold, M.G., 2018. Mechanisms for localising calcineurin and CaMKII in dendritic spines. *Cellular Signalling*, 49 (May), 46–58.
- Petrini, E.M. and Barberis, A., 2014. Diffusion dynamics of synaptic molecules during inhibitory postsynaptic plasticity. *Frontiers in Cellular Neuroscience*, 8 (September), 1–16.

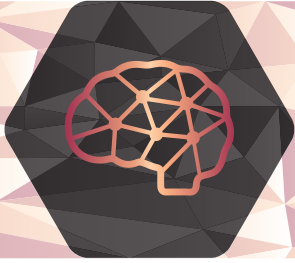
- 
- Petrini, E.M., Ravasenga, T., Hausrat, T.J., Iurilli, G., Olcese, U., Racine, V., Sibarita, J.-B., Jacob, T.C., Moss, S.J., Benfenati, F., Medini, P., Kneussel, M., and Barberis, A., 2014. Synaptic recruitment of gephyrin regulates surface GABAA receptor dynamics for the expression of inhibitory LTP. *Nature communications*, 5, 3921.
- Poirazi, P., Brannon, T., and Mel, B.W., 2003. Pyramidal neuron as two-layer neural network. *Neuron*, 37 (6), 989–999.
- Pulido, C., Trigo, F.F., Llano, I., and Marty, A., 2015. Vesicular Release Statistics and Unitary Postsynaptic Current at Single GABAergic Synapses. *Neuron*, 85 (1), 159–173.
- Ranganathan, G.N., Apostolides, P.F., Harnett, M.T., Xu, N.L., Druckmann, S., and Magee, J.C., 2018. Active dendritic integration and mixed neocortical network representations during an adaptive sensing behavior. *Nature Neuroscience*, 21 (11), 1583–1590.
- Sanderson, J.L., Gorski, J.A., Gibson, E.S., Lam, P., Freund, R.K., Chick, W.S., and Dell'Acqua, M.L., 2012. AKAP150-anchored calcineurin regulates synaptic plasticity by limiting synaptic incorporation of Ca<sup>2+</sup>-permeable AMPA receptors. *The Journal of neuroscience : the official journal of the Society for Neuroscience*, 32 (43), 15036–52.
- Schikorski, T. and Stevens, C.F., 1997. Quantitative Ultrastructural Analysis of Hippocampal Excitatory Synapses. *The Journal of Neuroscience*, 17 (15), 5858–5867.
- Schiller, J., Schiller, Y., Stuart, G., and Sakmann, B., 1997. Calcium action potentials restricted to distal apical dendrites of rat neocortical pyramidal neurons. *Journal of Physiology*, 505 (3), 605–616.
- Schuemann, A., Klawiter, A., Bonhoeffer, T., and Wierenga, C.J., 2013. Structural plasticity of GABAergic axons is regulated by network activity and GABAA receptor activation. *Frontiers in neural circuits*, 7 (June), 113.
- Schulte, J.T., Wierenga, C.J., and Bruining, H., 2018. Chloride transporters and GABA polarity in developmental, neurological and psychiatric conditions. *Neuroscience and Biobehavioral Reviews*, 90 (January), 260–271.
- Schulz, J.M., Knoflach, F., Hernandez, M.C., and Bischofberger, J., 2018. Dendrite-targeting interneurons control synaptic NMDA-receptor activation via nonlinear  $\alpha$ 5-GABAA receptors. *Nature Communications*, 9 (1).
- Smith, S.L., Smith, I.T., Branco, T., and Häusser, M., 2013. Dendritic spikes enhance stimulus selectivity in cortical neurons in vivo. *Nature*, 503 (7474), 115–120.
- Specht, C.G., Izeddin, I., Rodriguez, P.C., ElBeheiry, M., Rostaing, P., Darzacq, X., Dahan, M., and Triller, A., 2013. Quantitative nanoscopy of inhibitory synapses: Counting gephyrin molecules and receptor binding sites. *Neuron*, 79 (2), 308–321.
- Spruston, N., 2008. Pyramidal neurons: dendritic structure and synaptic integration. *Nature Reviews Neuroscience*, 9 (3), 206–221.
- Stoppini, L., Buchs, P. -a., and Muller, D., 1991. A simple method for organotypic cultures of nervous tissue. *Journal of Neuroscience Methods*, 37 (2), 173–182.

- Strack, S. and Colbran, R.J., 1998. Autophosphorylation-dependent Targeting of Calcium/ Calmodulin-dependent Protein Kinase II by the NR2B Subunit of the N -Methyl- d-aspartate Receptor. *Journal of Biological Chemistry*, 273 (33), 20689–20692.
- Takumi, Y., Ramirez-Leon, V., Laake, P., Rinvik, E., and Ottersen, O.P., 1999. Different modes of expression of AMPA and NMDA receptors in hippocampal synapses. *Nat Neurosci*, 2 (7), 618–24.
- Tran-Van-Minh, A., Cazé, R.D., Abrahamsson, T., Cathala, L., Gutkin, B.S., and DiGregorio, D.A., 2015. Contribution of sublinear and supralinear dendritic integration to neuronal computations. *Frontiers in Cellular Neuroscience*, 9 (March), 1–15.
- Tremblay, R., Lee, S., and Rudy, B., 2016. GABAergic Interneurons in the Neocortex: From Cellular Properties to Circuits. *Neuron*, 91 (2), 260–292.
- Turrigiano, G.G., 1999. Homeostatic plasticity in neuronal networks: the more things change, the more they stay the same. *Trends in neurosciences*, 22 (5), 221–7.
- Turrigiano, G.G., 2008. The self-tuning neuron: synaptic scaling of excitatory synapses. *Cell*, 135 (3), 422–35.
- Turrigiano, G.G., Leslie, K.R., Desai, N.S., Rutherford, L.C., and Nelson, S.B., 1998. Activity-dependent scaling of quantal amplitude in neocortical neurons. *Nature*, 391 (6670), 892–6.
- Turrigiano, G.G. and Nelson, S.B., 2004. Homeostatic plasticity in the developing nervous system. *Nature Reviews Neuroscience*, 5 (2), 97–107.
- Tyagarajan, S.K. and Fritschy, J.-M., 2014. Gephyrin: a master regulator of neuronal function? *Nature Reviews Neuroscience*, 15 (3), 141–156.
- Vasin, A., Zueva, L., Torrez, C., Volfson, D., Littleton, J.T., and Bykhovskaia, M., 2014. Synapsin Regulates Activity-Dependent Outgrowth of Synaptic Boutons at the Drosophila Neuromuscular Junction. *Journal of Neuroscience*, 34 (32), 10554–10563.
- van Versendaal, D., Rajendran, R., Saiepour, M.H., Klooster, J., Smit-Rigter, L., Sommeijer, J., De Zeeuw, C.I., Hofer, S.B., Heimel, J.A., Levelt, C.N., Versendaal, V., Rajendran, R., Saiepour, M.H., Klooster, J., Smit-Rigter, L., Sommeijer, J., Zeeuw, C.I. De, Hofer, S.B., Heimel, J.A., and Levelt, C.N., 2012. Article Elimination of Inhibitory Synapses Is a Major Component of Adult Ocular Dominance Plasticity. *Neuron*, 1 (2), 374–383.
- Vithlani, M., Terunuma, M., and Moss, S.J., 2011. The Dynamic Modulation of GABAA Receptor Trafficking and Its Role in Regulating the Plasticity of Inhibitory Synapses. *Physiological Reviews*, 91 (3), 1009–1022.
- Wenner, P., 2011. Mechanisms of GABAergic homeostatic plasticity. *Neural plasticity*, 2011, 489470.
- Wiegert, J.S. and Oertner, T.G., 2013. Long-term depression triggers the selective elimination of weakly integrated synapses. *Proceedings of the National Academy of Sciences*, 110 (47), E4510–E4519.
- Wierenga, C.J., 2017. Live imaging of inhibitory axons: Synapse formation as a dynamic trial-and-error process. *Brain Research Bulletin*, 129, 43–49.
- Wierenga, C.J., Becker, N., and Bonhoeffer, T., 2008. GABAergic synapses are formed without the involvement of dendritic protrusions. *Nature neuroscience*, 11 (9), 1044–52.



- 
- Wilson, D.E., Scholl, B., and Fitzpatrick, D., 2018. Differential tuning of excitation and inhibition shapes direction selectivity in ferret visual cortex. *Nature*, 560 (7716), 97–101.
- Wilson, D.E., Whitney, D.E., Scholl, B., and Fitzpatrick, D., 2016. Orientation selectivity and the functional clustering of synaptic inputs in primary visual cortex. *Nature Neuroscience*, 19 (8), 1003–1009.
- Wyszynski, M., Kharazia, V., Shanghvi, R., Rao, A., Beggs, a H., Craig, a M., Weinberg, R., and Sheng, M., 1998. Differential regional expression and ultrastructural localization of alpha-actinin-2, a putative NMDA receptor-anchoring protein, in rat brain. *The Journal of neuroscience : the official journal of the Society for Neuroscience*, 18 (4), 1383–92.
- Xue, M., Atallah, B. V., and Scanziani, M., 2014. Equalizing excitation-inhibition ratios across visual cortical neurons. *Nature*, 511 (7511), 596–600.
- Zipfel, W.R., Williams, R.M., and Webb, W.W., 2003. Nonlinear magic: Multiphoton microscopy in the biosciences. *Nature Biotechnology*, 21 (11), 1369–1377.





# Endocannabinoid signaling mediates local dendritic coordination between excitatory and inhibitory synapses

---

Hai Yin Hu\*<sup>1</sup>, Dennis L. H. Kruijssen\*<sup>1</sup>, Balázs Rózsa<sup>2</sup>,  
Casper C. Hoogenraad<sup>1</sup>, Corette J. Wierenga<sup>1</sup>

\* These authors contributed equally

<sup>1</sup> Department of Biology, Faculty of Science, Utrecht University, Utrecht, the Netherlands

<sup>2</sup> Institute of Experimental Medicine, Hungarian Academy of Sciences, Budapest, Hungary

*A revised version of this chapter has been accepted for publication in Cell Reports*



## Summary

Dendritic inhibitory synapses are most efficient in modulating excitatory inputs localized on the same dendrite, but it is unknown if their location is random or regulated. Here we show that formation of inhibitory synapses is directed by local excitatory synaptic activity. We stimulated dendritic spines close to a GABAergic axon crossing by pairing two-photon glutamate uncaging with postsynaptic depolarization in CA1 pyramidal cells. We found that repeated spine stimulation promoted growth of a new GABAergic bouton onto the same dendrite. The dendritic feedback signal required postsynaptic activation of DAGL, the enzyme that produces the endocannabinoid 2-AG, and it was mediated by CB1 receptors. We could also induce inhibitory bouton growth by local, brief applications of 2-AG. Together, our findings reveal a dendritic signaling mechanism to trigger growth of inhibitory boutons at dendritic locations with strong excitatory synaptic activity, which may serve to ensure inhibitory control over clustered excitatory inputs.

Keywords:

Two-photon microscopy, two-photon glutamate uncaging, inhibitory synapses, presynaptic boutons, synapse formation, endocannabinoid signaling, E/I balance, dendritic computation, activity-dependent adaptation

---

## Introduction

Inhibitory synapses are crucial in shaping neuronal activity in the brain. The majority of inhibitory synapses are made onto postsynaptic dendrites (Megías *et al.* 2001), where they regulate the integration of incoming synaptic signals. Dendritic inhibitory synapses are an important component of nonlinear dendritic computations (Branco and Häusser 2010, Bloss *et al.* 2016), and thereby essential for mediating complex behavior *in vivo* (Lovett-Barron *et al.* 2014). As inhibitory synapses exert local control over calcium signals and ion channel opening with high temporal and spatial precision (Jadi *et al.* 2012, Lovett-Barron *et al.* 2012, Müllner *et al.* 2015), the precise location of inhibitory synapses within the dendrite is an important factor in determining their functional impact.

Dendritic inhibitory synapses are formed by the emergence of new GABAergic boutons at axonal locations with pre-established contact to the dendrite (Wierenga *et al.* 2008), but it remains unclear if this process depends on dendritic location. *In vivo* studies have demonstrated that sensory activity can induce changes in dendritic inhibitory synapses (Keck *et al.* 2011, Froemke 2015), which are often coordinated with excitatory synapses on the same dendrite (Chen *et al.* 2012, 2015). Studies have shown that excitatory synaptic activity can affect plasticity of existing dendritic inhibitory synapses (Bourne and Harris 2011, Petrini *et al.* 2014, Chiu *et al.* 2018), but it is not known if the formation of new dendritic inhibitory synapses can be coordinated by the dendrite.

Here we hypothesized that excitatory and inhibitory synapses are coordinated within dendrites to maintain a local balance of synaptic inputs. We used two-photon glutamate uncaging to stimulate individual spines on dendrites of CA1 pyramidal neurons and observed that strong local excitation could trigger changes in a GABAergic axon that crossed the same dendrite. We found that the probability for GABAergic bouton growth was enhanced via a local retrograde signal from the stimulated dendrite. Such a local signaling system will coordinate the number of excitatory and inhibitory synapses within a dendritic branch in an activity-dependent manner.

## Results

To examine local coordination between dendritic excitatory and inhibitory synapses, we asked if inducing strong excitatory synaptic activity could trigger the formation of new inhibitory synapses on the same dendrite. We performed whole-cell patch clamp recordings of CA1 pyramidal cells in organotypic hippocampal slices of GAD65-GFP mice (López-Bendito et al. 2004). In these mice, approximately 20% of the CA1 interneurons are GFP-labeled, and they mostly express reelin or VIP and target dendrites. Parvalbumin and somatostatin cells are not labeled (Wierenga et al., 2010). The patch pipette contained the fluorescent red dye Alexa568 to visualize dendrites and spines of the recorded CA1 pyramidal cell (Figure 1A, B) (Wierenga *et al.* 2008, Müllner *et al.* 2015). We searched the labeled dendrites of the recorded neuron for a crossing with a GFP-labeled axon without an inhibitory presynaptic bouton. After the acquisition of four baseline images (5 min intervals), four spines close to the green axon crossing (range 1-12  $\mu\text{m}$ ; mean $\pm$ SEM =  $2.7 \pm 0.2 \mu\text{m}$ ) were individually stimulated using two-photon glutamate uncaging, while the postsynaptic cell was depolarized to 0 mV (Figure 1C; see methods for details). After spine stimulation, we continued to monitor the axon-dendrite crossing for up to 1 hour (5 min intervals). We often observed a new inhibitory bouton forming at the crossing (Figure 1D-I). In some cases, inhibitory boutons were formed *de novo* (Figure 1G-I), while in other cases a small irregularity of the axon was already present during baseline, which grew into a bouton after spine stimulation (Figure 1D-F). When we monitored inhibitory axon crossings at dendrites that were not stimulated, we only rarely observed spontaneous inhibitory bouton growth during the imaging period (Figure 1J-L), in agreement with a previous report (Wierenga *et al.* 2008). These observations suggest that the local activation of excitatory synapses promoted the growth of a nearby inhibitory bouton onto the same dendrite.

---

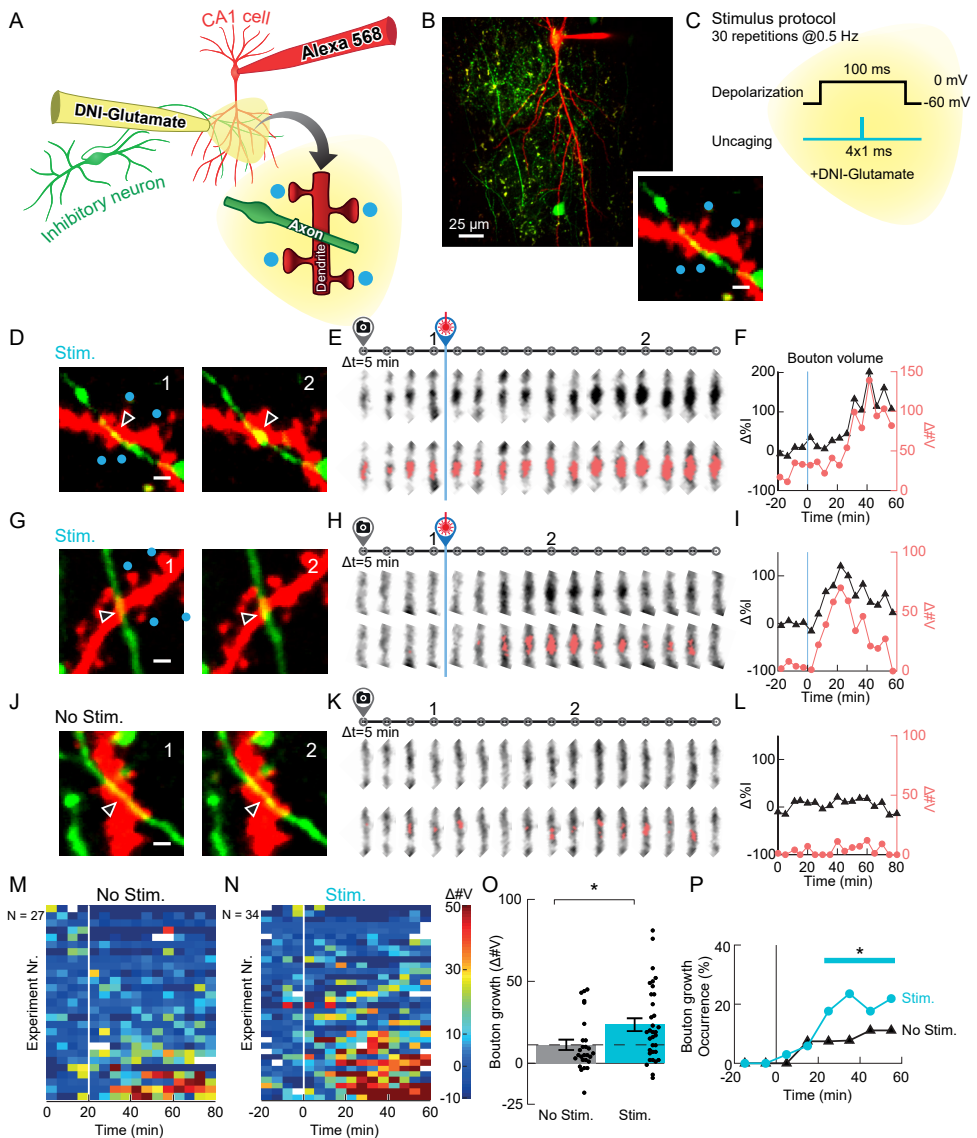
### Figure 1. Local dendritic stimulation promotes inhibitory bouton growth.

(A) Schematic representation of the experimental setup. A CA1 pyramidal cell was filled with Alexa 568 via a patch pipette. DNI-glutamate was locally applied, and glutamate uncaging was performed at 4 dendritic spines (blue dots) close to a crossing with a GFP-labeled inhibitory axon.

(B) Overview image of an example experiment. In red, a pyramidal cell is visible with a patch pipette attached. The inset shows a dendrite with a crossing inhibitory axon (green). Blue dots indicate uncaging locations.

(C) The spine stimulation protocol consisted of repeated (30x @0.5Hz) glutamate uncaging with postsynaptic depolarization to 0 mV. Uncaging was performed at 4 different spines near-simultaneously (1 ms each;  $\Delta t=0.1$  ms).

(D-F) Example of inhibitory bouton growth in response to local spine stimulation. (D) Images of time points indicated in E. Arrowheads point towards the axon crossing, blue dots indicate uncaging locations. Scale bar is 1  $\mu\text{m}$ . (E) Axonal segment at the crossing is displayed for all time points. The voxels above axon threshold are indicated in red in the lower panel. (F) Quantification of bouton volume over time, measured as the increase in number of voxels above axon threshold ( $\Delta\#V$ , red) and increase in relative intensity ( $\Delta\%I$ , black).



(G-I) As D-F, another example of inhibitory bouton growth after local spine stimulation.

(J-L) As in D-F, no change in the axon in the absence of stimulation.

(M,N) Heat maps showing bouton volumes over time of all experiments with (N; n=34) and without spine stimulation (M; n=27). Each row represents a single experiment. The vertical white line indicates the end of the baseline period (first 20 minutes). White squares indicate missing time points. Experiments are sorted by maximal bouton growth.

(O) Bouton growth per experiment (averaged over four consecutive time points) for experiments with ('stim') and without spine stimulation ('no stim'). Dashed line indicates bouton growth in the absence of spine stimulation. Bars indicate mean  $\pm$  SEM. Asterisk indicates  $p < 0.05$ , Student's t-test.

(P) Bouton growth occurrence over time in experiments in stimulated and non-stimulated conditions. Bouton growth in the stimulated condition was different compared to baseline, as tested by Cochran's Q test followed by McNemar's test (time points with  $p < 0.05$  are indicated by blue line). For non-stimulated condition, bouton growth was not different from baseline ( $p = 0.10$ ).

## Quantification of inhibitory bouton growth and time course

We quantified the morphological changes in the inhibitory axon to directly compare inhibitory bouton growth in experiments with and without spine stimulation. We determined inhibitory bouton volume as the number of voxels above axon intensity (pink voxels in Figure 1E, H, K, see methods for details; time course in Figure 1F, I, L). We plotted the change in bouton volumes for each time point in a heat map, in which each row represents an individual experiment (Figure 1M, N), illustrating the substantial variability in size of individual boutons over time (Wierenga *et al.* 2008, Schuemann *et al.* 2013). Inhibitory bouton growth was observed more often and more prolonged in experiments in which nearby spines were stimulated compared to experiments without stimulation. Maximal inhibitory bouton growth (averaged over 4 time points to avoid bias by single time point fluctuations) was significantly increased after spine stimulation compared to unstimulated controls (Figure 1O). To summarize the time course of inhibitory bouton growth over all experiments, we plotted the fraction of experiments in which bouton growth was above threshold over time (Figure 1P). In control experiments without stimulation, bouton growth occurrence did not deviate significantly from baseline during the entire imaging period ( $p=0.10$ ; Cochran's Q test). However, inhibitory bouton growth was significantly enhanced compared to baseline >25 minutes after spine stimulation ( $p<0.0001$ ; Cochran's Q test, asterisk indicates  $p<0.05$  McNemar's post hoc test). We verified that our conclusions did not depend on our quantification method or threshold (Figure S1). Together, our data demonstrate that local stimulation of dendritic spines significantly enhanced the probability of growing a new bouton on an inhibitory axon crossing at the same dendrite.

## Inhibitory bouton growth is mediated by the postsynaptic dendrite

We next asked if the postsynaptic dendrite has an active signaling role in triggering the inhibitory bouton growth, or if the uncaged glutamate directly affects the inhibitory axon, for instance via presynaptic glutamate receptors. There was no correlation between inhibitory bouton growth and the distance from the uncaging locations to the axon (Fig. S2), suggesting that glutamate diffusion to the axon is not a determining factor. We also directly tested whether inhibitory bouton growth could be induced by glutamate. We selected small segments of GFP-expressing inhibitory axons that were empty of boutons and performed two-photon glutamate uncaging at four locations close to the axon with the same stimulation protocol as used for spine stimulation (Figure 2A). While we observed fluctuations in axon intensity (Figure 2A-D), we never observed bouton growth at the location of the glutamate stimulation beyond control levels (Figure 2D, E). These experiments demonstrate that local glutamate exposure to the axon itself is not sufficient to induce bouton growth and indicates that the signal required for inducing inhibitory bouton growth is generated by the stimulated dendrite.

---

### Figure 2. Glutamate uncaging directly at inhibitory axons does not induce bouton growth.

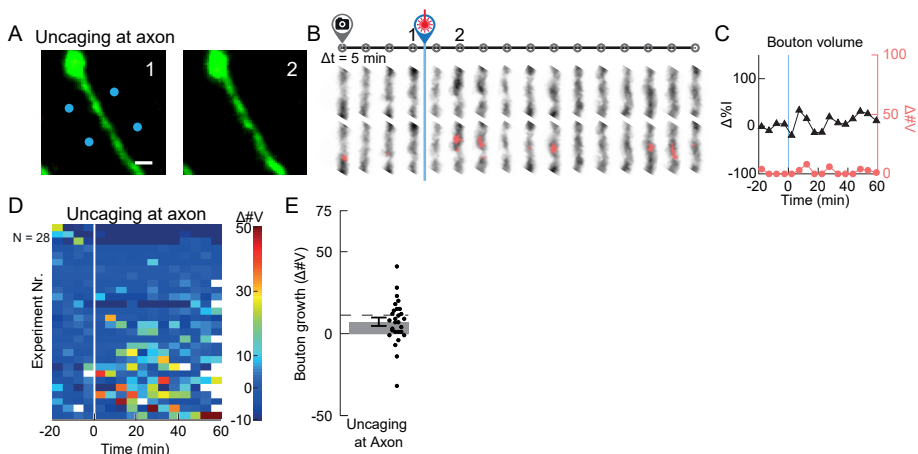
(A-C) Example of experiment in which glutamate uncaging was performed near a GFP-labeled axon. (A) Images of time points indicated in B. Blue dots indicate uncaging locations. Scale bar is 1  $\mu\text{m}$ . (B) Axonal segment is displayed for all time points. The voxels above axon threshold are indicated in red in the lower panel. (C) Quantification of bouton volume over time, measured as the increase in number of voxels above axon threshold ( $\Delta\#V$ , red) and increase in relative intensity ( $\Delta\%I$ , black).



## Inhibitory bouton growth is not tightly correlated with spine growth

Local stimulation of individual spines by glutamate uncaging evoked synaptic currents, which were recorded at the soma (Figure 3A). When the four spines were stimulated together, we often observed a small supralinear summation (average  $1.17 \pm 0.06$ ), reflecting opening of dendritic voltage-dependent ion channels (Losonczy and Magee 2006, Harnett *et al.* 2012, Weber *et al.* 2016). We did not find any correlation between this nonlinear component and inhibitory bouton growth (Figure 3B), suggesting that opening of voltage-gated ion channels is not a critical factor in the dendritic signaling pathway to induce inhibitory bouton growth.

Our stimulation protocol was designed to induce strong local excitation within the dendrite. Uncaging was performed in normal ACSF (without TTX) and paired with postsynaptic depolarization to allow NMDA receptor activation. In accordance with previous reports using similar stimulation protocols (Tanaka *et al.* 2008, Govindarajan *et al.* 2011), stimulated spines gradually increased in size during the first 10 minutes after the stimulation and then reached a plateau (Figure 3C). When averaged over all stimulated spines maximal spine size increased to  $131 \pm 2\%$ , compared to  $117 \pm 3\%$  ( $p < 0.001$ , Student's t-test) for spines on non-stimulated dendrites. In general agreement with previous reports (Harvey and Svoboda 2007, Oh *et al.* 2015), 49% of spines grew after spine stimulation, compared to 25% of spines growing spontaneously in the absence of stimulation ( $p < 0.005$ , Pearson's  $\chi^2$  test). To our surprise, we found no correlation between inhibitory bouton growth and the average growth of the four stimulated spines (Figure 3D), maximal spine growth, or the number of growing spines (Figure S3A, B). This indicates that spine growth after local glutamate stimulation is not directly linked to nearby inhibitory bouton growth, suggesting that local spine stimulation activates multiple signaling pathways in parallel.



(D) Heat map showing bouton volumes over time of all experiments ( $n=28$ ). Each row represents a single experiment. The vertical white line indicates the end of the baseline period (first 20 minutes). White squares indicate missing time points. Experiments are sorted by maximal bouton growth. (E) Bouton growth as a function of uncaging at axon. Bars indicate mean  $\pm$  SEM.  $p=0.33$ , Student's t-test, compared with control.

### **Inhibitory bouton growth requires NMDA receptor activation**

As we did not find a correlation between spine growth and bouton growth, we wondered whether inhibitory bouton growth may not require spine stimulation at all. Bouton growth may have directly resulted from the brief bouts of postsynaptic depolarization that were given during the spine stimulation protocol. We therefore imaged an axon-dendrite crossing as described before, but now applied the uncaging laser and postsynaptic depolarization protocol in absence of DNI-glutamate ('Mock' stimulation). Repeated depolarizations did not induce spine growth (Figure S3C) and in the absence of glutamate receptor activation on spines, inhibitory bouton growth did not occur beyond control levels (Figure 3E, H and S3D-F). This indicates that repeated postsynaptic depolarization by itself is not sufficient to induce inhibitory bouton growth. To specifically test for involvement of NMDA receptors, we repeated the glutamate uncaging experiments at four spines near an inhibitory axon crossing in the presence of 50  $\mu\text{M}$  APV to block NMDA receptor activation. APV completely blocked the increase in spine size (Figure S3C), and also blocked inhibitory bouton growth (Figure 3F, H and S3G-I), indicating that NMDA receptor activation was required.

To test if NMDA receptor activation was directly mediating inhibitory bouton growth, we repeated the uncaging experiments in  $\text{Mg}^{2+}$ -free ACSF in the presence of TTX, allowing strong NMDA receptor activation during the glutamate uncaging in the absence of postsynaptic depolarization. In accordance with previous reports (Harvey and Svoboda 2007, Tanaka *et al.* 2008), spines which are stimulated in low  $\text{Mg}^{2+}$ /TTX condition show a rapid, immediate growth within 5 minutes after stimulation. Our spine stimulation protocol (30x 1 ms pulses @0.5 Hz, without postsynaptic depolarization) induced clear spine growth in a similar number of spines compared to normal ACSF (55% of stimulated spines were growing), but spine growth was mostly transient (Figure S3C). Interestingly, inhibitory bouton growth was not induced under these conditions (Figure 3G, H and S3J-L), suggesting that postsynaptic glutamate receptor activation is not sufficient to trigger the feedback signal. Together, these results show that local activation of glutamate receptors is required, but that receptor activation alone is not sufficient to trigger inhibitory bouton growth after spine local stimulation.

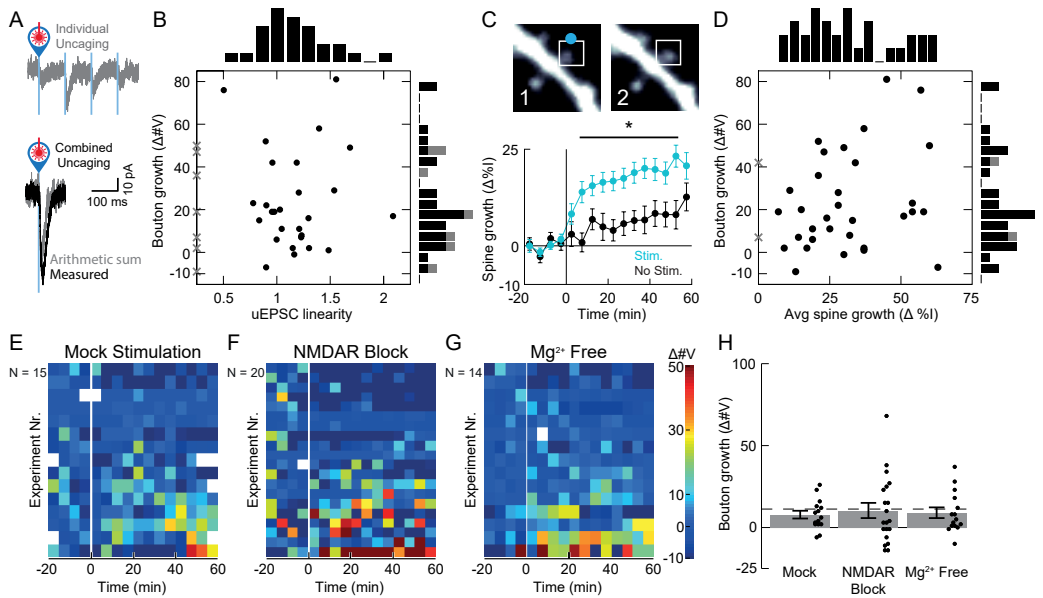


### Figure 3. Inhibitory bouton growth requires NMDA receptor activation

(A) Top: postsynaptic currents induced by glutamate uncaging (uEPSC) at 4 spines stimulated sequentially. Bottom: arithmetic sum of the four spine responses (gray) and the measured uEPSC when stimulated near-simultaneously (black).

(B) Scatter plot of uEPSC linearity against bouton growth. Gray crosses indicate experiments where uEPSC linearity could not be quantified. Inhibitory bouton growth was not correlated with uEPSC linearity ( $p=0.92$ , Spearman). Distributions are shown as histograms next to the scatter plot.

(C) Top: example of stimulated spine before (left) and after (right) the stimulus. The blue dot indicates the uncaging location. Bottom: spine growth, quantified as the increase in relative intensity ( $\Delta\%I$ ), over time. Local spine stimulation induced a gradual increase in spine size over time (blue;  $n=61$ ), which was absent in the non-stimulated condition (black;  $n=104$ ). Asterisk indicates  $p<0.05$  (Student's t-test with Bonferroni's correction).

(D) Scatter plot of average spine growth against bouton growth. Inhibitory bouton growth was not correlated with spine growth after local stimulation ( $p=0.22$ , Spearman). Gray crosses indicate two experiments in which we could not determine spine volume. Distributions are shown as histograms next to the scatter plot.

(E) Heat map showing bouton volumes over time of all experiments in which we performed the uncaging and depolarization stimulus in the absence of DNI-glutamate ('mock';  $n=15$ ). Each row represents a single experiment. The vertical white line indicates the end of the baseline period (first 20 minutes). White squares indicate missing time points. Experiments are sorted by maximal bouton growth.

(F) As in E, for experiments in the presence of APV ( $n=20$ ).

(G) As in E, for experiments in ACSF without  $Mg^{2+}$  and in the presence of TTX ( $n=14$ ).

(H) Bouton growth (averaged over four consecutive time points) for the experiments shown in E-G. Dashed line indicates control bouton growth without spine stimulation (from Figure 10). Bars indicate mean  $\pm$  SEM.  $p$ -values were 0.46, 0.87, and 0.65 (Student's t-test) for mock, APV and  $Mg^{2+}$ -free experiments, compared with control.

## Inhibitory bouton growth is mediated by retrograde endocannabinoid signaling

Endocannabinoids, a well-known class of retrograde messengers, are active lipolipids that are synthesized and released from the dendrite on demand (Castillo *et al.* 2012, Piomelli 2014) and mediate synaptic changes via presynaptic CB1 receptors (Cui *et al.* 2016, Monday and Castillo 2017). In our slices  $49 \pm 6\%$  of GFP-labeled axons showed clear immunostaining for CB1 receptors (Figure S4A-C). In accordance with recent *in vivo* data (Dudok *et al.* 2015), CB1 receptors uniformly decorated the entire surface of the axons, suggesting that CB1 signaling can occur in axonal stretches without boutons. Interestingly, we found that local spine stimulation could no longer trigger inhibitory bouton growth in the presence of AM251, a specific antagonist of CB1 receptors (Figure 4A, D and S4D-F), demonstrating the involvement of CB1 receptors.

Hippocampal CA1 dendrites and spines contain the enzyme DAGL, which produces the endocannabinoid 2-AG in an activity-dependent manner (Hashimoto *et al.* 2007, Piomelli 2014). We performed local spine stimulation experiments with THL, a lipase blocker with high specificity for DAGL, included in the patch pipette. Blocking postsynaptic DAGL blocked inhibitory bouton growth (Figure 4B, D and S4G-I), suggesting that inhibitory bouton growth requires 2-AG release from the dendrite.

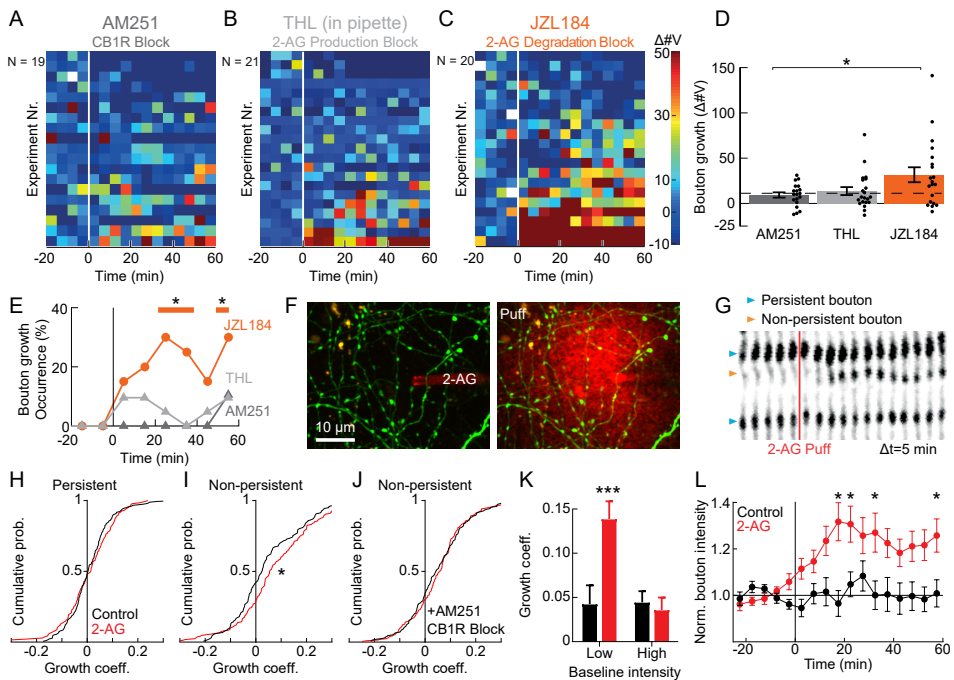


**Figure 4. Inhibitory bouton growth is mediated by endocannabinoid signaling**

(A) Heat map showing bouton volumes over time of all experiments in which spine stimulation was performed in the presence of the CB1 receptor antagonist AM251 ( $n=19$ ). Each row represents a single experiment. The vertical white line indicates the end of the baseline period (first 20 minutes). White squares indicate missing time points. Experiments are sorted by maximal bouton growth.

---

We also tested if we could facilitate inhibitory bouton growth by blocking the 2-AG degrading enzyme MAGL with JZL184 (Cui *et al.* 2016). In the presence of JZL184, local spine stimulation induced robust growth of nearby inhibitory boutons (Figure 4C, D and S4J-L), which was comparable to the level of bouton growth in experiments in the absence of pharmacological manipulation (Figure 10), although inhibitory bouton growth appeared to occur slightly earlier (Figure 4E). This experiment indicates that 2-AG degradation by MAGL does not limit the efficacy of the dendritic feedback signal. Together our results demonstrate that the dendritic feedback signal to induce inhibitory bouton growth after local spine stimulation requires CB1 receptor activation and depends on postsynaptic 2-AG production.

---

**(B)** As in A, for experiments in which THL was included in the patch pipette (n=21). THL is a lipase blocker with high affinity for the 2-AG production enzyme DAGL.

**(C)** As in B, for experiments in the presence of JZL184, an antagonist of the 2-AG degrading enzyme MAGL (n=20).

**(D)** Bouton growth per experiment (averaged over four consecutive time points) for the experiments shown in A (dark gray, 'AM251'), B (light gray, 'THL') and C (orange 'JZL184'). Dashed line indicates control bouton growth without spine stimulation (from Figure 10). Bars indicate mean±SEM. Asterisk indicates p=0.02 for JZL184 compared to AM251 (p=0.01 compared to control); p=0.44 THL vs AM251; p=0.06 JZL184 vs THL (Student's t tests).

**(E)** Bouton growth occurrence over time in experiments with AM251 (dark gray), THL (light gray) and JZL184 (orange). Orange line indicates time points where bouton growth in JZL184 was different compared to baseline, as tested by Cochran's Q test (p<0.0005) followed by McNemar's test (p<0.05 for individual time points). For AM251 and THL, p=0.125 and p=0.48, respectively (Cochran's Q test).

**(F)** 2-AG (and Alexa568 for visualization, red) was applied via a pipette close to inhibitory axons (green). Example images of a local application experiment before and during ('puff') local application.

**(G)** An axonal stretch (straightened) is shown for all time points. After 5 time points, 2-AG is applied (red line, '2-AG puff'). Blue arrows indicate persistent boutons (present in all time points) while the orange arrow indicates a non-persistent bouton (present in at least two, but not all, time points).

**(H)** Cumulative probability distributions of the growth coefficient of persistent boutons that were exposed to control ACSF (black; n=181 boutons) or 2-AG (red; n=135 boutons).

**(I)** Cumulative probability distributions of the growth coefficient of non-persistent boutons that were exposed to control ACSF (black; n=162 boutons) or 2-AG (red; n=167 boutons). (Mann-Whitney test, p<0.05).

**(J)** Cumulative probability distributions of the growth coefficient of non-persistent boutons that were exposed to control ACSF (black; n=195 boutons) or 2-AG (red; n=204 boutons) in the presence of CB1R antagonist AM251.

**(K)** Growth coefficient of non-persistent boutons with low and high baseline intensity. Bars represent mean±SEM. Asterisks indicate p<0.001 (2-way ANOVA followed by Sidak multiple comparisons test).

**(L)** Normalized bouton intensity over time for non-persistent boutons with low baseline intensity, that were exposed to control ACSF (black, n=54) or 2-AG (red, n=66). Bars represent mean±SEM. Asterisks indicate p<0.05 (2-way ANOVA followed by Sidak multiple comparisons test).

To test if mimicking 2-AG release is sufficient to induce inhibitory bouton growth, we used repeated short local applications of 2-AG or control ACSF from a pipette onto GFP-labeled inhibitory axons (Figure 4F; ~30  $\mu\text{m}$  diameter, see methods for details). When we locally applied 2-AG, we occasionally observed new boutons appearing along the inhibitory axon (Figure 4G). Growth or shrinkage of existing inhibitory synapses (persistent boutons) was not affected (Figure 4H). However, at axonal locations at which boutons were not always present (non-persistent boutons), local 2-AG application induced an overall shift towards more growth compared to control (Figure 4I). This shift was blocked by AM251 (Figure 4J). When we further distinguished between axonal locations with high and low baseline intensity (roughly reflecting axonal stretches with and without a bouton before 2-AG application), we found that 2-AG induced growth specifically at locations with low baseline intensity (Figure 4K). This growth was gradual and reached a plateau ~20 minutes after local 2-AG application (Figure 4L). These observations suggest that brief and local application of 2-AG can induce growth of inhibitory boutons via CB1 receptor activation preferably on empty axonal stretches. Local application of BDNF, another prominent activity-dependent dendritic retrograde signal (Gottmann *et al.* 2009, Harward *et al.* 2016), did not enhance bouton growth in GFP-labeled inhibitory axons (Figure S4M, N). Together, our experiments demonstrate that dendrites can trigger the growth of an inhibitory bouton at locations of strong excitatory synaptic activation through a local endocannabinoid feedback signal.

---

## Discussion

Dendritic inhibitory synapses are essential for dendritic computation because they can precisely shape local integration of excitatory synaptic inputs. Our data suggest that the formation of inhibitory synapses in the dendrite does not occur randomly, but that it can be directed by local excitatory synaptic activity in the dendrite. We describe a novel dendritic feedback signal to promote growth of inhibitory synapses in a dendritic region with strong synaptic activation. The signal from the dendrite to the axon requires local activation of glutamate receptors, including NMDA receptors. Furthermore, we show that inhibitory bouton growth after spine stimulation requires activation of CB1 receptors and depends on postsynaptic DAGL, the enzyme that produces the endocannabinoid 2-AG. The dendritic feedback signal could be mimicked by local application of 2-AG. The local signaling described here could provide inhibitory control at dendritic locations with strong excitatory synaptic activity and coordinate the number of excitatory and inhibitory synapses within dendrites in an activity-dependent manner.

The formation of dendritic inhibitory synapses is a highly dynamic process, which takes several hours (up to a day) and bouton growth is generally the first step in this process (Wierenga *et al.* 2008, Dobie and Craig 2011, Villa *et al.* 2016). In the hours after initial bouton formation, presynaptic vesicles and postsynaptic gephyrin and GABA<sub>A</sub> receptors are slowly recruited (Frias *et al.* 2018), but not all newly formed boutons will stabilize and form functional inhibitory synapses (Wierenga *et al.* 2008, Schuemann *et al.* 2013). The molecular events that take place during this maturation process and the signaling pathways regulating it are only partially known (Petrini *et al.* 2014, Flores *et al.* 2015, Krueger-Burg *et al.* 2017, Frias *et al.* 2018). The new boutons formed in our experiments will likely require several additional signals before becoming mature inhibitory synapses, which may well depend on local activity. Our current data identify a triggering mechanism for the formation of new inhibitory boutons at active dendrites which requires CB1 receptor activation. CB1 receptors are mostly known for mediating synaptic weakening (Monday and Castillo 2017). The mechanism described here could be related to the atypical endocannabinoid signaling that was recently found in synaptic strengthening (Cui *et al.* 2016, Wang *et al.* 2017).

Our data suggest that the formation of inhibitory synapses is locally coordinated by the dendrite via postsynaptic endocannabinoid production. We showed that blocking 2-AG production via postsynaptic DAGL interferes with inhibitory bouton growth. This suggests that 2-AG is the main endocannabinoid involved, but we do not rule out an additional role for other endocannabinoids (Piomelli 2014). During clustered spine stimulation, the postsynaptic production of endocannabinoids is likely triggered by a combination of postsynaptic depolarization and activation of local glutamate receptors (possibly both synaptic and extrasynaptic), as we found that each of these factors alone was not enough to trigger the dendritic feedback signal (Figure 3). Please note that in the low Mg<sup>2+</sup>/TTX condition, cell adhesion, neurotransmitter release or presynaptic activity may also have changed. Coincidence of multiple postsynaptic signals may be required to boost DAGL activity (Jung *et al.* 2012, Younts *et al.* 2013, Cui *et al.* 2016). The precise signaling pathways and the optimal conditions to induce the dendritic feedback signal should be addressed in

future experiments.

Dendrites receive and integrate synaptic signals from many different presynaptic partners. Our study suggests they can actively organize incoming synapses by sending a retrograde signal to promote the formation of inhibitory synapses at locations where clusters of excitatory synaptic inputs are strongly activated. Local clustered activation of inputs likely happens during physiological activation *in vivo*, as synaptic inputs with similar properties or activity patterns are often clustered on the same dendritic branch (Bloss *et al.* 2016, Wilson *et al.* 2016, Iacaruso *et al.* 2017). Clustering of excitatory inputs enhances the computational capacity of the postsynaptic neurons (Poirazi and Mel 2001, Branco and Häusser 2010) and inhibitory synapses at excitatory clusters will provide important local control over computations performed by individual dendritic branches (Lovett-Barron *et al.* 2012, Müllner *et al.* 2015, Bloss *et al.* 2016). The dendritic signaling mechanism described here would enable fine-tuning of dendritic inhibitory synapses in response to changes in activity of synaptic input clusters, allowing adaptation of dendritic inhibition during learning.

### **Acknowledgments**

The authors thank René van Dorland for excellent technical support. This research was supported by the Netherlands Organization for Scientific Research, as part of the VIDI program (CJW, HYH; #016.126.361), and as part of the research programme of the Foundation for Fundamental Research on Matter (FOM) (DLHK; #15PR3178-1), and by ERC Visionby3DSTIM, KFI16-1-2016-0177, NVKP16-1-2016-0043, GINOP2.1.1-15-2016-00979 (BR).

### **Author contributions**

CJW conceived and supervised the study, CJW, HYH and DLHK designed the experiments, HYH and DLHK performed the experiments and analysis, BR developed and provided DNI-glutamate, CCH provided critical input, CJW, HYH and DLHK wrote the paper with critical input from all authors.

### **Declarations of Interests**

BR is one of the founders of Femtonics Kft. and is a member of its scientific advisory board.



---

# Methods

## EXPERIMENTAL MODEL AND SUBJECT DETAILS

### Mice

In this study, male and female GAD65-GFP mice (López-Bendito *et al.* 2004) were used. GAD65-GFP mice express GFP in ~20% of GABAergic interneurons in the CA1 region of the hippocampus. The majority of GFP-labeled interneurons target dendrites and express reelin and VIP, while parvalbumin and somatostatin expression is nearly absent (Wierenga *et al.* 2010). We typically do not see many GFP-labeled boutons around the somata of CA1 pyramidal cells, indicating that basket cells are mostly not labeled in our slices. The sparse GFP expression allows monitoring of morphological changes in individual inhibitory axons (Wierenga *et al.* 2008, Schuemann *et al.* 2013). All animal experiments were performed in compliance with the guidelines for the welfare of experimental animals issued by the Federal Government of The Netherlands. All animal experiments were approved by the Animal Ethical Review Committee (DEC) of Utrecht University.

### Slice cultures

Organotypic hippocampal slice cultures were prepared at postnatal day 6-8 with a method slightly modified from Stoppini *et al.* (Stoppini *et al.* 1991). Mice were decapitated, followed by removal of the brain. The brain was placed in ice cold Gey's Balanced Salt Solution (GBSS, consisting of (mM): 137 NaCl, 5 KCl, 1.5 CaCl<sub>2</sub>, 1 MgCl<sub>2</sub>, 0.3 MgSO<sub>4</sub>, 0.2 KH<sub>2</sub>PO<sub>4</sub>, 0.85 Na<sub>2</sub>HPO<sub>4</sub>) supplemented with 12.5 mM HEPES, 25 mM glucose and 1 mM kynurenic acid (pH set at 7.2, osmolarity set at 320 mOsm, sterile filtered). Under sterile conditions, the frontal part of the brain and the cerebellum were dissected along the transverse plane and removed. The two hemispheres were then separated along the midline. For each hemisphere, the midbrain was carefully removed, and two incisions were made at the rostral and caudal ends of the hippocampus. The hippocampus was then carefully rolled out by flipping it 180 degrees over its long axis and a parallel incision was made in the cortex to dissect the hippocampus. Both hippocampi were placed in parallel on a PVC disk, excess liquid was removed, and slices were chopped perpendicularly to the long axis of the hippocampus with a thickness of 400 μm using a McIlwain Tissue Chopper. Slices were placed back in GBSS solution and carefully separated from each other. When needed, excess cortical tissue was removed from individual slices. Slices were washed in culturing medium (consisting of 48% MEM, 25% HBSS, 25% horse serum, 30 mM glucose and 12.5 mM HEPES, pH set at 7.3-7.4 and osmolarity set at 325 mOsm) before being placed on Millicell cell culture inserts (Millipore) in 6-well plates containing culturing medium. Slices were stored in an incubator (35 °C, 5% CO<sub>2</sub>) until use and culturing medium was completely replaced twice a week. Over time, slices attach to the membrane, flatten, and continue to develop in a physiological manner (De Simoni *et al.* 2003). Slices used in experiments were kept at least 7 days *in vitro* (DIV; average slice age was 14.4 DIV (with standard deviation=3.9; range 7-21)). There was no correlation between inhibitory bouton growth and slice age.

## METHOD DETAILS

### Two-photon microscopy and electrophysiology

Before the start of each experiment, a hippocampal slice was transferred, together with the piece of membrane it was plated on, from the incubator to the microscope recording chamber. During the experiment, the slice was perfused with carbogenated (95% O<sub>2</sub>, 5% CO<sub>2</sub>) artificial cerebrospinal fluid (ACSF, consisting of (mM): 126 NaCl, 3 KCl, 2.5 CaCl<sub>2</sub>, 1.3 MgCl<sub>2</sub>, 26 NaHCO<sub>3</sub>, 1.25 Na<sub>2</sub>H<sub>2</sub>PO<sub>4</sub>, 20 glucose and 1 Trolox) at a rate of approximately 1 ml/min at room temperature. Two-photon imaging was performed on a customized two-photon laser scanning microscope (Femto2D, Femtonics Ltd., Budapest, Hungary) using a Ti:Sapphire femtosecond pulsed laser (MaiTai, Spectra-Physics). This laser, tuned at 840 or 870 nm, was used to excite GFP and Alexa568 simultaneously and fluorescence was detected using two GaAsP photomultiplier tubes. For local application experiments, the laser was tuned at 910 nm.

A 4x air objective (Nikon Plan Apochromat) was used to locate the CA1 region of the slice culture and to roughly position the pipettes for whole-cell patch clamp (thick-walled borosilicate glass, World Precision Instruments) and for local DNI-glutamate application (thin-walled borosilicate glass, World Precision Instruments) using micromanipulators (LN Junior, Luigs & Neumann). Under a 60x water immersion objective (Nikon NIR Apochromat; NA=1.0), the opening of the application pipette was enlarged to approximately 5 μm by carefully tapping it against the patch pipette, and both pipettes were placed close to the imaging area. Whole-cell patch clamp of a CA1 pyramidal cell neuron was performed with the patch pipette (3-7 MΩ) filled with internal solution (consisting of (mM): 140 K-gluconate, 4 KCl, 0.5 EGTA, 10 HEPES, 4 MgATP, 0.4 NaGTP, 4 Na<sub>2</sub>Phosphocreatine, and 30 μM Alexa 568 (Thermo Fisher Scientific)). Cells were excluded when the initial resting membrane potential exceeded -50 mV, if the cell was firing spontaneously, or if R<sub>s</sub> exceeded 30 MΩ. The pyramidal cell was kept in voltage clamp at -60 mV throughout the experiment.

Crossings between the Alexa568-labeled dendrite and a GFP-labeled axon were identified using two-photon microscopy by overlap between the red and green channel (Wierenga *et al.* 2008, Müllner *et al.* 2015). After finding an inhibitory axon crossing with no or negligible bouton, the application pipette was placed with the opening towards the crossing (at ~40 μm distance and ~20 μm above the surface of the slice). The time needed for the search procedure and pipette placement was typically 10-15 minutes, and less than 30 minutes in all experiments. In most cases, dendrites were in stratum radiatum, with some experiments performed in stratum lacunosum moleculare. Image stacks of the axon-dendrite crossing were made every 5 minutes at a resolution of 9 pixels/μm with 0.5 μm z-steps (256x256 pixels, 28.4x28.4 μm).

### Spine stimulation

After acquiring four baseline time points, DNI-glutamate-TFA (Femtonics Ltd. (Tønnesen *et al.* 2014), 5 mM dissolved in HEPES-ACSF: (mM) 135 NaCl, 3 KCl, 2.5 CaCl<sub>2</sub>, 1.3 MgCl<sub>2</sub>, 1.25 Na<sub>2</sub>H<sub>2</sub>PO<sub>4</sub>, 20 Glucose, and 10 HEPES) was locally applied to the axon-dendrite crossing using

---

a Picospritzer II (General Valve Corporation; 8-12 mmHg) through the application pipette. A second Ti-Sapphire femtosecond pulsed laser (MaiTai, Spectra-Physics) tuned at 730 nm was used for two-photon uncaging. We selected four small spines close (range 1-12  $\mu\text{m}$ ; average  $2.7 \pm 0.2 \mu\text{m}$ ) to the axon crossing for stimulation. Usually spines were selected at both sides of the axon crossing. We optimized the excitation wavelength for visualizing changes in GFP-labeled axons, which may have compromised our ability to visualize the smallest spines. After locally applying caged glutamate for  $\sim 1$  minute, the laser scanned across lines of  $\sim 0.5 \mu\text{m}$  long and  $\sim 0.5 \mu\text{m}$  away from the spines for 1 ms. Laser intensity for glutamate uncaging was carefully chosen to evoke excitatory postsynaptic currents with physiological amplitude at individual spines (mean amplitude =  $10.9 \pm 0.6 \text{ pA}$ ; range 4-18 pA), measured at the soma. The amplitude of uncaging currents was not much affected by the presence of NMDA receptor antagonist APV (mean amplitude =  $9.2 \pm 0.8 \text{ pA}$ ;  $p=0.11$ , Student's t-test), in accordance with only a small NMDA receptor contribution to the synaptic current.

We also recorded the combined uEPSC when all four spines were stimulated together near-simultaneously (0.1 ms between spines). After recording the combined uEPSC, spine stimulation was performed. The four spines were stimulated together (1 ms pulses with 0.1 ms interval between spines) while the postsynaptic cell was depolarized to 0 mV, and this stimulation was repeated 30 times at 0.5 Hz (Figure 1C). Afterwards, the combined and individual uEPSCs were measured again. Experiments were only included if uEPSCs could be evoked after the stimulation protocol, verifying that glutamate uncaging had been successful. uEPSC linearity was determined by dividing the uEPSC amplitude of the combined response by the sum of individual uEPSC amplitudes.

For glutamate uncaging close to GFP-labeled axons, we selected small segments of GFP-expressing inhibitory axons that were empty of boutons and performed two-photon glutamate uncaging at four locations close to the axon with the same stimulation protocol as used for spine stimulation (30x 1ms pulses @0.5 Hz at four locations, interval between locations 0.1 ms). Glutamate uncaging spots were located close to the axon, at an average distance of  $1.2 \pm 0.2 \mu\text{m}$ . Even though there will be many unlabeled spines in close proximity to the uncaging spots, the likelihood that this uncaging protocol will activate multiple spines on a single dendrite will be low.

To perform two-photon uncaging in the absence of postsynaptic depolarization, regular ACSF was replaced by  $\text{Mg}^{2+}$ -free ACSF (regular ACSF without  $\text{MgCl}_2$ ) containing 0.5  $\mu\text{M}$  tetrodotoxin (TTX, Abcam).  $\text{Mg}^{2+}$ -free ACSF was washed in before imaging started. Regular ACSF was washed back in after the uncaging stimulus at  $\sim 15$  minutes. For these experiments, DNI-glutamate was dissolved in HEPES-ACSF without  $\text{MgCl}_2$  and containing 0.5  $\mu\text{M}$  TTX. To block NMDAR activation, 50  $\mu\text{M}$  DL-APV (Tocris) was added to regular ACSF and was applied to the slice during the entire experiment. To block CB1 receptors, 5  $\mu\text{M}$  AM251 (Tocris) was added to the bath and 10  $\mu\text{M}$  in the application pipette. To block 2-AG production by the enzyme DAGL in the postsynaptic dendrite, 5  $\mu\text{M}$  of Tetrahydrolipstatin (THL, Orlistat, Sigma) was added to the patch clamp intracellular solution. To block 2-AG degradation, 100 nM JZL184 (Tocris) was added to the bath.

### Local application of 2-AG and BDNF

For the local application of 2-AG, thick-walled application pipettes were filled with HEPES-ACSF + 50  $\mu$ M Alexa568 (for visualization) and 100  $\mu$ M 2-arachidonoylglycerol (2-AG, Tocris) + 0.1% DMSO or 0.1% DMSO control solution. In experiments when CB1 receptors were blocked, 5  $\mu$ M AM251 was added to the bath and the local application solution. We targeted axons in stratum radiatum, but we cannot exclude that a small population of GFP-labeled somatically targeting boutons were exposed and analyzed. Before the start of the experiment, the application pipette was placed inside the top layer of the slice, close to an area with multiple GFP-expressing inhibitory axons under visual control (excitation wavelength 840 nm for simultaneous visualization of Alexa568 and GFP). We adjusted the pressure of application pulses to set the diameter of the application area to  $\sim$ 30  $\mu$ m using a Picospritzer II (4-10 mmHg). This calibration procedure took <2 minutes. During the experiment, images (468x468 pixels, 51.5x51.5  $\mu$ m with 0.5  $\mu$ m z-steps) were taken at a wavelength of 910 nm every 5 minutes for 5 time points before and up to an hour after local application of 2-AG. 2-AG was applied in 30 bursts at 0.5 Hz (3 pulses of 50 ms per burst) to mimic the spine stimulation protocol. For BDNF application, we used 200 ng/ml Human recombinant BDNF (Merck) + 0.1% bovine serum albumin (BSA, Sigma) or 0.1% BSA control and 25-75 ms pulses at 2 Hz for 2 minutes.

### Immunohistochemistry and confocal microscopy

Slices were fixed by placing them in a 4% paraformaldehyde solution for 30 minutes at room temperature. After washing them thoroughly in phosphate buffered saline (PBS), the slices were permeabilized for 15 minutes in 0.5% Triton-X100 in PBS for 15 minutes, followed by 1 hour in a blocking solution consisting of 10% normal goat serum and 0.2% Triton-X100 in PBS. Primary antibody solution (mouse  $\alpha$ -CB1R, Synaptic Systems 258011; 1:500 in blocking solution) was applied at 4  $^{\circ}$ C overnight. Slices were washed thoroughly in PBS and placed in secondary antibody solution (goat  $\alpha$ -mouse (IgG2b) conjugated to Alexa594, Life Technologies A21145; 1:500 in blocking solution) for four hours at room temperatures. Finally, slices were washed thoroughly in PBS and mounted in Vectashield mounting medium (Vector labs). Confocal images were taken on a Zeiss LSM-700 confocal laser scanning microscopy system with a Plan-Apochromat 63x 1.4 NA oil immersion objective. Image stacks were acquired at 10 pixels per  $\mu$ m and with 0.3  $\mu$ m z steps.

## **QUANTIFICATION AND STATISTICAL ANALYSIS**

### Quantification of bouton and spine volumes

Experiments in which we imaged axon-dendrite crossings were only included in the analysis when the local maxima of the red and the green channel were not more than 1 optical section ( $\Delta z = 0.5 \mu$ m) apart (Wierenga *et al.* 2008, Müllner *et al.* 2015). Analysis and bouton volume quantification was performed on median filtered images using custom written Matlab scripts (Mathworks). A box of 9x9x5 voxels (i.e. 1x1x2.5  $\mu$ m) was positioned manually at the axon-dendrite crossing at each time point. An axon threshold was set to separate the boutons

---

from the axon, relative to the axon intensity (determined from the summed projection of 5 z-planes, modus along the entire axon) to account for possible intensity fluctuations between time points and differences between experiments (axon threshold was  $2.9 \pm 0.1$  for non-stimulated axons;  $2.8 \pm 0.1$  for stimulated axons;  $p=0.19$ , Student's t test). In a few experiments, bleach correction was applied. The absolute change in bouton volume ( $\Delta\#V$ ) was quantified as the number of voxels above bouton threshold minus the average volume of the baseline period. The relative change in bouton intensity ( $\Delta\%I$ ) was defined as the integrated intensity of all voxels inside the same  $9 \times 9 \times 5$  box, divided by the average intensity of the baseline period. As baseline intensity of the axon was sometimes very low,  $\Delta\%I$  gave very high values for boutons that were growing from dim axons. To avoid strong bias for these events, we used the absolute measure  $\Delta\#V$  for our comparisons. We verified that the two measures  $\Delta\#V$  and  $\Delta\%I$  were highly correlated (Pearson's  $r=0.82$ ,  $p<0.0001$ ) and that our conclusions do not critically depend on our quantification method (Figure S1). Bouton growth per experiment was defined as the maximum bouton volume after the baseline averaged over four consecutive time points. To show the average time course of bouton growth, we determined bouton growth occurrence as the fraction of experiments in which bouton growth exceeded an empirically chosen threshold (35 voxels for  $\Delta\#V$  and 50% for  $\Delta\%I$ ). We verified that our conclusions do not depend on the choice of this threshold (Figure S1E,F). Bouton growth occurrence was plotted in bins of 10 minutes to reduce noise and reduce the weight of boutons which last for only one time point.

Spine growth was determined as relative change in intensity ( $\Delta\%I$ ) over a volume of  $9 \times 9 \times 5$  voxels and spines were considered to grow when  $\Delta\%I > 25\%$ . Some stimulated spines which overlapped with the shaft or with neighboring spines were not analyzed. Maximal and average spine growth was determined as the maximum and mean of the 4 stimulated spines per experiment. Baseline spine volumes were similar between conditions ( $p=0.71$ , Student's t-test). Spine and bouton growth were induced in whole-cell recordings even after 20-40 minutes. We found no correlation between maximal spine growth or bouton growth with the time after breakthrough (Figure S1G,H).

#### Local application analysis

All image analysis was done blind to the experimental conditions. One to four axons (average length =  $38.5 \mu\text{m}$  with  $SD=7.3 \mu\text{m}$ ) within the field of view ( $468 \times 468$  pixels,  $51.5 \times 51.5 \mu\text{m} \mu\text{m}$ ) were analyzed. We quantified changes in axon intensity at all bouton locations (locations where inhibitory boutons were present at any time point during the imaging period). For each of these locations, we determined a growth coefficient which was normalized between -1 and +1, where negative values correspond to bouton shrinkage and positive values to growth. Bouton locations (axonal locations where boutons were present for at least 2 time points during the imaging period) were selected manually by the researcher, aided by the axon threshold calculated by the software (see above). The growth coefficient was calculated for each bouton to quantify its growth or shrinkage during the imaging period as  $(V2 - V1)/(V2 + V1)$ , in which  $V1$  is the average baseline bouton intensity and  $V2$  is the maximal bouton intensity, determined over a sliding window of 5 time points. A positive value of the growth coefficient indicates bouton growth, while a negative value

indicates bouton shrinkage. Persistent boutons were defined as boutons that are present at all time points, while non-persistent boutons are not present at all (but at least at two) time points. We further divided non-persistent boutons into two categories (low and high baseline intensity) using an baseline intensity of 20000 (arbitrary units) as an empirically determined threshold. This cutoff roughly divides the dataset into axon locations where no bouton is present in baseline ('low') and axon location where there is a bouton present in baseline ('high'). For the low baseline intensity boutons, we calculated the average intensity over time normalized to the baseline period.

#### Quantification of CB1R-positive axon fraction

In Fiji/ImageJ, all healthy looking axons in a maximum intensity projection (5-10 images) were manually selected based on the GFP channel. For each axon, colocalization with the CB1 receptor channel was determined. Per image stack, two or three maximum intensity projections were analyzed. The total amount of CB1 receptor-positive GFP axons in an image stack was divided by the total amount of quantified GFP-positive axons to determine the CB1 receptor-positive fraction.

#### Statistical analysis

Statistical differences between groups were tested with two-sample Student's t test and means are given  $\pm$  standard error of the mean (SEM), unless otherwise stated. Bouton growth occurrence per condition was tested for statistical significance against its own baseline period with a Cochran's Q test, followed by a post-hoc McNemar's test. Fractions of growing spines between conditions were tested with Pearson's  $\chi^2$  test. Possible correlations were tested with Spearman's ranked test and Pearson's correlation coefficient ( $r$ ) was determined. For the local application experiments, differences between the datasets were tested using a Mann-Whitney test. After subdividing the non-persistent boutons based on baseline intensity, data were tested using a two-way ANOVA, followed by a post-hoc Sidak's multiple comparisons test. This test was also performed on the normalized bouton intensity over time. Statistical analyses were performed using Matlab R2013a, Graphpad Prism 7, and SPSS Statistics 24.

## Supplementary Figures

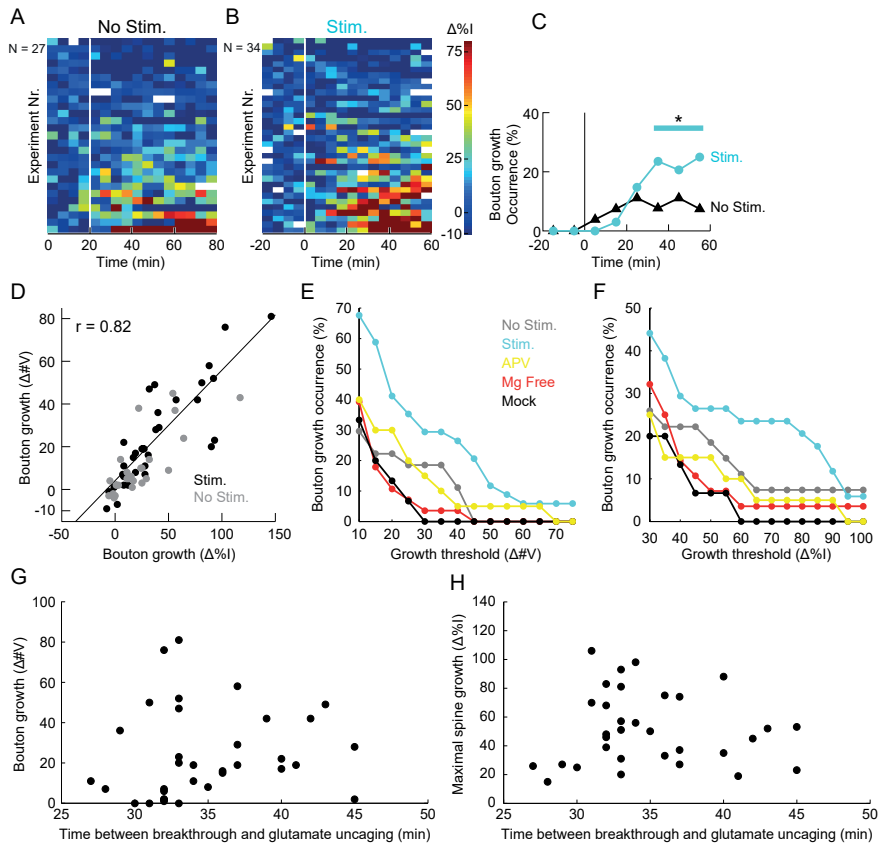


**Figure S1, related to figure 1: Bouton growth is independent of quantification method, threshold and time after breakthrough**

(A-B) As an alternative measure for bouton volume, we determined the relative increase in integrated intensity ( $\Delta\%I$ ) of the inhibitory axon at the crossing compared to its baseline intensity, a measure which is often used to quantify growth of small structures such as spines (Oh *et al.* 2015, Harward *et al.* 2016). Heat maps showing bouton intensity ( $\Delta\%I$ ) over time of all experiments in non-stimulated (A) and stimulated (B) conditions. Each row represents a single experiment. The vertical white line indicates the end of the baseline period (first 20 minutes). White squares indicate missing time points. Experiments are sorted by maximal bouton growth.

(C) Bouton growth occurrence over time in experiments in stimulated and non-stimulated conditions. Blue line indicates timepoints where bouton growth was different compared to baseline, as tested by Cochran's Q test followed by post-hoc McNemar's test.  $p < 0.05$

(D) Scatter plot of absolute bouton volume growth ( $\Delta\#V$ ) against relative bouton intensity growth ( $\Delta\%I$ ) from experiments with (black) and without (gray) spine stimulation. The two measures of bouton growth are highly correlated. Pearson's  $r = 0.82$  ( $p < 10^{-18}$ , Spearman).

(E, F) Bouton growth occurrence plotted against growth threshold ( $\Delta\#V$  in E and  $\Delta\%I$  in F) for No Stim (gray), Stim (blue), APV (yellow),  $Mg^{2+}$  free (red) and Mock (black) experiments. These graphs indicate that our conclusions do not depend on the choice of this threshold.

(G, H) Bouton growth (G) and maximal spine growth (H) plotted against the time between whole-cell breakthrough and glutamate uncaging for all 'Stim' experiments (Fig. 1M). These graphs suggest that washout in not a major factor in our experiments.

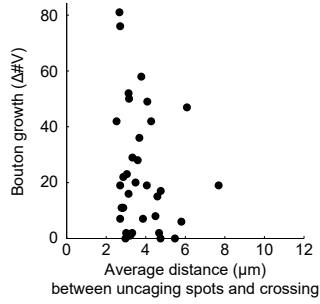


**Figure S2, related to figure 2: Bouton growth is not correlated with distance to uncaging spot**

Scatter plot of bouton growth versus the average distance between the axon-dendrite crossing and the 4 uncaging spots.  $p=0.21$ , Spearman.



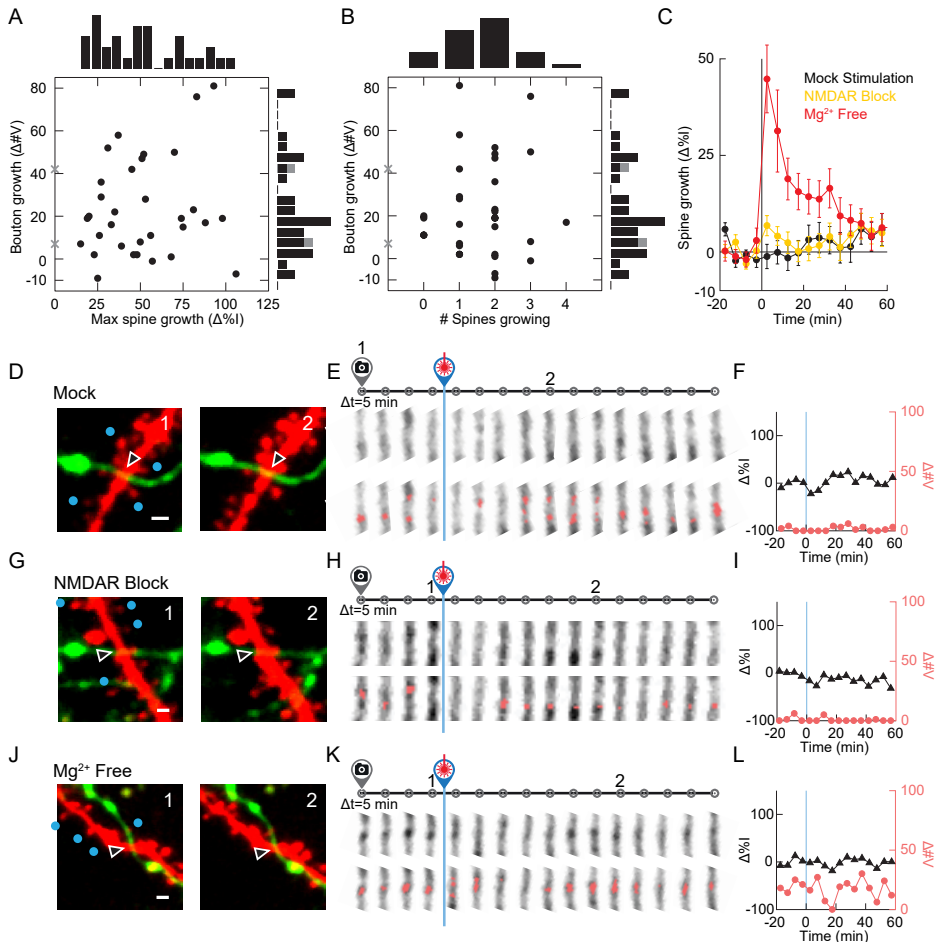


**Figure S3, related to figure 3: Bouton growth and spine growth are not correlated**

(A) Scatter plot of maximal spine growth against bouton growth per experiment. No correlation was found ( $p=0.54$ , Spearman). Gray crosses indicate two experiments in which we could not determine spine volumes. Distributions are shown as histograms next to the scatter plot.

(B) Scatter plot of number of growing spines against bouton growth per experiment. No correlation was found ( $p=0.61$ , Spearman).

(C) Average spine growth over time after spine stimulation in the absence of DNI-glutamate ('mock stimulation', black), when NMDA receptors were blocked with APV ('NMDAR block', yellow), and in Mg<sup>2+</sup> free ACSF ('Mg<sup>2+</sup> free', red).

(D-F) Example of an experiment in which spine stimulation and postsynaptic depolarization were applied in absence of DNI-glutamate ("Mock"). (D) Images of two time points indicated in E. Arrowheads point towards the axon crossing, blue dots indicate uncaging locations. Scale bar is 1 μm. (E) Axonal segment at the crossing is displayed for all time points. The voxels above axon threshold are indicated in red in the lower panel. (F) Quantification of bouton volume over time, measured as the increase in number of voxels above axon threshold (Δ#V, red) and increase in relative intensity (Δ%I, black).

(G-I) As D-F, example of an experiment in which spine stimulation was performed in presence of the NMDAR antagonist DL-APV.

(J-L) As in D-F, example of an experiment in which spine stimulation was performed without depolarization in absence of extracellular Mg<sup>2+</sup> and in presence of TTX.

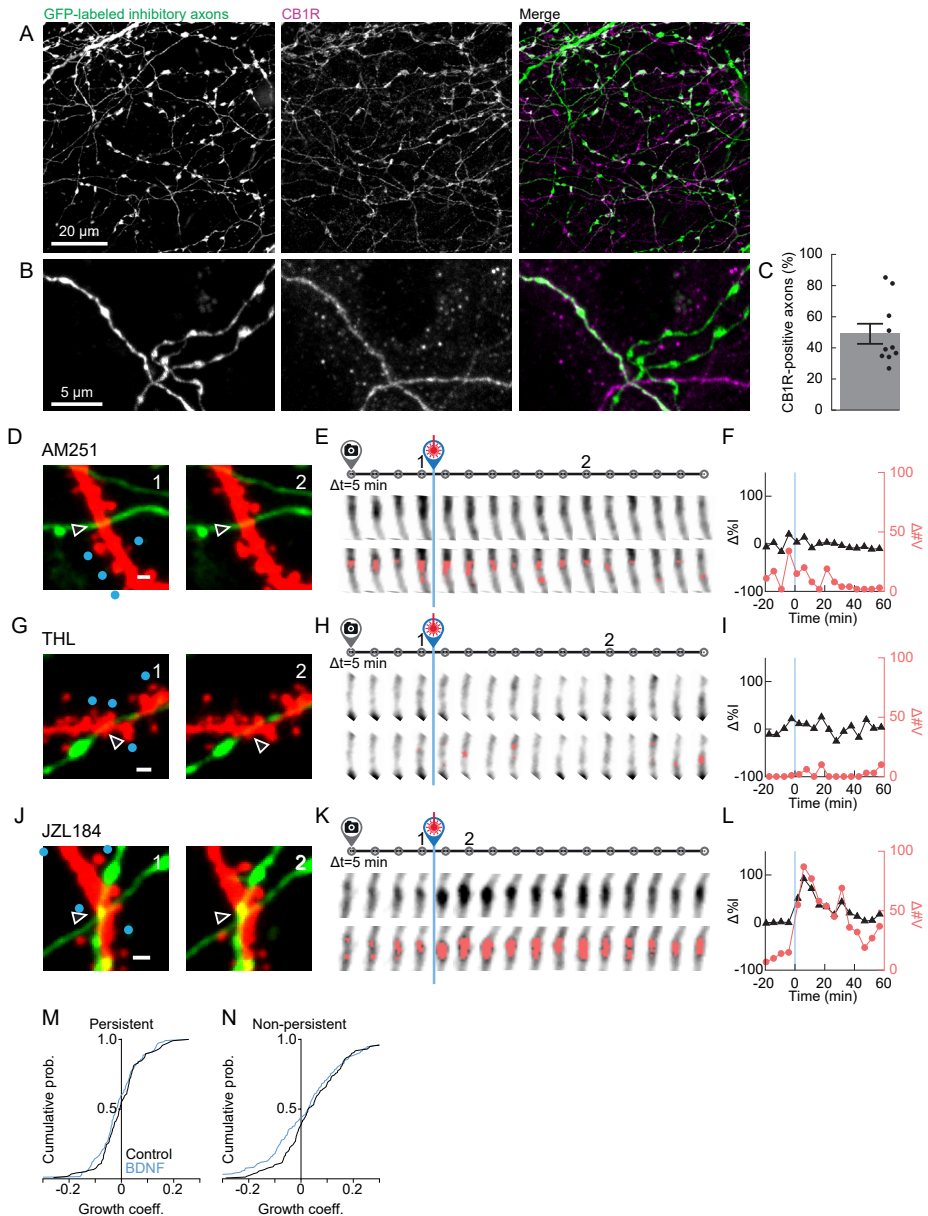


**Figure S4, related to figure 4: Quantification of CB1-positive GFP-labeled inhibitory axons**

**(A)** Example of immunohistochemistry against the CB1 receptor. Left panel: GFP-positive axons. Middle panel: CB1 receptors. Right panel: merged image. In accordance with the reported low expression levels at postsynaptic dendrites and spines and glia cells (Kano *et al.* 2009), we did not detect substantial CB1 receptor immunostaining in non-axonal structures.

**(B)** As in A. Example showing CB1R-positive and CB1R-negative GFP-labeled axons and CB1R-positive unlabeled axon.

**(C)** Quantification of the percentage of GFP-labeled axons positive for the CB1 receptor. Bar represents mean  $\pm$  SEM. (n=10 image stacks, N=3 slices).

- 
- (D-F)** Example of an experiment in which spine stimulation was performed in presence of the CB1-receptor antagonist AM251. (D) Images of two time points indicated in E. Arrowheads point towards the axon crossing, blue dots indicate uncaging locations. Scale bar is 1  $\mu\text{m}$ . (E) Axonal segment at the crossing is displayed for all time points. The voxels above axon threshold are indicated in red in the lower panel. (F) Quantification of bouton volume over time, measured as the increase in number of voxels above axon threshold ( $\Delta\#V$ , red) and increase in relative intensity ( $\Delta\%I$ , black).
- (G-I)** As D-F, example of an experiment in which spine stimulation was performed with THL in the patch pipette. THL is a lipase blocker with high affinity for the 2-AG synthesis enzyme DAGL.
- (J-L)** As in D-F, example of an experiment in which spine stimulation was performed in presence of JZL184, a blocker of 2-AG degradation enzyme MAGL.
- (M)** Cumulative probability distributions of the growth coefficient of persistent boutons that were exposed to control ACSF (black; n=118 boutons) or BDNF (blue; n=124 boutons).
- (N)** Cumulative probability distributions of the growth coefficient of non-persistent boutons that were exposed to control ACSF (black; n=160 boutons) or BDNF (blue; n=195 boutons).

## References

- Bloss, E.B., Cembrowski, M.S., Karsh, B., Colonell, J., Fetter, R.D., and Spruston, N., 2016. Structured Dendritic Inhibition Supports Branch-Selective Integration in CA1 Pyramidal Cells. *Neuron*, 89 (5), 1016–1030.
- Bourne, J.N. and Harris, K.M., 2011. Coordination of size and number of excitatory and inhibitory synapses results in a balanced structural plasticity along mature hippocampal CA1 dendrites during LTP. *Hippocampus*, 21 (4), 354–73.
- Branco, T. and Häusser, M., 2010. The single dendritic branch as a fundamental functional unit in the nervous system. *Current opinion in neurobiology*, 20 (4), 494–502.
- Castillo, P.E., Younts, T.J., Chávez, A.E., and Hashimoto, Y., 2012. Endocannabinoid Signaling and Synaptic Function. *Neuron*, 76 (1), 70–81.
- Chen, J.L., Villa, K.L., Cha, J.W., So, P.T.C., Kubota, Y., and Nedivi, E., 2012. Clustered Dynamics of Inhibitory Synapses and Dendritic Spines in the Adult Neocortex. *Neuron*, 74 (2), 361–373.
- Chen, S.X., Kim, A.N., Peters, A.J., and Komiyama, T., 2015. Subtype-specific plasticity of inhibitory circuits in motor cortex during motor learning. *Nature Neuroscience*, 18 (8), 1109–1115.
- Chiu, C.Q., Martenson, J.S., Yamazaki, M., Natsume, R., Sakimura, K., Tomita, S., Tavalin, S.J., and Higley, M.J., 2018. Input-Specific NMDAR-Dependent Potentiation of Dendritic GABAergic Inhibition. *Neuron*, 97 (2), 368–377.e3.
- Cui, Y., Prokin, I., Xu, H., Delord, B., Genet, S., Venance, L., and Berry, H., 2016. Endocannabinoid dynamics gate spike-timing dependent depression and potentiation. *eLife*, 5 (FEBRUARY2016), 1–32.
- Dobie, F.A. and Craig, A.M., 2011. Inhibitory Synapse Dynamics: Coordinated Presynaptic and Postsynaptic Mobility and the Major Contribution of Recycled Vesicles to New Synapse Formation. *Journal of Neuroscience*, 31 (29), 10481–10493.
- Dudok, B., Barna, L., Ledri, M., Szabó, S.I., Szabadits, E., Pintér, B., Woodhams, S.G., Henstridge, C.M., Balla, G.Y., Nyilas, R., Varga, C., Lee, S.-H., Matolcsi, M., Cervenak, J., Kacsokovics, I., Watanabe, M., Sgheddu, C., Melis, M., Pistis, M., Soltesz, I., and Katona, I., 2015. Cell-specific STORM super-resolution imaging reveals nanoscale organization of cannabinoid signaling. *Nature Neuroscience*, 18 (1), 75–86.
- Flores, C.E., Nikonenko, I., Mendez, P., Fritschy, J.-M., Tyagarajan, S.K., and Muller, D., 2015. Activity-dependent inhibitory synapse remodeling through gephyrin phosphorylation. *Proceedings of the National Academy of Sciences of the United States of America*, 112 (1), E65-72.
- Frias, C.P., Bresser, T., Scheefhals, L., Hu, H.Y., Van Bergen en Henegouwen, P.M.P., Hoogenraad, C.C., and Wierenga, C.J., 2018. Semaphorin4D induces inhibitory synapse formation by rapid stabilization of presynaptic boutons via MET co-activation. *BioRxiv*, 100271, doi: <https://doi.org/10.1101/100271>.
- Froemke, R.C., 2015. Plasticity of Cortical Excitatory-Inhibitory Balance. *Annual Review of Neuroscience*, 38 (1), 195–219.

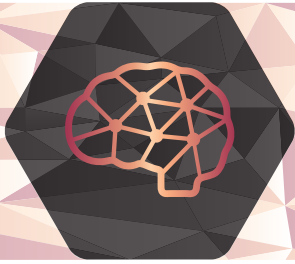
- 
- Gottmann, K., Mittmann, T., and Lessmann, V., 2009. BDNF signaling in the formation, maturation and plasticity of glutamatergic and GABAergic synapses. *Experimental Brain Research*, 199 (3–4), 203–234.
- Govindarajan, A., Israely, I., Huang, S.-Y., and Tonegawa, S., 2011. The dendritic branch is the preferred integrative unit for protein synthesis-dependent LTP. *Neuron*, 69 (1), 132–46.
- Harnett, M.T., Makara, J.K., Spruston, N., Kath, W.L., and Magee, J.C., 2012. Synaptic amplification by dendritic spines enhances input cooperativity. *Nature*, 491, 599–602.
- Harvey, C.D. and Svoboda, K., 2007. Locally dynamic synaptic learning rules in pyramidal neuron dendrites. *Nature*, 450 (7173), 1195–1200.
- Harward, S.C., Hedrick, N.G., Hall, C.E., Parra-bueno, P., Milner, T.A., Pan, E., Laviv, T., Hempstead, B.L., and Yasuda, R., 2016. Autocrine BDNF-TrkB signalling within a single dendritic spine. *Nature*, 538 (7623), 99–103.
- Hashimoto-dani, Y., Ohno-shosaku, T., and Kano, M., 2007. Ca<sup>2+</sup>-assisted receptor-driven endocannabinoid release: mechanisms that associate presynaptic and postsynaptic activities. *Current Opinion in Neurobiology*, 17, 360–365.
- Iacaruso, M.F., Gasler, I.T., and Hofer, S.B., 2017. Synaptic organization of visual space in primary visual cortex. *Nature*, 547 (7664), 449–452.
- Jadi, M., Polsky, A., Schiller, J., and Mel, B.W., 2012. Location-dependent effects of inhibition on local spiking in pyramidal neuron dendrites. *PLoS Computational Biology*, 8 (6).
- Jung, K.-M., Sepers, M., Henstridge, C.M., Lassalle, O., Neuhofer, D., Martin, H., Ginger, M., Frick, A., DiPatrizio, N. V., Mackie, K., Katona, I., Piomelli, D., and Manzoni, O.J., 2012. Uncoupling of the endocannabinoid signalling complex in a mouse model of fragile X syndrome. *Nature Communications*, 3, 1080.
- Kano, M., Ohno-Shosaku, T., Hashimoto-dani, Y., and Watanabe, M.U.M., 2009. Endocannabinoid-mediated control of synaptic transmission. *Physiol Rev*, 89, 309–380.
- Keck, T., Scheuss, V., Jacobsen, R.I., Wierenga, C.J., Eysel, U.T., Bonhoeffer, T., and Hübener, M., 2011. Loss of sensory input causes rapid structural changes of inhibitory neurons in adult mouse visual cortex. *Neuron*, 71 (5), 869–882.
- Krueger-Burg, D., Papadopoulos, T., and Brose, N., 2017. Organizers of inhibitory synapses come of age. *Current Opinion in Neurobiology*, 45, 66–77.
- López-Bendito, G., Sturgess, K., Erdélyi, F., Szabó, G., Molnár, Z., and Paulsen, O., 2004. Preferential origin and layer destination of GAD65-GFP cortical interneurons. *Cerebral Cortex*, 14 (10), 1122–1133.
- Losonczy, A. and Magee, J.C., 2006. Integrative properties of radial oblique dendrites in hippocampal CA1 pyramidal neurons. *Neuron*, 50 (2), 291–307.
- Lovett-Barron, M., Kaifosh, P., Kheirbek, M.A., Danielson, N., Zarembka, J.D., Reardon, T.R., Turi, G.F., Hen, R., Zemelman, B. V., and Losonczy, A., 2014. Dendritic inhibition in the hippocampus supports fear learning. *Science*, 343 (February), 857–863.

- Lovett-Barron, M., Turi, G.F., Kaifosh, P., Lee, P.H., Bolze, F., Sun, X.H., Nicoud, J.F., Zemelman, B. V., Sternson, S.M., and Losonczy, A., 2012. Regulation of neuronal input transformations by tunable dendritic inhibition. *Nature Neuroscience*, 15 (3), 423–430.
- Megías, M., Emri, Z., Freund, T.F., Gulyás, A.I., and Megias, M., 2001. Total number and distribution of inhibitory and excitatory synapses on hippocampal CA1 pyramidal cells. *Neuroscience*, 102 (3), 527–540.
- Monday, H.R. and Castillo, P.E., 2017. Closing the gap: long-term presynaptic plasticity in brain function and disease. *Current Opinion in Neurobiology*, 45, 106–112.
- Müllner, F.E., Wierenga, C.J., and Bonhoeffer, T., 2015. Precision of Inhibition: Dendritic Inhibition by Individual GABAergic Synapses on Hippocampal Pyramidal Cells Is Confined in Space and Time. *Neuron*, 87 (3), 576–589.
- Oh, W.C., Parajuli, L.K., and Zito, K., 2015. Heterosynaptic Structural Plasticity on Local Dendritic Segments of Hippocampal CA1 Neurons. *Cell Reports*, 10 (2), 162–169.
- Petrini, E.M., Ravasenga, T., Hausrat, T.J., Iurilli, G., Olcese, U., Racine, V., Sibarita, J.-B., Jacob, T.C., Moss, S.J., Benfenati, F., Medini, P., Kneussel, M., and Barberis, A., 2014. Synaptic recruitment of gephyrin regulates surface GABAA receptor dynamics for the expression of inhibitory LTP. *Nature communications*, 5, 3921.
- Piomelli, D., 2014. More surprises lying ahead. The endocannabinoids keep us guessing. *Neuropharmacology*, 76 (PART B), 228–234.
- Poirazi, P. and Mel, B.W., 2001. Impact of active dendrites and structural plasticity on the memory capacity of neural tissue. *Neuron*, 29 (3), 779–796.
- Schuemann, A., Klawiter, A., Bonhoeffer, T., and Wierenga, C.J., 2013. Structural plasticity of GABAergic axons is regulated by network activity and GABAA receptor activation. *Frontiers in neural circuits*, 7 (June), 113.
- De Simoni, A., Griesinger, C.B., and Edwards, F.A., 2003. Development of rat CA1 neurones in acute versus organotypic slices: role of experience in synaptic morphology and activity. *Journal of Physiology*, 550 (Pt 1), 135–47.
- Stoppini, L., Buchs, P. -a., and Muller, D., 1991. A simple method for organotypic cultures of nervous tissue. *Journal of Neuroscience Methods*, 37 (2), 173–182.
- Tanaka, J.-I., Horiike, Y., Matsuzaki, M., Miyazaki, T., Ellis-Davies, G.C.R., and Kasai, H., 2008. Protein synthesis and neurotrophin-dependent structural plasticity of single dendritic spines. *Science (New York, N.Y.)*, 319 (5870), 1683–7.
- Tønnesen, J., Katona, G., Rózsa, B., and Nägerl, U.V., 2014. Spine neck plasticity regulates compartmentalization of synapses. *Nature Neuroscience*, (February).
- Villa, K.L., Berry, K.P., Subramanian, J., Cha, J.W., Oh, W.C., Kwon, H.B., Kubota, Y., So, P.T.C., and Nedivi, E., 2016. Inhibitory Synapses Are Repeatedly Assembled and Removed at Persistent Sites In Vivo. *Neuron*, 89 (4), 756–769.

- 
- Wang, W., Jia, Y., Pham, D.T., Palmer, L.C., Jung, K.-M., Cox, C.D., Rumbaugh, G., Piomelli, D., Gall, C.M., and Lynch, G., 2017. Atypical Endocannabinoid Signaling Initiates a New Form of Memory-Related Plasticity at a Cortical Input to Hippocampus. *Cerebral Cortex*, (July), 1–14.
- Weber, J.P., Andrásfalvy, B.K., Polito, M., Magó, Á., Ujfalussy, B.B., and Makara, J.K., 2016. Location-dependent synaptic plasticity rules by dendritic spine cooperativity. *Nature Communications*, 7, 11380.
- Wierenga, C.J., Becker, N., and Bonhoeffer, T., 2008. GABAergic synapses are formed without the involvement of dendritic protrusions. *Nature neuroscience*, 11 (9), 1044–52.
- Wierenga, C.J., Müllner, F.E., Rinke, I., Keck, T., Stein, V., and Bonhoeffer, T., 2010. Molecular and electrophysiological characterization of GFP-expressing CA1 interneurons in GAD65-GFP mice. *PloS one*, 5 (12), e15915.
- Wilson, D.E., Whitney, D.E., Scholl, B., and Fitzpatrick, D., 2016. Orientation selectivity and the functional clustering of synaptic inputs in primary visual cortex. *Nature Neuroscience*, 19 (8), 1003–1009.
- Younts, T.J., Chevaleyre, V., and Castillo, P.E., 2013. CA1 Pyramidal Cell Theta-Burst Firing Triggers Endocannabinoid-Mediated Long-Term Depression at Both Somatic and Dendritic Inhibitory Synapses. *Journal of Neuroscience*, 33 (34), 13743–13757.







# Intuitive and semi-automated analysis tool for axonal bouton dynamics

---

Hai Yin Hu, Corette J. Wierenga

Department of Biology, Faculty of Science, Utrecht University, Utrecht, the Netherlands

*In preparation*



## Summary

Synapses are essential to neuronal processes and their form is diverse and dynamic. Here we present a toolbox we developed in Matlab to study the dynamic nature of presynaptic ‘en passant’ boutons in fluorescently labeled axons. To do so, the procedure is divided over two separate modules for axon tracing, and subsequent bouton detection. Both modules are executed semi-automatically and lowering the workload, while still offering a large degree of freedom to fine-tune. The graphical interface enables the researcher to visually inspect every step and offers a comprehensive overview.

## Introduction

Neurons communicate via specialized structures called synapses. The number and strength of synapses varies over time as synaptic connections are continuously being formed, lost, potentiated, or depressed in response to experience. These synapse dynamics are considered an essential aspect of adaptation and learning processes in the brain (Caroni *et al.* 2012). Research on synapse dynamics has mostly concentrated on postsynaptic changes (e.g. changes in dendritic spines), but an increasing number of studies have reported specific presynaptic structural changes during learning and structural changes in axons and their presynaptic terminals (boutons) are also important in brain diseases (Monday and Castillo 2017). Despite increased interest in studying axonal bouton plasticity, not many tools are available for analysis of structural presynaptic plasticity. Studies of presynaptic dynamics rely on fluorescence microscopy where images of live fluorophore-labelled axons are acquired over time. Most axons have a relatively simple structure, with a thin ( $\sim 0.1-0.5 \mu\text{m}$ ) axonal shaft and presynaptic terminals can be distinguished relatively easy as varicosities of varying sizes (*‘en passant’* boutons) along the axon (Fig. 1A). Time-lapse imaging of axons *in vivo* and *in vitro* has revealed that boutons are dynamic structures, which can change in shape, size and intensity and boutons appear, disappear and reappear over time (Fig. 1B) (Stettler *et al.* 2006, Schuemann *et al.* 2013). Manual image analysis of large number of axons and presynaptic boutons is usually unpractical, time consuming, and difficult to reproduce between researchers. However, fully automated analysis is prone to error as axons can display varying fluorescence intensities and neighboring axons may overlap. For three dimensional samples, the limited depth resolution further increases the risk of introducing errors by automated analysis.

We have developed an open-source analysis software tool written in Matlab for the semi-automatic analysis of axonal boutons. Packaged in an intuitive graphical user interface, our software tool assists researchers in axon tracing and bouton detection through semi-automated algorithms.

A prominent feature of the software is the comprehensive overview it generates per axon, which displays each traced time point together in a single view. A full overview of all time points allows the researcher to directly verify the outcome of the algorithm and to correct the tracing when necessary. We believe our analysis tool is a valuable addition to existing software, which currently only allows comparison between two time points or afterwards

---

(Song *et al.* 2016, Gala *et al.* 2017). Furthermore, our tool gives the researcher the freedom to overrule the algorithm in an intuitive manner, offering great flexibility. The relatively simple structure of axons allows the same set of bouton analysis tools analysis for a wide range of cell types and for *in vitro* as well as *in vivo* data sets.

---

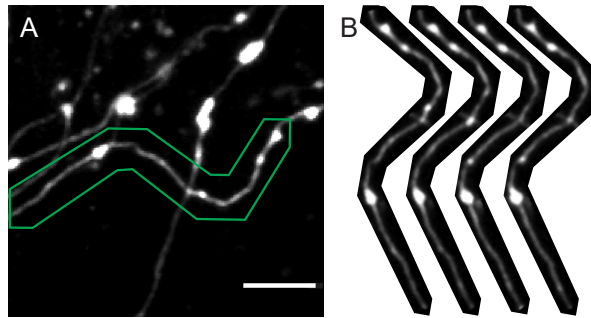


**Figure 1. Dynamics of axon and their presynaptic boutons**

(A) Mean projection of an example two-photon microscopy image stack of GFP-labeled fluorescent axons. The axons are recognizable by their elongated thin structure, the swellings along the axons are the presynaptic boutons. Note that density and size of these boutons can vary substantially.

(B) Zoom in of the axon stretch in A captured at several time points over one hour. Boutons can appear, disappear, and vary in size over time. Scale bar is 5  $\mu\text{m}$ .

---

## Description of the software

Our software tool divides bouton analysis in four sequential steps: axon tracing, bouton detection, bouton categorization, and bouton volume quantification.

### Axon tracing

We present a semi-automated approach in which the axon backbone is initially traced manually by sparsely placing nodes along the axon in the *tiffreader* software tool. The sparse axon backbone is then completed automatically in two steps. First, the gaps between the nodes are connected with a custom pathfinding algorithm that searches for the local maximum fluorescence intensity in 3D. The resulting backbone is then expanded along the orthogonal axis to envelop the entire axon (width can be adjusted by the user). In the second step, the node locations are optimized by finding the maximum intensity along the orthogonal axis. The average intensity projection of the straightened traced axon is displayed for additional visual guidance. The linear transformation of the traced axon facilitates the comparison of the axon between multiple time points. Small misalignments between the nodes can easily be corrected manually (Fig. 2A).

Node coordinates are determined separately for XY and XZ planes, allowing the researcher to correct both planes individually. During the optimization of the trace, the software will

place additional nodes near locations where the axon bends. These locations are determined by the change in the direction of the slope of the axon backbone. Automatic placement of nodes can be prone to errors when there are bright fluorescent spots close to the axon, which can cause misalignment. To minimize abrupt ‘jumps’, the axon backbone is smoothed using a robust local regression which excludes obvious outliers. The researcher can improve the precision of the automated tracing by placing additional nodes near crowded fluorescent crossings during the first step of manual tracing. However, automatic placement can still fall short, for instance at unusually crowded samples. Our software tool provides the option to adjust the position of any node manually after the automated optimization procedure.

Bouton dynamics are determined by monitoring the same axon over multiple time points. When tracing subsequent time points, the software uses the backbone of the earlier traced axon as a template. This template is then corrected for translational drift. The horizontal and vertical drift between the image stacks is determined by first making a Z-projection of each time point and taking its Fourier transform. Then, the translational difference between all subsequent time points is determined (Szeliski 2006). To determine Z drift between different stacks, first a Z-profile is composed by summing over X and Y. This profile is then compared over time with cross correlation to estimate the Z drift. If the sample drift is too large, the drift correction may fail. In such cases, the researcher can either adjust the drift, or trace the axons manually per time point.

The results of the axon tracing procedure are displayed in a linearized two-dimensional preview, which is updated in real-time whenever a node of the backbone is manually adjusted. Traced axons at all time points are displayed together in the same figure for a complete overview. This allows for direct comparison over time, giving the researcher visual feedback and facilitating the alignment process (Fig. 2B). The XYZ coordinates of the traced axons are saved in an output file, allowing the researcher to export the results and use them for other purposes.

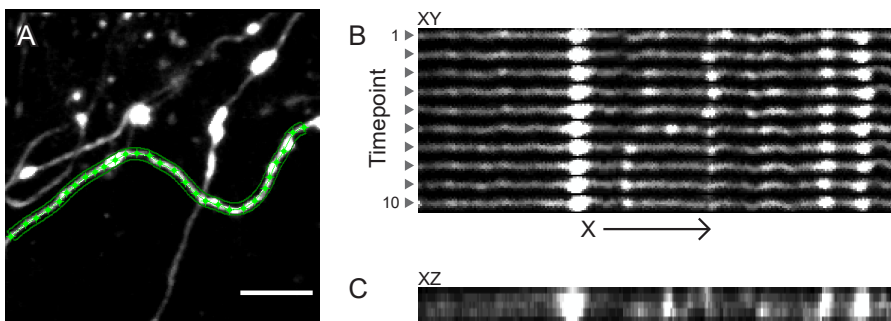


**Figure 2. Axon tracing in fluorescence microscopy imaging data using *tiffreader***

(A) Axon traced and optimized with *tiffreader*. Red diamond symbols indicate the node locations along the axonal backbone (dotted line). The width of the traced axon is indicated by the parallel red lines.

(B) Linearized view of the traced axon in A. Linearization facilitates visual inspection and allows manual corrections.

(C) The linearized axon from images at multiple time points. Each row represents a single time point.

---

## Bouton detection

In a separate software tool *boutonfinder*, the traced axons at different time points are loaded and displayed together for visual assessment of bouton dynamics (Fig. 1D). Along the traced axons, putative boutons can be identified as local increases in width and fluorescence intensity. Bouton locations are determined by a semi-automatic bouton detection algorithm, by applying an intensity threshold on the traced axon. The bouton threshold is determined for each axon separately as the fluorescence intensity can vary significantly between axons, due to differences in (expression level of) the fluorescent label, imaging depth, and laser power.

The *boutonfinder* software first identifies the parts of the axon without boutons ('shaft'), based on the center voxels of the traced axon (the center along XY and the maximum intensity along Z). These intensity values are sorted, and a shaft threshold is determined from the histogram (Fig. 2A). Parts of the axon with center voxel intensity values below this shaft threshold are considered 'shaft' compartments without boutons (blue shading in figure 2B). These 'shaft' compartments of the traced axon will be used later to determine intensity fluctuations between timepoints.

A shaft threshold was set to be able to classify the boutons from the shaft. To determine this threshold, the sum of the traced intensity was taken over Z (5-stacks) and the average over Y. This reduces the axon trace to the one dimension, X. These intensities are then sorted, the average over the lower half is taken as the threshold (earlier iteration of the analysis software uses a different approach), which can be used to account for possible intensity fluctuations between time points and differences between experiments.

The bouton threshold is defined as twice average intensity value of the shaft threshold intensity. After thresholding the image, a one-dimensional intensity curve is constructed from the traced axon by taking the maximum over the Z axis and the sum across the orthogonal axis (Fig. 3A). The locations of individual boutons are determined by applying a peak finding algorithm on this curve (Fig. 3B). The estimated shaft threshold can be poor if the intensity distribution is non-continuous, which could occur when the traced axon is short. For this reason, the multiplicative factor between the shaft and bouton thresholds can be set manually.

## Bouton categorization

After all boutons are detected for every time point, reoccurring boutons are categorized based on their location on the axon. We first map the locations where boutons have occurred during the entire imaging period and determine their distribution (Fig. 3C). Peaks in this distribution are detected and correspond to axon locations at which a bouton was present at multiple time points (the more often a bouton occurred at a certain location, the higher the peak). These bouton peak locations are used align the individually detected boutons by matching them to the closest peak location (Fig. 3D).

The assignment procedure respects the following conditions: A bouton cannot be assigned

to multiple bouton peak locations and a bouton peak location cannot have more than one bouton assigned per time point. For boutons which cannot be assigned to any bouton peak location, are assigned their own category. The success of the location assignment depends on the alignment during *tiffreader* and misalignments can hamper bouton categorization. The researcher visually inspects the estimate by *boutonfinder* and can overrule and manually correct the bouton categorization if needed.

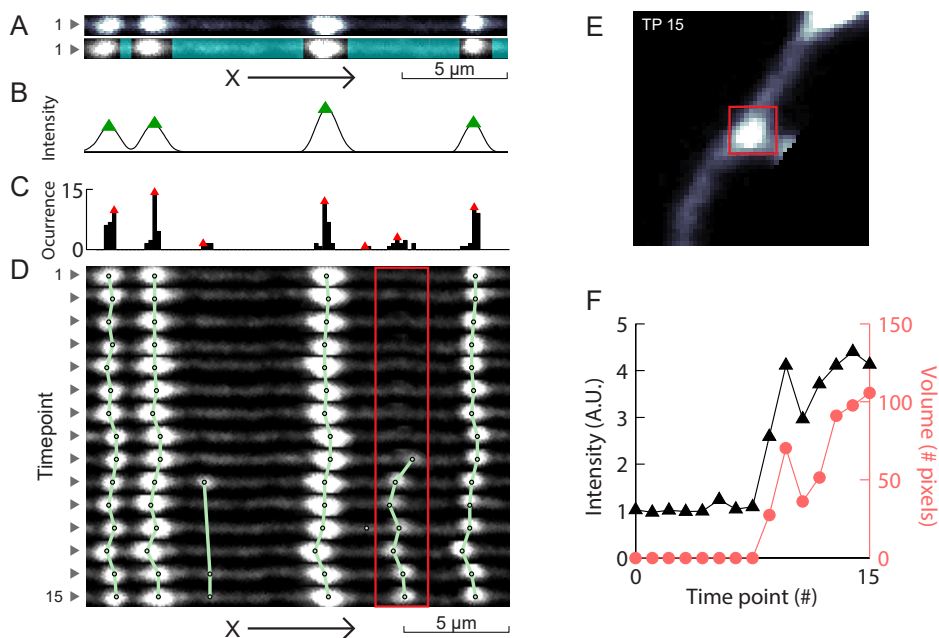


**Figure 3. Determining bouton threshold and detection of boutons using *boutonfinder***

(A) Distribution of the fluorescent intensity from the voxels at the axon backbone. The shaft threshold is determined as the average over the lower half of voxel intensity. Identification of 'shaft' compartments (blue shading), based on the shaft threshold.

(B) Intensity profile of voxels along the axon backbone, after subtracting the bouton threshold from the image. Boutons are detected using a peak algorithm (green triangles).

(C) Distribution of detected bouton locations for all time points. Red triangles indicate identified bouton locations.

(D) Categorical assignment of recurring boutons. Connected boutons (green lines) are categorized as the same bouton recurring over multiple time points.

(E) Example bouton (red box in D; time point 15) in original untransformed image with quantification box (red,  $1 \times 1 \mu\text{m}$ ).

(F) Quantification of bouton size (example from red box in D) as fluorescence intensity (black) as well as number of voxels (red) for all time points

---

## Quantification of bouton size

The linearized axon view (Fig. 3D) grants a comprehensive overview of the axon and its boutons over all time points. However, the linearization distorts any quantification as voxels near curvatures are missed or oversampled. We therefore quantify the size of the boutons in the untransformed dataset, in a 3-dimensional quantification window around the center of the bouton (Fig. 3E). This window is linked to the coordinates in the linearized axon view, which allows inspecting the boutons in the overview in parallel. In time points in which the bouton is absent, the XYZ coordinates of the bouton are interpolated from the surrounding time points when possible and otherwise extrapolated.

An increase in fluorescence intensity can be interpreted as volume growth, which makes bouton intensity a practical estimate for volume. However, the absolute bouton intensity can strongly vary depending on external factors such as the amount of fluorescent label (e.g. GFP in our case), sample depth, and laser power. These factors can vary for boutons on different axons, even within the same experiment, and this makes absolute intensity often not a good measure for bouton volume. Our software reports two measures of bouton size which allow comparison between different axons and experiments (Fig. 3F). The absolute change in bouton volume ( $\Delta\#V$ ) was quantified as the number of voxels above bouton threshold minus the average volume of the baseline period. The relative change in bouton intensity ( $\Delta\%I$ ) was defined as the integrated intensity of all voxels inside the same  $1 \times 1 \times 2.5 \mu\text{m}$  box ( $9 \times 9 \times 5$  pixels in example), divided by the average intensity of the baseline period. As this latter is a relative measure,  $\Delta\%I$  can give very high values for boutons that are growing from dim axons.

## Correction for intensity fluctuations

When imaging the same area repeatedly, variations in fluorescence intensity can occur between recording sessions which do not reflect physiological changes e.g. due to bleaching, sample drift or laser power fluctuations. These fluorescence fluctuations can impair the comparison of bouton intensity over time. *In vivo* data sets will be even more susceptible to these intensity variations compared to *in vitro* data. To account for intensity fluctuations over time, *boutonfinder* offers the option to normalize individual time points. We take the intensity of the axonal shaft (without boutons) as reference for the normalization. The rationale behind this approach is that fluorescent fluctuations due to experimental conditions are expected to be similar in boutons and the axonal shaft, while the intensity of the axonal shaft should be independent of changes in bouton intensity reflecting bouton dynamics.

First, background intensity (determined as the mode of the image stack in *tiffreader*) is subtracted from the traced axon intensity values for each time point. Next, we use the shaft threshold intensity for each individual time point for normalization. The researcher can inspect how normalization affects the bouton intensity and decide to apply or remove this normalization.

Our correction method for intensity fluctuations is different from previous software tools.

EPBscore uses the median of the axon backbone as a reference for normalizing each time point (Song *et al.* 2016). By including the boutons, however, the median is subject to change when the density of boutons changes. As a result, the normalization in EPBscore will be dependent on the bouton dynamics, the subject of study. In an alternative approach (Gala *et al.* 2017), axon intensity was determined by fitting the smoothed traced axon with a Gaussian along the length of the backbone. This has the advantage that normalization values can vary along the axon, which becomes important when the axon displays strong fluctuations in fluorescence intensity, for instance when the axon traverses a large number of Z planes. However, the axon intensity may not always be properly described by the Gaussian fit. In our hands, we find that estimating each individual time point with a gaussian fit is not always achievable and can actually introduce noise when the fit is poor, especially for shorter stretches of axon.

### **Generality**

The results of the analysis are listed in Matlab files, which contain the coordinates of the axonal backbone and detected boutons at each time point. These coordinates are given with respect to the original image, to facilitate connecting this software to independent analysis tools or programs within or without Matlab.

### **Conclusion**

We present a semi-automatic analysis tool for tracing axons and detecting ‘en passant’ boutons. Our analysis tool is designed with the researcher in mind. It provides the ease and speed of automated detection, but leaves the researcher in full control, via a comprehensive visual inspection of the data at each stage of the analysis and the possibility to correct the detection algorithm if necessary. Although fully automated detection has the advantage of being 100% objective, it does not have the guarantee to be 100% right. In many cases, the researcher needs to use his/her biological insight to judge exceptions and border cases, or to identify unexpected phenomena. Furthermore, fully automated detection can be difficult to implement reliably, e.g. due to large range in fluorescence intensities and bouton sizes. Our software tool offers the researcher a large degree of freedom, while maintaining the advantages of fully automated bouton analysis such as reproducibility. Using the visual overview and intuitive controls, a trained eye can quickly judge the semi-automated axon tracing and bouton detection and adjust when deemed necessary. This allows direct comparison between image analysis between researchers or research groups in a controlled and reproducible manner. The software is versatile and can be adapted to specific data or analysis requirements.

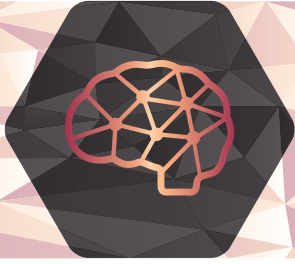


---

## References

- Caroni, P., Donato, F., and Muller, D., 2012. Structural plasticity upon learning: regulation and functions. *Nature Reviews Neuroscience*, 13 (7), 478–490.
- Gala, R., Lebrecht, D., Sahlender, D.A., Jorstad, A., Knott, G., Holtmaat, A., and Stepanyants, A., 2017. Computer assisted detection of axonal bouton structural plasticity in in vivo time-lapse images. *eLife*, 6, 1–20.
- Monday, H.R. and Castillo, P.E., 2017. Closing the gap: long-term presynaptic plasticity in brain function and disease. *Current Opinion in Neurobiology*, 45, 106–112.
- Schuemann, A., Klawiter, A., Bonhoeffer, T., and Wierenga, C.J., 2013. Structural plasticity of GABAergic axons is regulated by network activity and GABAA receptor activation. *Frontiers in neural circuits*, 7 (June), 113.
- Song, S., Grillo, F.W., Xi, J., Ferretti, V., Gao, G., and De Paola, V., 2016. EPBscore: a Novel Method for Computer-Assisted Analysis of Axonal Structure and Dynamics. *Neuroinformatics*, 14 (1), 121–7.
- Stettler, D.D., Yamahachi, H., Li, W., Denk, W., and Gilbert, C.D., 2006. Axons and synaptic boutons are highly dynamic in adult visual cortex. *Neuron*, 49 (6), 877–887.
- Szeliski, R., 2006. Image Alignment and Stitching: A Tutorial. *Foundations and Trends® in Computer Graphics and Vision*, 2 (1), 1–104.





4

# Semaphorin4D induces inhibitory synapse formation by rapid stabilization of presynaptic boutons via MET co-activation

---

Cátia P. Frias<sup>1</sup>, Tom Bresser<sup>1</sup>, Lisa Scheefhals<sup>1</sup>, Hai Yin Hu<sup>1</sup>,  
Paul M. P. van Bergen en Henegouwen<sup>1</sup>, Casper C. Hoogenraad<sup>1</sup>, Corette J. Wierenga<sup>1</sup>

Department of Biology, Faculty of Science, Utrecht University, Utrecht, the Netherlands

*A revised version of this chapter has been accepted for publication in The Journal of Neuroscience*



## Summary

Changes in inhibitory connections are essential for experience-dependent circuit adaptations. Defects in inhibitory synapses are linked to neurodevelopmental disorders, but the molecular processes underlying inhibitory synapse formation are not well understood. Here we use high resolution two-photon microscopy in organotypic hippocampal slices to examine the signaling pathways induced by the postsynaptic signaling molecule Semaphorin4D (Sema4D) during inhibitory synapse formation. By monitoring changes in individual GFP-labeled presynaptic boutons we found that the primary action of Sema4D is to induce stabilization of presynaptic boutons within tens of minutes. Stabilizing boutons rapidly recruited synaptic vesicles, which was followed by accumulation of postsynaptic gephyrin. Newly formed inhibitory synapses were complete and functional after 24 hours, as determined by electrophysiology and immunohistochemistry. We further showed that Sema4D signaling is regulated by network activity and can induce a local increase in bouton density, suggesting a possible role in circuit adaptation. We further examined the intracellular signaling cascade triggered by Sema4D and found that bouton stabilization occurred through rapid remodeling of actin, and this could be mimicked by the actin-depolymerizing drug Latrunculin B or by reducing ROCK activity. The intracellular signaling cascade required activation of the receptor tyrosine kinase MET, which is a well-known autism risk factor. Our immunohistochemistry data suggests that MET may be localized to presynaptic inhibitory axons. Together, our data yield important insights in the molecular pathway underlying activity-dependent Sema4D-induced synapse formation and reveal a novel role for MET in inhibitory synapses.

## Author contributions

CPF and CJW designed the experiments. CPF performed and analyzed most experiments, with specific experiments performed by TB (5A-D) and LS (6G). HYH performed and analyzed all electrophysiological recordings. PMPvB and CCH provided reagents. CPF and CJW wrote the manuscript with critical input from all other authors. CJW conceived and supervised the research.

## Acknowledgements

We would like to thank G. Szábo for kindly providing the GAD65-GFP mice, R. van Dorland for technical support, M. van Kesteren for analysis of LatB immunodata, S. Paradis for helpful comments and scientific discussions and A. Akhmanova, G.G. Turrigiano and R.J. Pasterkamp for critically reading the manuscript. This work was supported by the People Programme (Marie Curie Actions) of the European Union's Seventh Framework Programme FP7/2007-2013/ under REA grant agreement 289581 (C.P.F.), a Marie Curie Reintegration Grant 256284 (C.J.W.) and the Netherlands Organization for Scientific Research (NWO38 VIDI, C.J.W., NWO-VICI, C.C.H.).

---

## Introduction

GABAergic synapses provide the main inhibitory control over neuronal activity in the brain and are indispensable for shaping network function (Isaacson and Scanziani 2011). In postnatal brain tissue, in which the majority of inhibitory connections have been established, synapse formation and disassembly is still ongoing (Caroni *et al.* 2012). Formation and disassembly of inhibitory synapses in the brain play an important role in experience-dependent circuit adaptation (Hensch 2005, Keck *et al.* 2011, Chen *et al.* 2015, Froemke 2015, Sprekeler 2017) and defects in GABAergic synapses have been observed in many neurodevelopmental disorders (Marín 2012, Cellot and Cherubini 2014, Nelson and Valakh 2015). We and others have previously shown that inhibitory axons are dynamic structures with boutons forming and disappearing with apparently stochastic dynamics (Fu and Huang 2010, Dobie and Craig 2011, Kuriu *et al.* 2012, Frias and Wierenga 2013). These ongoing bouton dynamics allow quick updating of connections in response to changes in the neuronal circuitry (Staras 2007, Frias and Wierenga 2013). New inhibitory synapses form by the emergence of new presynaptic boutons at pre-existing axon-dendrite crossings (Wierenga *et al.* 2008, Schuemann *et al.* 2013). However, the signaling pathways that regulate the multiple steps during inhibitory synapse formation are not well understood (Wierenga 2017).

In the recent years, enormous progress has been made by the identification and characterization of proteins that are involved in the formation of inhibitory synapses (Siddiqui and Craig 2011, Krueger-Burg *et al.* 2017, Lu *et al.* 2017). The class 4 semaphorin Sema4D, originally identified as an axon guidance factor (Kolodkin *et al.* 1993, Pasterkamp 2012), has been shown to play a crucial role in this process. Formation of GABAergic synapses was shown to depend on Sema4D signaling, as knockdown of postsynaptic Sema4D led to a 30% reduction of GABAergic synapses in primary cultures (Paradis *et al.* 2007). In addition, acute activation of Sema4D pathway by adding a soluble form of the extracellular part of Sema4D to primary hippocampal cultures induces rapid increase of GABAergic synapses (Kuzirian *et al.* 2013, Raissi *et al.* 2013). The observation that somatic and dendritic synapses responded equally to Sema4D signaling (Kuzirian *et al.* 2013) suggests that Sema4D could be acting on a broad range of (or perhaps all) inhibitory synapses.

Despite its well-characterized physiological importance, relatively little is known about the cellular mechanism by which Sema4D induces inhibitory synapse formation. It was shown that Sema4D acts as a postsynaptic protein and requires its receptor PlexinB1 to induce inhibitory synapses (Kuzirian *et al.* 2013, Raissi *et al.* 2013). The signal cascades that are triggered by Sema4D-PlexinB1 interaction have been well studied in other cells and these studies revealed that Sema4D action is highly cell-specific (Zhou *et al.* 2008, Cagnoni and Tamagnone 2014). For instance, Sema4D has been reported to either suppress or enhance cellular adhesion and/or migration, depending on the cell type (Oinuma *et al.* 2006, Basile *et al.* 2007, Giacobini *et al.* 2008, Swiercz *et al.* 2008). The intracellular molecular events downstream of Sema4D/PlexinB1 signaling that lead to inhibitory synapse induction are currently not known.

In the current study, we used high resolution two-photon microscopy in organotypic hippocampal slices to characterize Sema4D regulation of inhibitory synapse formation in intact tissue and to examine the underlying molecular pathway. We found that Sema4D signaling specifically regulates the rapid stabilization of inhibitory boutons along the axon and that local bouton stabilization by Sema4D can result in local changes in bouton density within tens of minutes. These rapid presynaptic changes are followed by subsequent recruitment of pre- and postsynaptic proteins to complete the formation of functional inhibitory synapses over the course of the next hours. We also found that Sema4D-induced bouton stabilization is activity-dependent. The intracellular pathway for bouton stabilization involves specific remodeling of the actin cytoskeleton, and requires the activation of the receptor tyrosine kinase MET. Our data unravel an important regulatory pathway of activity-dependent inhibitory synapse formation and reveal a novel role for the receptor tyrosine kinase MET in Sema4D-induced formation of inhibitory synapses.

---

## Experimental Procedures

### Animals

All animal experiments were performed in compliance with the guidelines for the welfare of experimental animals issued by the Federal Government of The Netherlands. All animal experiments were approved by the Animal Ethical Review Committee (DEC) of Utrecht University.

### Hippocampal slice cultures

Hippocampal slice cultures (400  $\mu\text{m}$  thick) were prepared from postnatal day 5-7 of both male and female GAD65-GFP mice (López-Bendito *et al.* 2004) as previously described (Müllner *et al.* 2015). In short, the hippocampi were dissected in ice-cold HEPES-GBSS (containing 1.5 mM  $\text{CaCl}_2 \cdot 2\text{H}_2\text{O}$ , 0.2 mM  $\text{KH}_2\text{PO}_4$ , 0.3 mM  $\text{MgSO}_4 \cdot 7\text{H}_2\text{O}$ , 5 mM KCl, 1 mM  $\text{MgCl}_2 \cdot 6\text{H}_2\text{O}$ , 137 mM NaCl, 0.85 mM  $\text{Na}_2\text{HPO}_4$  and 12.5 mM HEPES) supplemented with 1 mM kynurenic acid and 25 mM glucose, and plated in a MEM-based medium (MEM supplemented with 25 % HBSS, 25 % horse serum, 30 mM glucose and 12.5 mM HEPES). In GAD65-GFP mice, approximately 20% of the CA1 interneurons express GFP from early embryonic developmental stage into adulthood (López-Bendito *et al.* 2004, Wierenga *et al.* 2010). The majority of GFP-labeled interneurons expresses reelin and VIP, while parvalbumin and somatostatin expression is nearly absent (Wierenga *et al.* 2010). For our study, the relatively low number of GFP-positive axons is crucial for proper analysis of individual boutons.

The slices were kept in culture for at least one week before the experiments (range 7-21 days *in vitro*) at 35 °C in 5 %  $\text{CO}_2$ . For live imaging experiments, slices were transferred to an imaging chamber, where they were continuously perfused with carbogenated artificial cerebrospinal fluid (ACSF; containing 126 mM NaCl, 3 mM KCl, 2.5 mM  $\text{CaCl}_2$ , 1.3 mM  $\text{MgCl}_2$ , 1.25 mM  $\text{NaH}_2\text{PO}_4$ , 26 mM  $\text{NaHCO}_3$ , 20 mM glucose and 1mM Trolox). The temperature of the chamber was maintained at 37°C. Treatment and control experiments were conducted in slices from sister cultures.

### Pharmacological treatments

The following drugs were used: 0.1/0.2 % DMSO, 1 nM Fc and Sema4D-Fc (amino acids 24-711) (both R&D Systems), 100 nM Latrunculin B (Santa Cruz Biotechnology), 200 nM Jasplakinolide (Tocris Bioscience), 1  $\mu\text{M}$  PHA-665752 (Sigma-Aldrich) and 10  $\mu\text{M}$  Y-27632 (Sigma-Aldrich). We used the small molecule PHA-665752 (PHA), a highly specific MET inhibitor (Christensen *et al.* 2003, Deguchi *et al.* 2016), to decrease endogenous phosphorylation of MET, without affecting MET expression or neuronal cell viability. We used 10 nM Fc or Sema4D for the local puffing experiments.

For treatments that were followed by immunostaining of inhibitory synapses, 1 nM Fc or Sema4D-Fc was added to the culturing medium and slices were left in the incubator for 2, 6 or 24 h before fixation.

## Two-photon imaging

For acute treatments, drugs were added to the perfusion ACSF after a baseline period of 40 minutes (5 time points) and we continued imaging for an additional 10 time points in the wash-in period (total imaging period is 140 minutes). In longer treatments, we treated the slices for 6 hours after the baseline period (5 imaging time points) at the microscope and restarted imaging for 5 time points, for a total treatment period of 6 hours and 40 minutes (400 minutes). For activity blockade, 0.5  $\mu\text{M}$  tetrodotoxin citrate (TTX; Tocris Bioscience) was added to the perfusion ACSF prior to the transfer of the slice to the imaging chamber. Time-lapse two-photon microscopy images were acquired on a Femtonics 2D two-photon laser-scanning microscope (Budapest, Hungary), with a Nikon CFI Apochromat 60X NIR water-immersion objective. GFP was excited using a laser beam tuned to 910 nm (Mai Tai HP, Spectra Physics). The 3D images (93.5  $\mu\text{m}$  x 93.5  $\mu\text{m}$  in xy, 1124 x 1124 pixels) consisted of 29-33 z stacks (0.5  $\mu\text{m}$  step size in z). Small misalignments due to drift were manually compensated during the acquisition.

For the local treatment, we used HEPES-ACSF (containing 126 mM NaCl, 3 mM KCl, 2.5 mM  $\text{CaCl}_2$ , 1.3 mM  $\text{MgCl}_2$ , 1.25 mM  $\text{NaH}_2\text{PO}_4$ , 20 mM glucose, and 10 mM HEPES; pH 7.41) with 20  $\mu\text{M}$  Alexa 568 (Invitrogen), in order to visualize the spread of the local puff. Sema4D or Fc was added to the HEPES-ACSF to a final concentration of 10 nM. The solution was loaded into a patch pipette (4-6 M $\Omega$ ), and was locally applied to a GFP labeled axon using a Picospritzer II (General Valve). Time-lapse two photon microscopy imaging was performed as described previously, except that a second laser (Spectra Physics) was used at 840 nm to visualize the area of the puff. The 3D images (51.3  $\mu\text{m}$  x 51.3  $\mu\text{m}$  in xy, 620 x 620 pixels) consisted of 18-22 z stacks (0.5  $\mu\text{m}$  step size in z). After a baseline period of 20 minutes (5 TPs), the pipette was put into position before the stimulation. The stimulation consisted of 300 puffs of 20-50 ms at 2 Hz. The pipette was carefully retracted before continuing the time series for 10 additional time points (total imaging period of 70 minutes).

## Two-photon image analysis

The analysis of inhibitory bouton dynamics was performed semi-automatically using ImageJ (US National Institute of Health) and Matlab-based software (Mathworks). The 3D coordinates of individual axons were selected at every time point by using the CellCounter plugin (Kurt De Vos, University of Sheffield, Academic Neurology). For each image, 1-5 stretches of axons (average length 78  $\mu\text{m}$  with standard deviation 18  $\mu\text{m}$ , with average of 31 boutons per axon with standard deviation 11; for local treatment experiments, average length 39  $\mu\text{m}$  with standard deviation 8  $\mu\text{m}$ , with average of 14 boutons per axon with standard deviation of 4) were selected for analysis.

A 3D intensity profile along the selected axons was constructed at each time point, and individual boutons were identified in a two-step process using custom-made Matlab software (Schuemann *et al.* 2013). In brief, an axon threshold was calculated to differentiate the axon from the background (2 standard deviations above mean intensity); subsequently, a local threshold (0.5 standard deviation above mean axon intensity) identified the boutons along the selected axon. Only boutons with at least 5 pixels above bouton threshold were included. Each image stack was visually examined, and false positives and negatives were



---

corrected manually. Only raw data was analyzed; images were median-filtered for illustration purposes only.

Boutons were classified as persistent when they were present during all time points, and non-persistent when they were absent during one or more time points during the imaging session. The average fraction of persistent and non-persistent boutons was calculated by normalization to the average number of boutons per axon. To bias our analysis towards synaptic events (Schuemann *et al.* 2013), we restricted our analysis to boutons that appeared for at least 2 time points at the same location during the imaging period. We verified that our main conclusions did not change when this restriction was released. Based on their presence during baseline and treatment periods, we defined five subgroups of non-persistent boutons: new boutons (not present during baseline), lost boutons (not present during wash-in), stabilizing boutons (non-persistent during baseline, persistent during wash-in), destabilizing boutons (persistent during baseline, non-persistent during wash-in), and transient boutons (non-persistent in baseline and wash-in) (Fig. 1). Average fraction of each subgroup of boutons was normalized to the total average number of non-persistent (NP) boutons per axon. The duration of each bouton was defined as the number of time points present divided by the total number of time points per period. Bouton density was calculated as the average number of boutons at all time points divided by the 3D axon length.

## **Electrophysiology**

During the experiment, the slice was placed in a recording chamber perfused with oxygenated artificial cerebral spinal fluid (ACSF) at a rate of 1 ml/min. The recording ACSF consisted of 126 mM NaCl, 3 mM KCl, 2.5 mM CaCl<sub>2</sub>, 1.3 mM MgCl<sub>2</sub>, 1.25 mM Na<sub>2</sub>H<sub>2</sub>PO<sub>4</sub>, 26 mM NaHCO<sub>3</sub>, and 20 mM glucose. Whole cell voltage clamp recordings were performed at 35 °C in CA1 cells of GAD65-GFP slice cultures at DIV 13-19. Recordings were made on a Multiclamp 700B amplifier (Molecular Devices) and stored using pClamp 10 software. To isolate sIPSCs, 20 μM DNQX and 50 μM APV were added to the recording ACSF. For mIPSCs, 0.5 μM TTX was added as well. Thick walled borosilicate pipettes of 3-6 MΩ were filled with an internal solution containing 70 mM K-gluconate, 70 mM KCl, 0.5 mM EGTA, 10 mM HEPES, 4 mM MgATP, 0.4 mM NaGTP, and 4 mM Na<sub>2</sub>Phosphocreatine. Cells were excluded from analysis if the series resistance increased more than 35 %. IPSCs were automatically detected in Clampfit and further analyzed in custom Matlab scripts. Detected events within 3 ms of each other were merged and events smaller than 3 times the RMS of the signal were excluded. The cumulative distributions for individual experiments were interpolated to generate the average distribution.

## **Immunohistochemistry, confocal imaging and image analysis**

For post hoc immunohistochemistry, organotypic hippocampal slices were fixed in 4 % (w/v) paraformaldehyde for 30 minutes at room temperature. Slices were rinsed in phosphate buffer and permeabilized with 0.5 % TritonX-100 in phosphate buffer for 15 minutes. Slices were blocked with 0.2 % TritonX-100, 10 % goat serum (ab7481, Abcam) in phosphate buffer for 60 minutes. Primary antibodies were applied overnight at 4°C in blocking solution. After washing, slices were incubated with secondary antibodies in blocking solution for 4h at

room temperature. Slices were washed and mounted on slides in Vectashield mounting medium (Vector Labs).

The following primary and secondary antibodies were used: rabbit  $\alpha$ -VGAT (1:1000; Synaptic Systems, 131 003), mouse  $\alpha$ -gephyrin (1:1000; Synaptic Systems, 147 011), guinea pig  $\alpha$ -VGLUT (1:400; Millipore, AB5905), rabbit  $\alpha$ -Homer (1:1000; Synaptic Systems, 160002), mouse  $\alpha$ -myc (1:100; Oncogene Research Products, OP10), mouse  $\alpha$ -MET (1:500; Santa Cruz Biotechnology, sc-8057), Alexa405-, Alexa-488 and Alexa-568 conjugated secondary antibodies (Invitrogen). For staining MET we used a previously described myc-tagged nanobody, which was shown to recognize MET with low nanomolar affinity (Heukers *et al.* 2014). We visualized the nanobody with an antibody against the C-terminal myc tag. We validated the nanobody staining in primary hippocampal cultures using a previously described immunostaining protocol (Esteves da Silva *et al.* 2015).

For immunostainings, high resolution confocal laser scanning microscopy was performed on a Zeiss LSM-700 system with a Plan-Apochromat 63x 1.4 NA oil immersion objective. Each image was a z-series of 11-35 images (0.3  $\mu$ m z step size), each averaged 4 times. The imaging area in the CA1 region was 78 x 78  $\mu$ m (1024 x 1024 pixels). The confocal settings were kept the same to compare fluorescence intensities between slices.

For the quantification of VGAT and gephyrin intensities per image, we determined per image the mean intensity of 3 randomly chosen areas of 10 x 10  $\mu$ m of the average projection image from the 5 middle z-layers. For the cumulative plots individual values (per area) were used. Synaptic puncta size and number were determined using the PunctaAnalyzer plugin, and inhibitory synapses were defined as overlapping VGAT and gephyrin puncta. For determining co-localization of GFP-labeled boutons with synaptic marker VGAT or with MET, we manually inspected individual boutons through all z-sections. A bouton was only considered positive when at least one z stack of the bouton overlapped with VGAT or MET staining. The images were median-filtered only for illustration purposes.

## Statistical Analysis

Data are represented as mean values  $\pm$  standard error of the mean, unless stated otherwise. Statistical analysis was performed using GraphPad Prism software. Results from treatment and control experiments were compared using the Mann-Whitney U test (MW). The ChiSquare test ( $\chi^2$ ) was used for comparing the fraction of axons with/without stabilizing boutons. For comparing multiple groups, we used the Kruskal-Wallis test (KW) followed by a posthoc Dunn's comparison test. We used a One-Way ANOVA followed by a Dunnett's multiple comparison test (One-Way ANOVA) to compare the effect of wash-in of PHA over time. We used a Two-Way ANOVA followed by a Sidak's multiple comparisons test (TwoWay ANOVA) to compare treatment effects at multiple time points. For the comparison of cumulative distributions, we used the Kolmogorov-Smirnov (KS) test. We have indicated the tests and p-values in the figure legends. Differences between control and treatment were considered significant when  $p < 0.05$  (\*,  $p < 0.05$ ; \*\*,  $p < 0.01$ ; \*\*\*,  $p < 0.001$ ). In all figure legends and text, N indicates the number of independent experiments, and n indicates the number of axons/images analyzed.

---

## Results

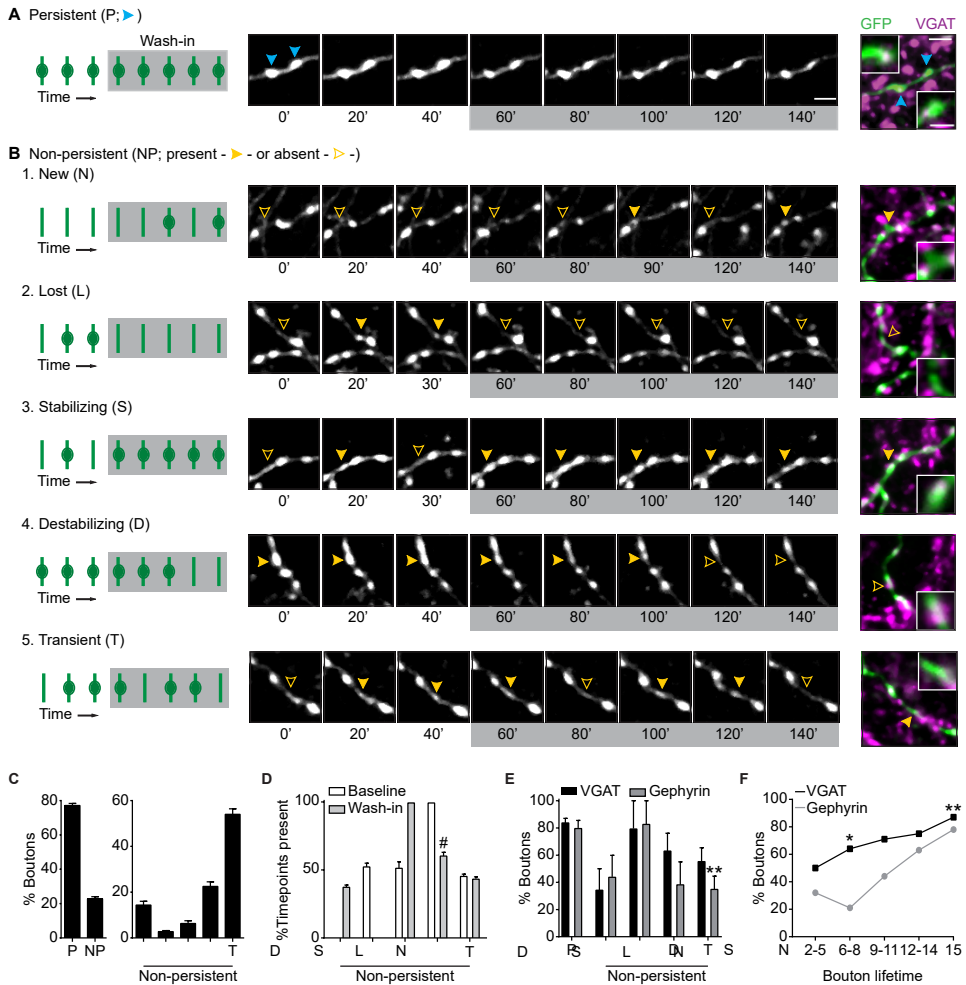
We performed time-lapse two-photon microscopy in organotypic hippocampal cultures from GAD65-GFP mice to monitor the dynamics of inhibitory boutons in the CA1 region of the hippocampus (Wierenga *et al.* 2008, Schuemann *et al.* 2013). In GAD65-GFP mice, approximately 20% of the CA1 interneurons express GFP. The majority of GFP-labeled interneurons express reelin and VIP, while parvalbumin and somatostatin expression is nearly absent (López-Bendito *et al.* 2004, Wierenga *et al.* 2010). High-resolution image stacks of GFP-labeled inhibitory axons were acquired every 10 minutes, for a total period of 150 minutes (15 time points). Inhibitory boutons were remarkably dynamic and many boutons appear, disappeared and reappeared during the course of the imaging period. To bias our analysis towards synaptic events, we only included boutons that appeared for at least 2 time points at the same location during the imaging period. We distinguished two main classes of boutons: persistent boutons, which were present during all time points, and non-persistent boutons, which were absent during one or more time points during the imaging session (Fig. 1A,B). Approximately 77 % (with standard deviation of 12 %) of inhibitory boutons at any given time point were persistent (Fig. 1C), and they reflect inhibitory synapses (Wierenga *et al.* 2008, Müllner *et al.* 2015). Non-persistent boutons reflect locations where inhibitory synapses are 'in transition', e.g. where synapses are being formed or disassembled (Wierenga *et al.* 2008, Dobie and Craig 2011, Fu *et al.* 2012, Schuemann *et al.* 2013). Based on the presence or absence of non-persistent boutons during a baseline and wash-in period (details are given in the methods section), we distinguished 5 subgroups of non-persistent boutons: new (N; absent during baseline), lost (L; absent during wash-in), stabilizing (S; non-persistent during baseline, persistent during wash-in), destabilizing (D; persistent during baseline, non-persistent during wash-in) and transient (non-persistent in both periods). These different subgroups of non-persistent boutons not only differed in their incidence and duration (Fig. 1C,D), but also in their molecular composition, as assessed by immunostaining for the presynaptic vesicular GABA transporter (VGAT) and the postsynaptic scaffold gephyrin (Fig. 1E). Stabilizing boutons, which were present for at least 90 minutes before fixation, showed similar association with VGAT and gephyrin as persistent boutons, indicating that they are nascent inhibitory synapses that have started to recruit pre- and postsynaptic proteins within this period. Newly formed boutons, which were present for a short period before fixation, showed a lower percentage of VGAT and gephyrin association. Boutons with longer total lifetime before fixation showed higher association with VGAT and gephyrin, suggesting a gradual recruitment of proteins over the imaging period (Fig. 1F). Recruitment of gephyrin appeared delayed compared to VGAT, as previously reported (Wierenga *et al.* 2008, Dobie and Craig 2011). These data demonstrate that inhibitory presynaptic boutons are dynamic structures that are continuously being formed and disassembled along the axons, and suggest that non-persistent boutons reflect boutons at different stages of inhibitory synapse assembly and disassembly.

## Inhibitory bouton stabilization during treatment with Sema4D

It was recently shown that class 4 semaphorin Sema4D can rapidly induce an increase of functional inhibitory synapses in hippocampal dissociated cultures (Kuzirian *et al.* 2013). However, these data could not resolve if Sema4D directly promotes synapse formation or rather prevents ongoing synapse elimination, thereby indirectly increasing synaptic density. To examine the effect of Sema4D on ongoing inhibitory bouton dynamics, we bath applied the extracellular domain of mouse Sema4D conjugated to the Fc region of mouse IgG2A (Sema4D; 1 nM) and compared inhibitory bouton dynamics during a baseline period of 5 time points and during Sema4D treatment in the subsequent 10 time points (Fig. 2A). We used Fc alone (1 nM) as a control treatment (Kuzirian *et al.* 2013). Bath application of Sema4D did not affect overall axonal morphology (Fig. 2A) and did not change the density of inhibitory boutons (Fig. 2B). However, when we analyzed the different subgroups of non-persistent boutons, we found that Sema4D treatment specifically enhanced the fraction of stabilizing boutons from  $6 \pm 2\%$  to  $16 \pm 3\%$  (Fig. 2C). Indeed, this effect was also clear when we analyzed the absolute density of boutons. The density of stabilizing boutons was increased by >2-fold, while other subgroups of boutons were unaffected (Fig. 2D-H). To examine how Sema4D-induced stabilization developed over time, we quantified the number of boutons that were present for 5 consecutive time points during the baseline and the wash-in period. We found that Sema4D induced a marked increase in these boutons over the course of the wash-in period (% stabilization, Fig. 2I), and strongly enhanced the number of boutons that had stabilized at the end of this period (last 5 time points; Fig. 2J). Stabilizing boutons are relatively rare in our slices, as under control conditions only 40% of the axons display one or more stabilizing boutons. Treatment with Sema4D significantly increased this fraction to 77% (Fig. 2K). Altogether, these data show that Sema4D treatment in intact tissue specifically promotes the stabilization of inhibitory boutons within tens of minutes, without affecting synapse elimination.

### Figure 1. Classification of presynaptic inhibitory boutons by their dynamics.

(A) Time-lapse two-photon images of two inhibitory boutons (blue arrowheads) along a GAD65-GFP-labeled axon in the CA1 region of the hippocampus. These boutons were present at all time points, and therefore categorized as persistent boutons. Only every second image is shown for clarity. On the right, the same region is shown after fixation and staining against vesicular GABA transporter (VGAT, magenta). The zoom shows a single optical plane through the bouton to demonstrate overlap (white) of VGAT and GFP boutons. Time in minutes. Scale bars 2  $\mu\text{m}$  and 1  $\mu\text{m}$  (zoom). (B1-5) Same as in A, showing examples of new (B1; absent during baseline), lost (B2; absent during wash-in), stabilizing (B3; non-persistent during baseline, and persistent during wash-in), destabilizing (B4; persistent during baseline, and non-persistent during wash-in) and transient (B5; non-persistent during both baseline and wash-in) boutons. Filled yellow arrowheads indicate that the bouton is present, and empty yellow arrowheads indicate that the bouton is absent at the time point shown. (C) Average fraction of persistent (P) and non-persistent (NP) boutons at any given time point, and average fraction of the 5 subgroups of non-persistent boutons normalized to the total number of non-persistent boutons (N – new; L – lost; S – stabilizing; D –



destabilizing; T – transient). **(D)** Percentage of time points in which boutons were present during baseline (white) and wash-in (gray) periods. #: value for D was significantly different from N and T for wash-in ( $\chi^2$ ; D vs N,  $p = 0.002$ ; D vs T,  $p = 0.002$ ). **(E)** Fraction of boutons positive for VGAT and gephyrin per axon. Two-way ANOVA analysis showed a significant effect on bouton type ( $p = 0.0098$ ). For gephyrin, P vs T,  $p = 0.001$  (Sidak's multiple comparisons test). **(F)** Fraction of boutons co-localizing with VGAT or gephyrin as a function of bouton lifetime (total number of time points (#TPs) present during the imaging period). Lost boutons ('L' in C,D) were not included.  $\chi^2$ : TP2-5,  $p = 0.21$ ; TP6-8,  $p = 0.02$ ; TP9-11,  $p = 0.13$ ; TP12-14,  $p = 0.35$ ; TP15,  $p = 0.008$ . Confocal images in A are maximum intensity projections of 5-8 z stacks, while two-photon images are maximum intensity projections of 13-15 z stacks. Data are represented as mean  $\pm$  SEM. Data in C and D from 90 axons from 24 independent experiments, data in E and F from 21 axons from 5 independent experiments for the VGAT 902 staining (P:  $n=282$  boutons; N:  $n=13$ ; S:  $n=6$ ; D:  $n=17$ ; T:  $n=45$ ) and from 15 axons from 4 independent experiments for the gephyrin staining (P:  $n=232$  boutons; N:  $n=15$ ; S:  $n=6$ ; D:  $n=1$ ).

## Sema4D-induced stabilization of inhibitory boutons is the first step of inhibitory synapse formation

We next assessed whether Sema4D-induced bouton stabilization also results in an increase of inhibitory synapses in our slices. We first examined if longer Sema4D treatment could enhance the bouton stabilization effect. We compared dynamics of individual boutons during baseline and after 6 h treatment (400 minutes total treatment) and found that longer Sema4D treatment also induced prominent bouton stabilization, measured as fraction as well as absolute density (Fig. 3A,B). However, the 6 h treatment did not increase bouton stabilization beyond the 2 h level (Fig. 3C), suggesting that only a limited number of inhibitory boutons can be stabilized by Sema4D treatment, resulting in saturation of the treatment effect already after 2 hr. In addition to promoting bouton stabilization, with longer treatments we also detected a small reduction in the fraction of transient boutons (Fig. 3A). This effect was only revealed by analyzing the changes in density over time (Fig. 3D), which suggest that this may reflect an indirect effect of prolonged bouton stabilization. These results indicate that the Sema4D-induced stabilization of inhibitory boutons persists, but does not further increase, with longer treatments.

We next asked if Sema4D-induced inhibitory bouton stabilization leads to the formation of functional synapses. We treated organotypic hippocampal slices with 1 nM Fc or 1 nM Sema4D for 24 h, and determined overall inhibitory synapse density by immunohistochemistry. We used antibodies against presynaptic VGAT and postsynaptic gephyrin to visualize inhibitory synapses (Fig. 3E,F). Sema4D induced a clear  $24 \pm 7\%$  increase in the density of inhibitory synapses (Fig. 3G), suggesting that the observed Sema4D-induced bouton stabilization after 2 h resulted in the formation of new synapses after 24 h. We used electrophysiological recordings to verify that these synapses were functional. In agreement with the immunohistochemistry results, we found that 24 h treatment with Sema4D increased the frequency of miniature inhibitory postsynaptic currents (mIPSCs) by 37% (from  $5.2 \pm 0.5$  to  $7.1 \pm 0.5$  Hz), while mIPSC amplitude was not affected (Fig. 3H-K). To determine the time course of the recruitment of pre- and postsynaptic elements during synapse formation, we quantified VGAT and gephyrin immunostaining after 2, 6 and 24 h treatments. Treatment with Sema4D induced an increase in the area of VGAT puncta, without affecting their density (Fig. 4A-C). For gephyrin, Sema4D treatment caused an increase in puncta density, but not in their size (Fig. 4D-F). The average puncta intensity was not affected (at 24 h, VGAT:  $107 \pm 4\%$  of control,  $p = 0.35$  (MW); gephyrin:  $106 \pm 5\%$  of control,  $p = 0.51$  (MW)). Interestingly, the time course for presynaptic and postsynaptic changes was different. Whereas an increase in presynaptic VGAT area could already be detected after 6 h, the increase in postsynaptic gephyrin density was only evident after 24 h. These data are consistent with gradual increase in presynaptic vesicle content and subsequent acquisition of postsynaptic scaffolds at newly formed inhibitory synapses (Wierenga *et al.* 2008, Dobie and Craig 2011). Together, these data indicate that the initial Sema4D-induced stabilization of inhibitory boutons is followed by a slower maturation process, resulting in an overall increase in functional inhibitory synapses after Sema4D treatment. 5; T:  $n=39$ ). In F,  $n=14-28$  per TP, except for TP15.

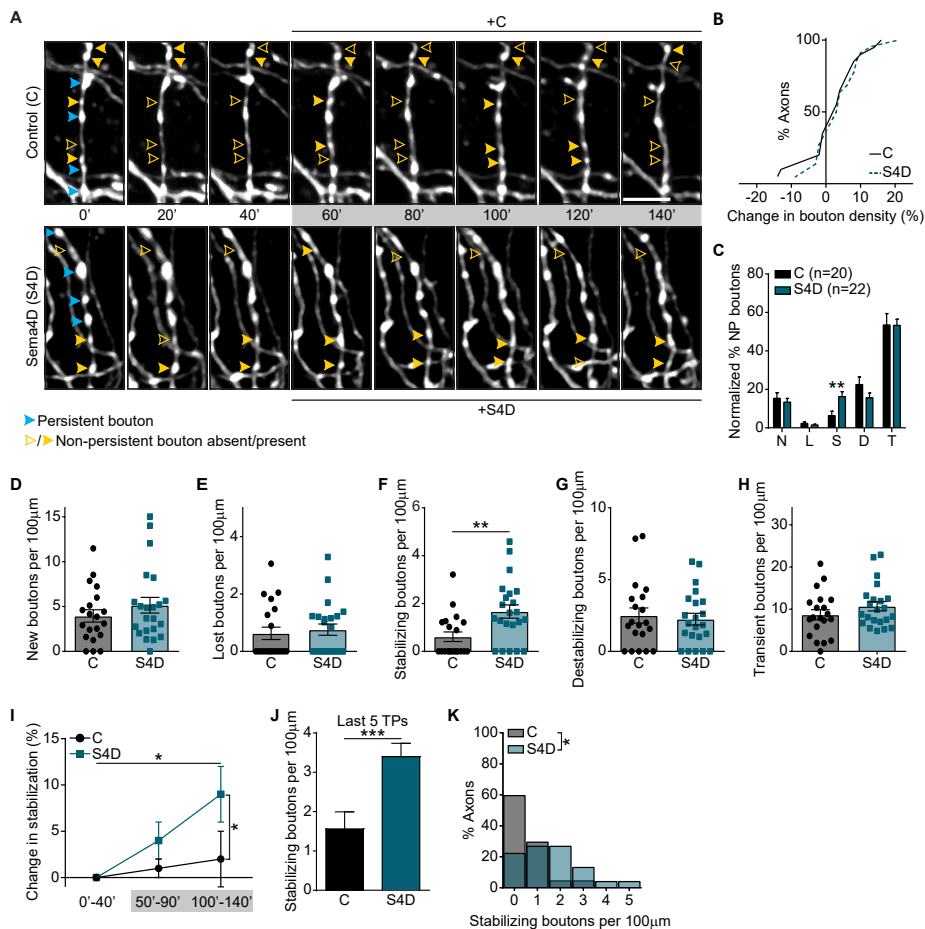


## Figure 2. Sema4D treatment promotes inhibitory bouton stabilization.

(A) Time-lapse two-photon images of GFP-labeled inhibitory axons in the CA1 region of the hippocampus during baseline (5 time points) and wash-in (10 time points; grey box) of 1 nM Fc - control (C; upper panel) or 1 nM Sema4D-Fc (S4D; bottom panel). Only every second image is shown for clarity. Persistent (blue) and non-persistent (yellow) boutons are indicated by arrowheads. Filled arrowheads indicate that the bouton is present, and empty arrowheads indicate that the bouton is absent at that time point. Images are maximum intensity projections of 11-18 z stacks. Time in minutes. Scale bar 5  $\mu$ m. (B) Cumulative distribution of the change in mean bouton density during the wash-in period compared to baseline after wash-in of C or S4D (MW,  $p = 0.83$ ). (C) Average fraction of subgroups of non-persistent boutons in C- and S4D-treated axons: N - new (MW,  $p = 0.86$ ); L - lost (MW,  $p = 0.93$ ); S - stabilizing (MW,  $p = 0.003$ ); D - destabilizing (MW,  $p = 0.25$ ); T - transient (MW,  $p = 0.89$ ). (D-H) Density of new (D; MW,  $p = 0.41$ ), lost (E; MW,  $p = 0.61$ ), stabilizing (F; MW,  $p = 0.003$ ), destabilizing (G; MW,  $p = 0.84$ ) and transient (H; MW,  $p = 0.34$ ) boutons in axons treated with 1 nM Fc (C) and 1 nM Sema4D-Fc (S4D). Each dot represents an individual axon. (I) Stabilization of inhibitory boutons, as determined by the change (compared to baseline) in density of boutons that were present at 5 consecutive time points during the imaging period: 0'-40' (baseline), 50'-90' (wash-in) and 100'-140' (wash-in). Two-way ANOVA analysis showed a significant effect of both treatment ( $p = 0.04$ ) and time ( $p = 0.03$ ). (J) Density of boutons that stabilized in the last 5 time points (TPs) (MW,  $p = 0.0008$ ). (K) Frequency distribution of the stabilizing bouton density in C- and S4D-treated axons ( $\chi^2$ ,  $p = 0.03$ ). Data are represented as mean  $\pm$  SEM. Data from 20 control axons (N=6) and 22 S4D-treated axons (N=5).

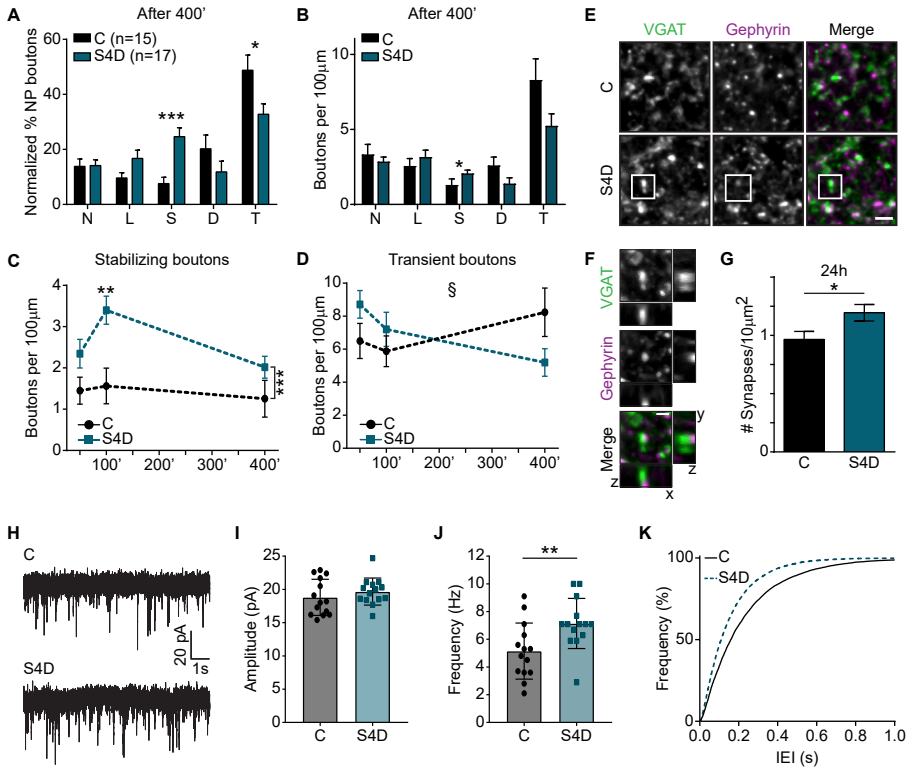


### Figure 3. Sema4D increases overall inhibitory synaptic density.

(A) Fraction of non-persistent boutons after treatment 935 with 1 nM Fc (control; C) or 1 nM Sema4D-Fc (S4D) for 6 hours (400 minutes of total treatment). N - new (MW,  $p = 0.91$ ) L - lost (MW,  $p = 0.13$ ); S - stabilizing (MW,  $p = 0.0003$ ); D - destabilizing (MW,  $p = 0.16$ ); T - transient (MW,  $p = 0.02$ ). (B) Density of non-persistent boutons after treatment with 1 nM Fc (C) or 1 nM Sema4D-Fc (S4D) for 6 hours. N: MW,  $p = 0.74$ ; L: MW,  $p = 0.29$ ; S: MW,  $p = 0.03$ ; D: MW,  $p = 0.09$ ; T: MW,  $p = 0.11$ . (C) Density of stabilizing boutons after treatment with Fc or S4D for 50, 100 and 400 minutes. Two-way ANOVA analysis showed that S4D increased bouton density independent of time ( $p = 0.0002$ ). At 100',  $p = 0.005$  (Sidak's multiple comparisons test). (D) Same as B, but for transient boutons. Two-Way ANOVA analysis indicated a significant interaction between treatment and time (§;  $p = 0.03$ ). (E) Representative images of CA1 dendritic area of GAD65-GFP hippocampal slices treated with 1 nM Fc (C) or 1 nM Sema4D-Fc (S4D) for 24 h, and immunostained for VGAT (green) and gephyrin (magenta). Images are average intensity projections of 5 z stacks. Scale bar 2  $\mu\text{m}$ . (F) Example of an inhibitory synapse (white box in D), identified as the apposition of VGAT (green) and gephyrin (magenta) puncta. The respective xz and yz projections show the close apposition of the two markers. Images are maximum intensity projections of 6 z stacks. Scale bar 1  $\mu\text{m}$ . (G) Density of inhibitory synapses in slices treated with Fc or S4D for 24 h (MW,  $p = 0.03$ ). (H) Representative whole-cell voltage-clamp recordings of miniature inhibitory postsynaptic currents (mIPSCs) from CA1 pyramidal cells in organotypic hippocampal slices treated for 24 h with 1 nM Fc/DMSO (C) or 1 nM S4D/DMSO (S4D). (I-J) Mean mIPSC amplitude (I) and frequency (J) in CA1 cells after 24 h treatment with Fc or S4D (H: MW,  $p = 0.35$ ; I: MW,  $p = 0.008$ ). (K) Cumulative distribution of inter-event interval (IEI) of mIPSCs. Data are represented as mean  $\pm$  SEM. Data in A,B from 15 control axons (N=4) and 17 S4D-treated axons (N=4), data in G from 15 control images (N=3) and 15 S4D images (N=3), and data in H-K from 14 control cells (N=5) and 14 S4D-treated cells (N=7).



## Sema4D-induced bouton stabilization relies on network activity

We previously showed that inhibitory bouton dynamics are regulated by neuronal activity (Schuemann *et al.* 2013). We therefore asked whether Sema4D-induced stabilization of inhibitory boutons depended on network activity. Blocking activity by bath application of tetrodotoxin (TTX) slightly decreased overall bouton dynamics in our slices (data not shown), which is in accordance with our previous findings (Schuemann *et al.* 2013). However, we found that in the presence of TTX Sema4D treatment no longer induced stabilization of inhibitory boutons, and that Sema4D treatment even led to a reduction in bouton stabilization compared to control (Fig. 5A,B). Indeed, whereas under control conditions Sema4D treatment increased the number of axons that displayed stabilizing boutons, it led to a decrease in the presence of TTX (Fig. 5C,D). These findings demonstrate that Sema4D treatment affects bouton dynamics in an activity-dependent manner, and indicate that Sema4D promotes the stabilization of inhibitory presynaptic boutons only in active neuronal networks.

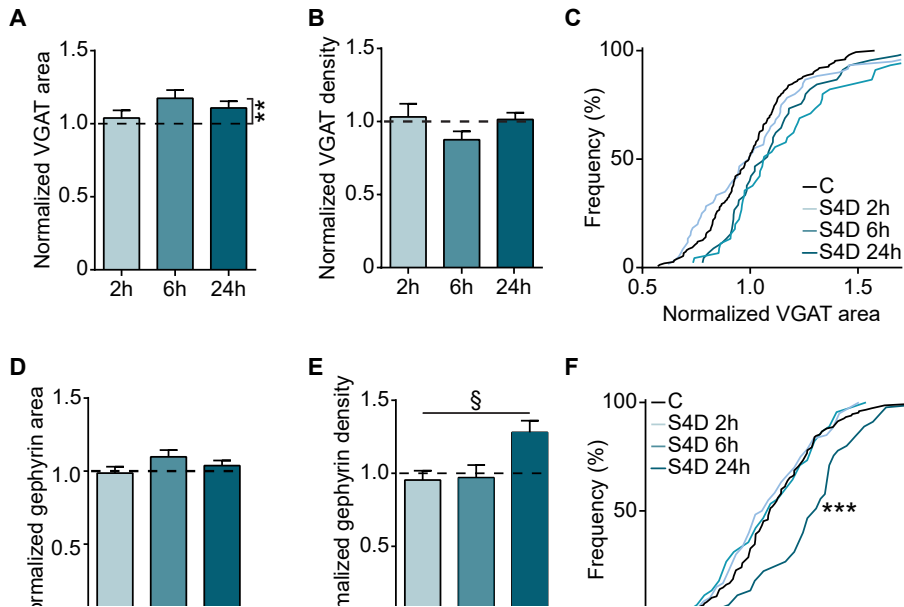


**Figure 4. VGAT and gephyrin undergo different changes in response to Sema4D.**

(**A**) Normalized area of presynaptic vesicular GABA transporter 968 (VGAT) puncta (after treatment with 1 nM S4D for 2 h, 6 h and 24 h). Dotted line represents control (treatment with 1nM Fc for 2 h, 6 h and 24 h). Two-way ANOVA analysis showed that S4D treatment increased VGAT area independent of time ( $p = 0.005$ ). (**B**) Normalized density of VGAT puncta, after treatment with 1 nM S4D for 2 h, 6 h and 24 h. Dotted line represents control (treatment with 1nM Fc for 2 h, 6 h and 24 h). (**C**) Cumulative distributions of the normalized area of VGAT after treatment with 1 nM S4D for 2, 6 and 24 h. Black line represents the normalized control values.  $p = 0.81$ ,  $p = 0.08$  and  $p = 0.14$  (KS) for 2, 6 and 24 h, respectively. (**D-E**) Same as in A-B, but for normalized area (D) and density (E) of postsynaptic gephyrin puncta. Two-way ANOVA analysis showed a significant effect of time ( $p = 0.04$ ) and an interaction between treatment and time (§;  $p = 0.04$ ) in E. (**F**) Same as in C, but for normalized gephyrin density.  $p = 0.99$ ,  $p = 0.99$  and  $p < 0.0001$  (KS) for 2, 6 and 24 h, respectively. Data are represented as mean  $\pm$  SEM. Data from 15-20 control images (N=3-4) and 15-20 S4D images (N=3-4) per time point.

## Local Sema4D-induced bouton stabilization

Under physiological circumstances, Sema4D is a membrane-attached protein acting locally (Pasterkamp 2012, Raissi *et al.* 2013). Presynaptic boutons along the same axon interact and share presynaptic proteins vesicles (Staras 2007, Bury and Sabo 2016) and we wondered if local Sema4D signaling would act differently compared to ubiquitous activation of Sema4D signaling during bath application. We therefore locally applied Sema4D to short stretches (~40  $\mu\text{m}$ ) of inhibitory axons (Fig. 5E). Local application with control solution appeared to slightly reduce local bouton stabilization (compare control curves in 5F and 2I), possibly from mechanical pressure. In contrast, local application of Sema4D induced robust stabilization of inhibitory boutons in these axons (Fig. 5F), resulting in a significant increase in local bouton density in these short axon stretches (Fig. 5G). This indicates that local application of Sema4D is more potent to induce axonal changes than bath application, which failed to induce a change in overall bouton density (compare Fig. 2B). This suggests that stabilizing boutons may compete for presynaptic components within individual axons when Sema4D is bath applied, limiting overall bouton density. Together, our results demonstrate that Sema4D signaling is capable to mediate rapid changes in local bouton density of inhibitory axons in an activity-dependent manner.

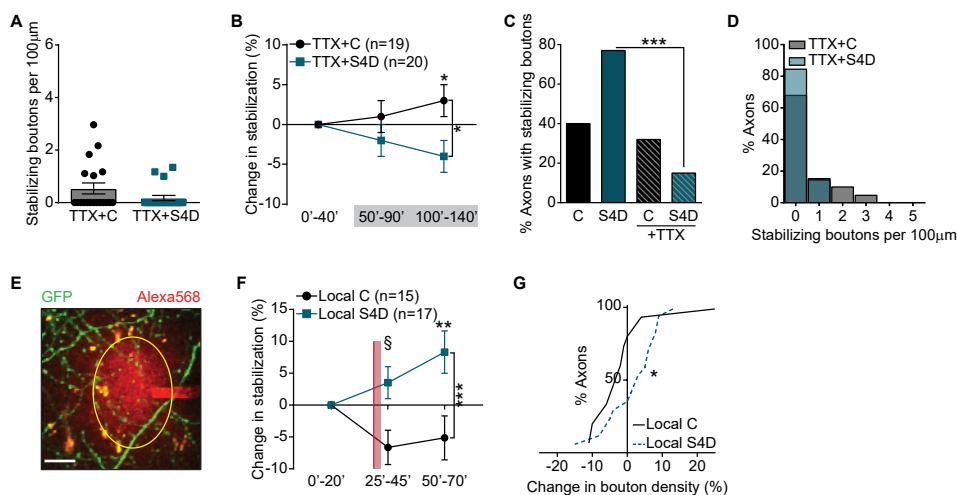


**Figure 5. Sema4D induces local stabilization of inhibitory boutons.**

(A) Density of stabilizing boutons in axons treated with 1 nM Fc (C) and 1 nM Sema4D-Fc (S4D), in the presence of 0.5  $\mu\text{M}$  TTX (MW,  $p = 0.17$ ). (B) Stabilization of inhibitory boutons upon treatment with C or S4D in the presence of 0.5  $\mu\text{M}$  TTX, determined by the change (compared to baseline) in density of boutons that were present at 5 consecutive time points during the imaging period: 0'-40' (baseline), 50'-90' (wash-in) and 100'-140' (wash-in). Two-way ANOVA analysis showed a significant effect of treatment ( $p = 0.01$ ). At 100'-140',  $p = 0.04$  (Sidak's multiple comparisons test). (C) Fraction of axons with stabilizing boutons in axons treated with C or S4D, in normal or activity-depleted slices with TTX ( $\chi^2$  (p-values are Bonferroni-corrected): C vs S4D,  $p = 0.01$ ; C vs C+TTX,  $p = 0.58$ ; C+TTX vs S4D+TTX,  $p = 0.22$ ; S4D vs S4D+TTX,  $p < 0.0001$ ). (D) Frequency distribution of the stabilizing bouton density in C- and S4D-treated axons, in the presence of 0.5  $\mu\text{M}$  TTX ( $\chi^2$ ,  $p = 0.17$ ). (E) Representative image

---

## Actin remodeling by low doses of LatrunculinB promotes stabilization of inhibitory boutons

The Sema4D effect on inhibitory synapses was previously shown to be dependent on its receptor PlexinB1 (Kuzirian *et al.* 2013). Sema4D/PlexinB1 signaling induces changes in the intracellular actin cytoskeleton via multiple small GTPase signaling pathways in many different cell types (Zhou *et al.* 2008, Cagnoni and Tamagnone 2014). Some of these downstream signaling pathways, which can modify actin in multiple ways, are mediated by receptor tyrosine kinases, such as MET and ErbB-2, acting as co-receptors for PlexinB1. It was shown in breast carcinoma cells that, when MET is co-activated, Sema4D/PlexinB1 signaling reduces RhoA levels and this results in actin depolymerization, while co-activation of ErbB-2 leads, via RhoA activation, to actin polymerization (Swiercz *et al.* 2008, Sun *et al.* 2012). To examine how the actin cytoskeleton is involved in inhibitory bouton dynamics, we studied the effect of two actin remodeling drugs in our system with intended opposite effects: the actin monomer sequestering drug LatrunculinB (LatB), which is generally considered an actin depolymerizing drug, and the actin filament stabilizer Jasplakinolide (Jasp), which promotes actin polymerization. In the low concentrations that we use here (100 nM LatB and 200 nM Jasp) these drugs perturb the actin cytoskeleton without affecting synaptic function (Honkura *et al.* 2008, Rex *et al.* 2009). None of the treatments changed overall axon morphology (Fig. 6A). We found that the fraction of stabilizing boutons was increased in the presence of LatB, but not in the presence of Jasp (Fig. 6B,C). The effect of LatB seemed highly specific for stabilizing boutons, as the other bouton subgroups were not affected. Indeed, we found that LatB specifically increased the absolute density of stabilizing boutons by almost 2-fold (Fig. 6D) and increased the fraction of axons with stabilizing boutons (Fig. 6E). The rapid and highly specific action of LatB suggests a direct action on the local actin cytoskeleton. The changes in bouton dynamics after LatB treatment were surprisingly similar to Sema4D treatment (Fig. 2F and 2K). Our findings suggest that inhibitory bouton dynamics are regulated by specific changes in the actin cytoskeleton and that conditions favoring actin depolymerization promote bouton stabilization. The similarity between stabilization of inhibitory boutons induced by treatment with LatB or Sema4D suggests that both treatments may induce a similar effect on intracellular actin. As we found that only a specific subset of inhibitory boutons was stabilized by Sema4D treatment (Fig. 2C), we wondered if these were the same boutons that responded to LatB. To test this, we treated slices with a combination of LatB and Fc or LatB and Sema4D. We found that bouton

---

1000 of the local treatment of GFP-labeled inhibitory axons in the CA1 region of the hippocampus. The pipette was filled with Alexa568 (red) to visualize the area of the puff (yellow circle). Scale bar 10  $\mu\text{m}$ . (F) Same as B, but for local treatment with 10 nM Fc (control, C) or 10 nM S4D. Red line marks the puffing. Two-way ANOVA analysis showed a significant effect of treatment ( $p = 0.0002$ ) and an interaction between treatment and time ( $\S$ ;  $p = 0.02$ ). At 50'-70',  $p = 0.003$  (Sidak's multiple comparisons test). (G) Cumulative distribution of the change in mean bouton density after local treatment with C or S4D compared to baseline (MW,  $p = 0.045$ ). Data are represented as mean  $\pm$  SEM. Data in A-D from 19 control axons (N=5) and 20 S4D-treated axons (N=5), and in F-G from 15 control axons (N=6) and 17 S4D-treated axons (N=6).

stabilization by LatB occluded a further increase by co-application with Sema4D (Fig. 6F and 6G), although it did increase the fraction of new boutons. These results suggest that LatB and Sema4D treatment act to stabilize a specific, overlapping, subset of inhibitory boutons.

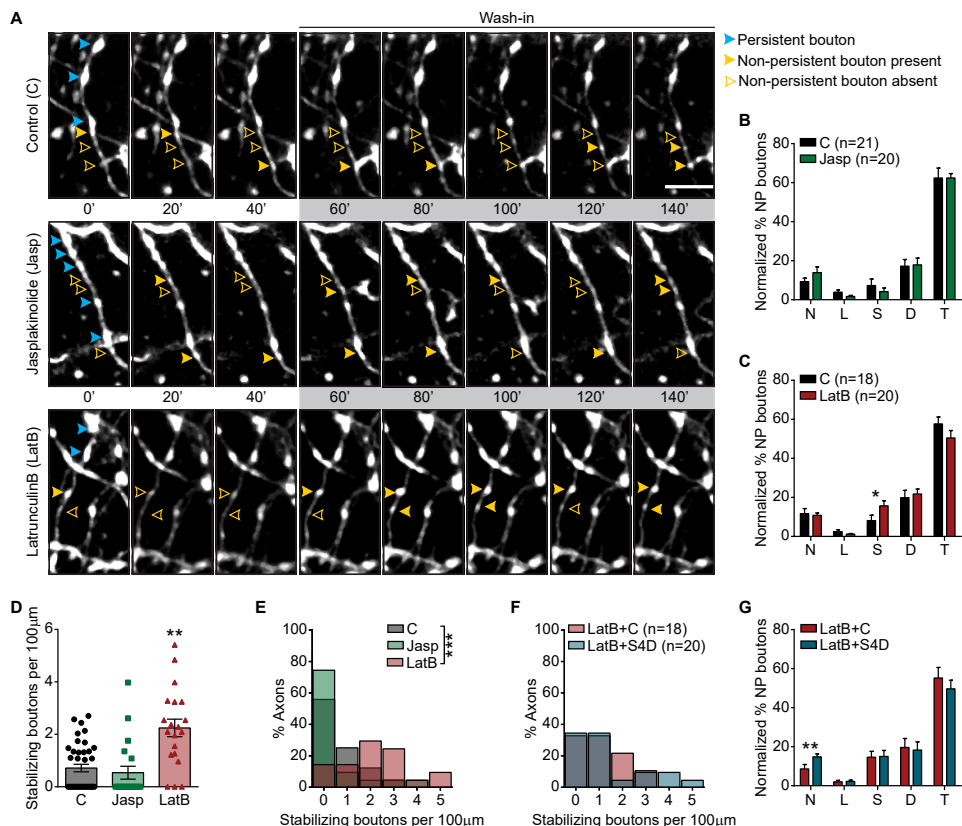


**Figure 6. Inhibitory bouton dynamics are regulated by actin.**

(A) Time-lapse two-photon images of GAD65-GFP-labeled axons in the CA1 region of the hippocampus during baseline (5 time points) and wash-in (10 time points; grey box) of DMSO - control (C; upper panel), 200 nM Jasplakinolide (Jasp; middle panel) or 100 nM LatrunculinB (LatB; bottom panel). Only every second image is shown for clarity. Persistent and non-persistent boutons are indicated as in Figure 2. Images are maximum intensity projections of 12-14 z stacks. Time in minutes. Scale bar 5 μm. (B) Fraction of non-persistent (NP) boutons in C and Jasp-treated axons: N - new (MW,  $p = 0.37$ ); L - lost (MW,  $p = 0.18$ ); S - stabilizing (MW,  $p = 0.49$ ); D - destabilizing (MW,  $p = 0.95$ ); T - transient (MW,  $p = 0.93$ ). (C) Same as in B, but for C and LatB-treated axons (N: MW,  $p = 0.99$ ; L: MW,  $p = 0.66$ ; S: MW,  $p = 0.01$ ; D: MW,  $p = 0.6$ ; T: MW,  $p = 0.29$ ). (D) Density of stabilizing boutons in control, Jasp- (MW:  $p = 0.55$ ) and LatB-treated axons (MW:  $p = 0.005$ ). (E) Frequency distribution of the stabilizing bouton density in C, Jasp- and LatB-treated slices ( $\chi^2$ ; C vs Jasp,  $p = 0.31$ ; C vs LatB,  $p = 0.0005$ ). (F) Same as E, but for combined treatment with 100 nM LatB/1 nM Fc (LatB+C) or 100 nM LatB/1 nM Sema4D (LatB+S4D) ( $\chi^2$ ,  $p = 0.37$ ). (G) Same as B, but for combined treatment with LatB+C or LatB+S4D (N: MW,  $p = 0.005$ ; L: MW,  $p = 0.58$ ; S: MW,  $p = 0.96$ ; D: MW,  $p = 0.82$ ; T: MW,  $p = 0.52$ ). Data are represented as mean  $\pm$  SEM. Data in B from 1033 21 control axons (N=6) and 20 Jasp-treated axons (N=5), in C from 18 control axons (N=5) and 20 LatB-treated axons (N=5) and in F-G from 18 LatB+Fc (N=4) and 20 LatB+S4D-treated axons (N=5).

We then wondered if treatment with the actin depolymerizing drug LatB would be sufficient to induce inhibitory synapse formation, similarly to the Sema4D treatment. Interestingly, we observed that although LatB induced changes in VGAT and gephyrin puncta after 2 h (Fig. 484 inhibitory synapses (Fig. 7G). Gephyrin and VGAT staining returned to baseline with longer LatB treatment. Together, our data suggest that LatB and Sema4D induce rapid stabilization of the same subgroup of inhibitory boutons, but that only Sema4D signaling leads to coordinated pre- and postsynaptic changes resulting in inhibitory synapse formation. This indicates that presynaptic bouton stabilization alone is not enough to induce inhibitory synapse formation and that additional signaling may be required.

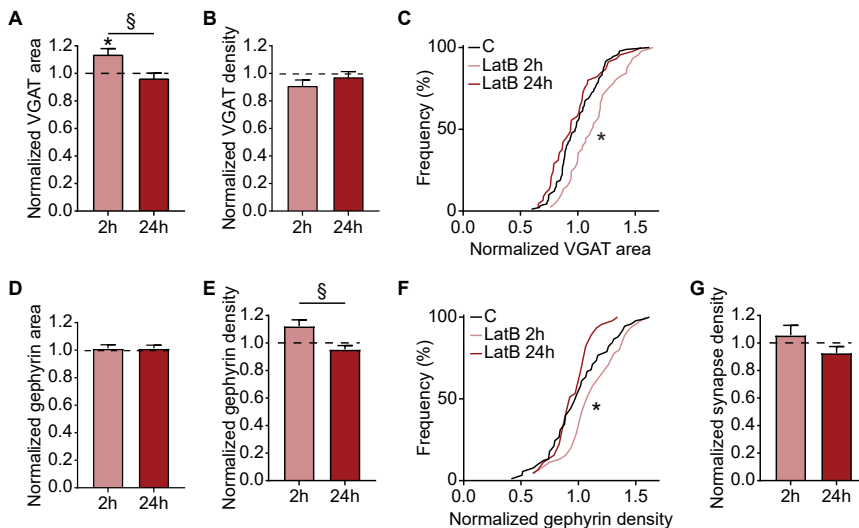


**Figure 7. Latrunculin B treatment does not promote inhibitory synapse formation.**

(A) Normalized area of presynaptic vesicular GABA transporter (VGAT) puncta (after treatment with 100 nM LatB for 2 h and 24 h). Dotted line represents control (treatment with DMSO for 2 h and 24 h). Two-way ANOVA analysis indicated a significant effect of time ( $p = 0.02$ ) and an interaction between treatment and time ( $\S$ ,  $p = 0.02$ ). (B) Normalized density of VGAT, after treatment with 100 nM LatB for 2 h and 24 h. Dotted line represents control (treatment with DMSO for 2 h and 24 h). (C) Cumulative distributions of the normalized area of VGAT after treatment with 100 nM LatB for 2 and 24 h. Black line represents the normalized control values.  $p = 0.047$  and  $0.33$  (KS) for 2 and 24 h, respectively. (D-E) Same as in A-B, but for the area (D) and density (E) of postsynaptic gephyrin puncta. In E, Two-way ANOVA analysis showed a significant effect of time ( $p = 0.04$ ) and interaction between treatment and time ( $\S$ ,  $p = 0.04$ ). (F) Same as in I, but for normalized gephyrin density.  $p = 0.047$  and  $0.33$  (KS) for 2 and 24 h, respectively. (G) Same as A, but for normalized density of inhibitory synapses. Data are represented as mean  $\pm$  SEM. Data from 15 control images ( $N=3$ ) and 15 LatB images ( $N=3$ ) per time point.

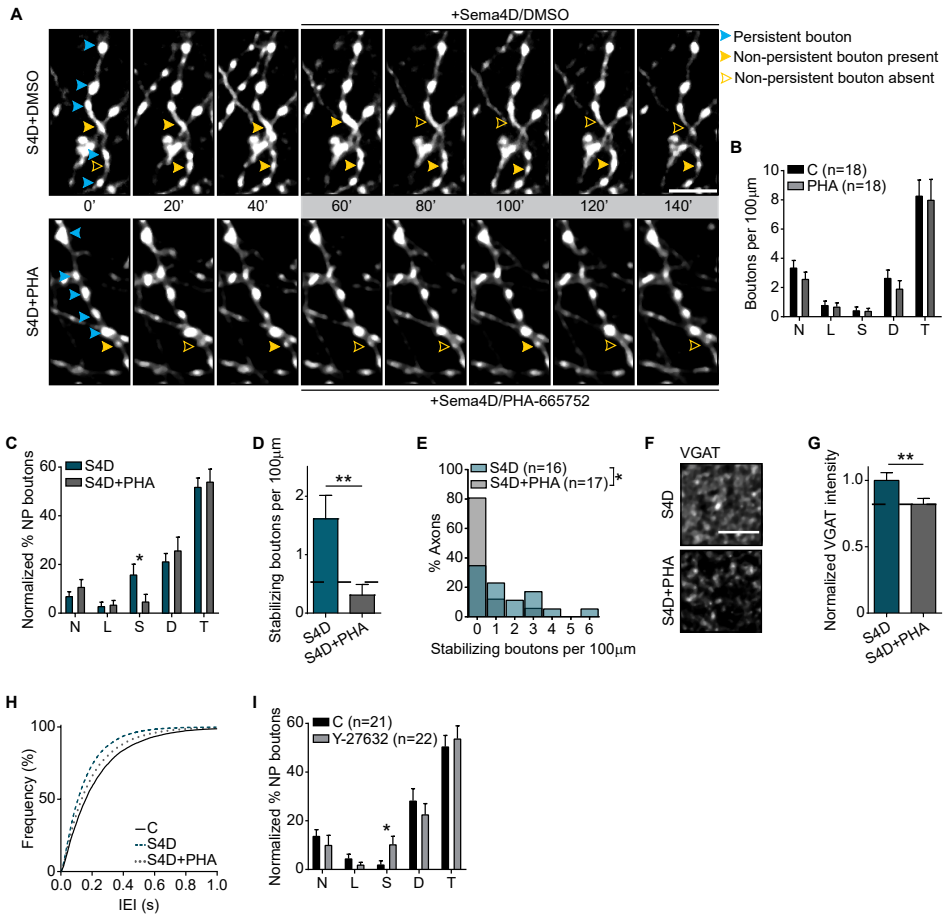
## Inhibitory bouton stabilization by Sema4D requires MET

Our observation that LatB could mimic the Sema4D-induced stabilization of inhibitory boutons points to a possible involvement of MET in this process. We therefore assessed if MET activation is necessary for the observed Sema4D-induced stabilization of boutons by making use of the highly specific MET inhibitor PHA-665752 (PHA) (Christensen *et al.* 2003, Deguchi *et al.* 2016). We first verified that adding PHA alone did not affect bouton dynamics (Fig. 8B) or spontaneous inhibitory postsynaptic currents (data not shown), indicating that MET is not very active under baseline conditions in our slices. Next, we treated our slices with Sema4D to induce bouton stabilization and compared bouton dynamics in the presence or absence of PHA (Fig. 8A, C-D). Blocking MET with PHA completely abolished the Sema4D-induced increase in the density of stabilizing boutons (Fig. 8D). In fact, blocking MET in combination with Sema4D treatment almost entirely abolished the occurrence of stabilizing boutons on our slices (Fig. 8E), while the other bouton subgroups were not much affected (8C). Consistent with the live imaging data, inhibiting MET with PHA also blocked the increase in VGAT staining intensity (Fig. 8F,G) and mIPSC frequency (Fig. 8H) after Sema4D treatment. Taken together, these data indicate that activation of MET is required for the Sema4D-induced stabilization of inhibitory boutons.

As the actin depolymerization pathway downstream of Sema4D/PlexinB1 signaling via MET was previously shown to reduce intracellular RhoA activity (Swiercz *et al.* 2008, Sun *et al.* 2012), we tested if stabilization of inhibitory boutons could also be achieved by directly reducing ROCK activity, a well-known downstream effector of RhoA (Amano *et al.* 2010). We found that reducing ROCK signaling with the specific ROCK inhibitor Y-27632 also resulted in an increase in the density of stabilizing boutons in our slices (Fig. 8I), which was similar to the effect of LatB and Sema4D treatments. This suggests that the intracellular pathway that is activated by Sema4D/PlexinB1 signaling to induce stabilization of inhibitory boutons involves activation of MET receptor tyrosine kinase and reduction of ROCK activity to promote specific changes in the actin cytoskeleton.

### Figure 8. Inhibitory bouton stabilization by Sema4D requires MET.

(A) Time-lapse two-photon images of GAD65-GFP-labeled axons in organotypic hippocampal slices during wash-in (grey box) of combination of 1 nM Sema4D and DMSO (S4D; upper panel) or combination of 1 nM Sema4D with 1  $\mu$ M PHA-665752 (S4D+PHA; bottom panel). Only every second image is shown for clarity. Persistent and non-persistent boutons are indicated as in Figure 2. Images are maximum intensity projections of 15-16 z stacks. Scale bar 5  $\mu$ m. (B) Density of non-persistent boutons in slices treated with DMSO (C) and 1  $\mu$ M PHA-665752 (PHA): N – new (MW,  $p = 0.28$ ); L – lost (MW,  $p = 0.77$ ); S – stabilizing (MW,  $p = 0.98$ ); D – destabilizing (MW,  $p = 0.24$ ); T – transient (MW,  $p = 0.67$ ). (C) Fraction of non-persistent (NP) boutons in S4D- and S 1066 4D+PHA-treated axons: N: MW,  $p = 0.34$ ; L: MW,  $p = 0.74$ ; S: MW,  $p = 0.01$ ; D: MW,  $p = 0.64$ ; T: MW,  $p = 0.53$ . (D) Density of stabilizing boutons in slices treated with S4D or S4D+PHA (MW,  $p = 0.006$ ). Dotted line represents control values. (E) Frequency distribution of the stabilizing bouton density in S4D- and S4D+PHA-treated slices ( $\chi^2$ ,  $p = 0.048$ ). (F) Representative images of hippocampal slices treated with S4D (upper panel) or S4D+PHA (bottom panel) for 100', and stained for presynaptic VGAT. Images are average intensity projections of 5 z stacks. Scale bar 5  $\mu$ m.



**(G)** Normalized mean staining intensity for VGAT in S4D- and S4D+PHA-treated slices (MW,  $p = 0.009$ ). Control value is indicated with dotted line. **(H)** Cumulative distribution of inter-event interval (IEI) of mIPSCs from CA1 pyramidal cells in organotypic slices after treatment with 1 nM Fc/DMSO (C), 1 nM S4D/DMSO (S4D) or 1 nM S4D/1 μM PHA-665752 (S4D+PHA) for 24 h. C and S4D as in Figure 3K. **(I)** Fraction of non-persistent boutons in axons treated with MQ (control) or 10 μM Y-27632 (ROCK inhibitor): N: MW,  $p = 0.05$ ; L: MW,  $p = 0.39$ ; S: MW,  $p = 0.02$ ; D: MW,  $p = 0.38$ ; T: MW,  $p = 0.78$ . Data are represented as mean  $\pm$  SEM. Data in B from 18 control axons (N=4) and 18 PHA-treated axons (N=4), in C-E from 17 S4D-treated axons (N=4) and 16 S4D+PHA-treated axons (N=4), in F-G from 16 images of S4D-treated slices (N=3) and 23 images of S4D+PHA-treated slices (N=4); in H from 14 control cells (N=5), 14 S4D-treated cells (N=7) and 17 S4D+PHA-treated cells (N=5), and in I from 21 control axons (N=5) and 22 Y-27632-treated axons (N=5).

**MET is enriched at a subset of inhibitory presynaptic boutons**

Our pharmacological experiments do not address if Sema4D-induced changes in actin occur at the pre- or postsynaptic compartment. The subcellular localization of Sema4D and PlexinB1 is not known (Paradis *et al.* 2007), but the localization of MET has been described. Interestingly, it was reported that in postnatal tissue the majority of MET is localized in axons (Judson *et al.* 2009) and detailed EM analysis showed clusters of MET in the shaft of unmyelinated axons and in small presynaptic terminals (Eagleson *et al.* 2013). The majority of these terminals are glutamatergic (Tyndall and Walikonis 2006, Xie *et al.* 2016), but possible MET expression in GABAergic axons was never addressed directly. To address the localization of MET in our slices, we made use of an antibody (Qiu *et al.* 2014) and a nanobody (Heukers *et al.* 2014) with demonstrated specificity for MET. We first confirmed that both label synapses in primary hippocampal cultures (Fig. 9A-C). The majority of MET puncta overlapped with excitatory synapses (Fig. 9A,B) in line with previous reports (Tyndall and Walikonis 2006, Eagleson *et al.* 2013, Xie *et al.* 2016). However, clear association of MET with inhibitory presynapses was also observed in these cultures (Fig. 9B,C). We then used the MET nanobody and antibody to label MET in our hippocampal slices of GAD65-GFP mice (Fig. 9D). Although there was a quantitative difference, presumably reflecting a difference in labeling affinity, both methods clearly showed that a subset of GFP-labeled inhibitory boutons was enriched for MET (Fig. 9E). Comparison between the MET staining pattern with staining for postsynaptic gephyrin (compare Figs. 9F and 3F) suggests a presynaptic localization of MET at these inhibitory synapses, as MET puncta were often completely embedded in the GFP-labeled bouton. These data suggest that MET may be present in inhibitory axons and terminals to mediate Sema4D/plexinB1 signaling.



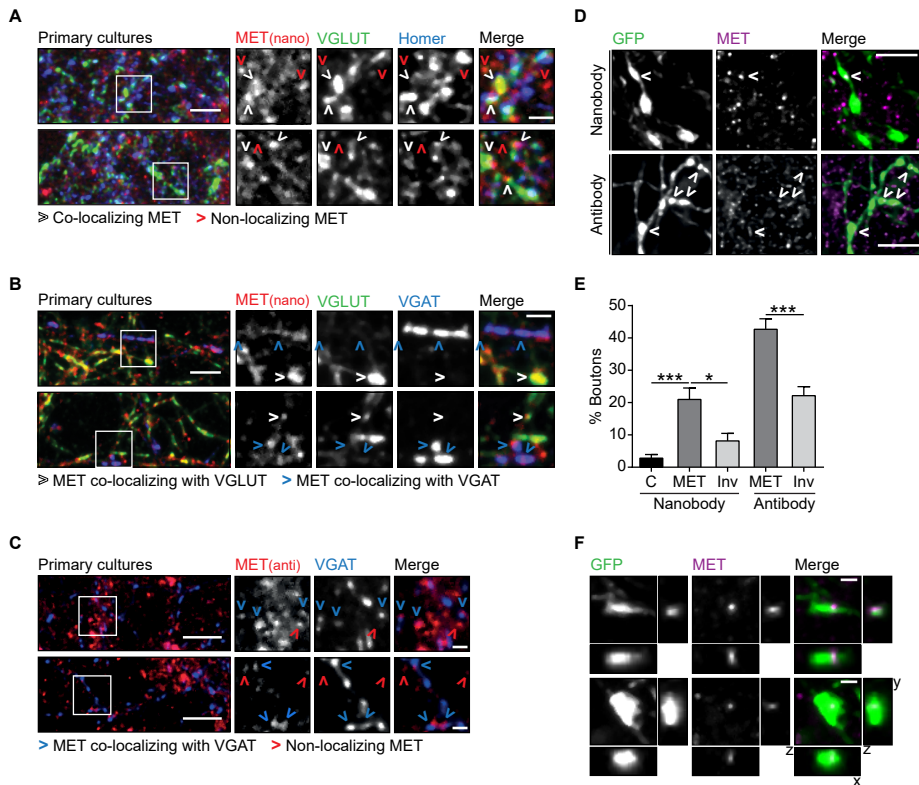


### Figure 9. MET is enriched in a subset of inhibitory presynaptic boutons.

(A) Images of primary cultures of hippocampal neurons immunostained with MET nanobody (red) and markers for excitatory synapses: presynaptic vesicular glutamate transporter (VGLUT; green) and postsynaptic Homer (blue). The majority of MET puncta co-localize with one or both markers (white arrows), but some MET puncta do not co-localize (red arrows). Images are maximum intensity projections of 13 stacks. Scale bar 5  $\mu\text{m}$  (overview) and 2  $\mu\text{m}$  (zoom). (B) Same as A, but neurons were stained with MET nanobody (red) and markers for excitatory presynapses (VGLUT; green) and inhibitory presynapses (vesicular GABA transporter VGAT; blue). White arrows indicate MET co-localizing with VGLUT and blue arrows indicate MET co-localizing with VGAT. Images are maximum intensity projections of 12 stacks. Scale bar 5  $\mu\text{m}$  (overview) and 2  $\mu\text{m}$  (zoom). (C) Same as A, but hippocampal neurons were stained with MET antibody (red) and VGAT (blue). Blue arrows highlight MET puncta co-localizing with VGAT, while red arrows indicate MET puncta that do not co-localize with VGAT. Images are maximum intensity projections of 17-21 stacks. Scale bar 10  $\mu\text{m}$  (overview) and 2  $\mu\text{m}$  (zoom). (D) Representative images of GFP-labeled inhibitory boutons (green) in hippocampal slices, stained with a nanobody (upper) and an antibody (lower panels) against MET (magenta). Images are maximum intensity projections of 5-6 z stacks. White arrows indicate MET enrichment in GFP-labeled boutons. Scale bar 5  $\mu\text{m}$ . (E) Fraction of GFP boutons positive for MET. Aspecific staining was determined by anti-staining without nanobody ('C'; black) and random co-localization was determined by inverting the MET channel ('Inv'; light gray) (Nanobody: KW,  $p = 0.002$ ; Antibody: MW,  $p < 0.0001$ ). (F) Example of two inhibitory boutons (green) in hippocampal slices showing enrichment in MET (magenta), and the respective xz and yz projections. Images are maximum intensity projections of 6 z stacks. Scale bar 1  $\mu\text{m}$ . Data are represented as mean  $\pm$  SEM. Data in F from 10 control images (N=2), 12 images in MET and inverted group (N=3) for the nanobody staining and 15 images in MET and inverted group (N=3) for the antibody staining.

## Discussion

By monitoring individual boutons over time in live brain slices, we observed that the primary action of Semaphorin 4D (Sema4D) signaling is to stabilize presynaptic boutons of inhibitory axons within tens of minutes. These stabilizing boutons develop into mature, functional inhibitory synapses over the course of several hours. They rapidly acquire presynaptic vesicles as evidenced by an increase in VGAT staining, while recruitment of postsynaptic gephyrin was slower. We demonstrate for the first time that Sema4D-induced bouton stabilization is activity-dependent and that Sema4D signaling can induce local changes in bouton density. We found that inhibitory axons respond differently to Sema4D signaling in active and inactive networks (Fig. 5). These results suggest that inhibitory axons can respond very rapidly to local signals in their environment, but that the response is modulated by the state of the network and/or the local internal state of the axon. It was previously shown that Sema4D in inhibitory synapses signals via the PlexinB1 receptor. We now show that this signaling pathway requires co-activation of the receptor tyrosine kinase MET. The downstream intracellular pathway involves specific remodeling of the actin cytoskeleton, which can be mimicked by bath application of low levels of the actin depolymerizing drug LatB or by reducing ROCK activity. Our immunohistochemistry data suggest that MET is localized to the presynaptic compartment of GABAergic synapses. Our data is the first to show a role for the autism-linked MET in inhibitory synapses.

Our live imaging experiments give unique insight in the dynamics of inhibitory synapse formation in brain slices, which remain undetected with methods using stationary comparisons before and after treatment. In our slices, the majority of GFP-labeled boutons are persistent and display pre- and postsynaptic markers of mature inhibitory synapses, but a significant portion (~20-25%) of inhibitory boutons are non-persistent and represent locations where inhibitory synapses are 'in transition'. At these axonal locations, inhibitory synapses are formed and disassembled in an apparent trial-and-error fashion (Wierenga *et al.* 2008, Dobie and Craig 2011, Fu *et al.* 2012, Schuemann *et al.* 2013, Wierenga 2017). We found that Sema4D signaling did not induce formation of inhibitory synapses *de novo*, but specifically stabilized boutons at locations where a bouton had occurred before. We also observed that Sema4D-induced bouton stabilization was not further enhanced by longer treatment (>2 h) or by co-application with LatB, suggesting that the number of boutons susceptible to Sema4D at any given time is limited. This suggests that Sema4D signaling is involved only at a specific stage during synapse formation and that boutons which are more mature or too immature do not respond to Sema4D. In primary cultures, a larger fraction of synapses are immature compared to intact tissue (Dobie and Craig 2011, Kuriu *et al.* 2012), which may explain why the Sema4D effect on inhibitory synapses is stronger in primary neurons (Kuzirian *et al.* 2013). In our slices, Sema4D treatment increased inhibitory synapse density by ~20% after 24 hours (Fig. 3G), which is comparable to experience-dependent changes in inhibitory synapses observed *in vivo* (Keck *et al.* 2011, Chen *et al.* 2015, Villa *et al.* 2016).

One of the key observations of this study is that the primary action of Sema4D is to stabilize presynaptic boutons of inhibitory axons within tens of minutes. These stabilizing boutons

---

develop into mature, functional inhibitory synapses over the course of several hours. It was previously shown that inhibitory synapses can be induced by postsynaptic gephyrin clustering (Flores *et al.* 2015), and rapid formation of new gephyrin clusters was observed after Semaphorin 4D treatment in primary cultures (Kuzirian *et al.* 2013), suggesting that Semaphorin 4D may promote inhibitory synapse formation via a postsynaptic mechanism. However, our data clearly show that gephyrin clustering after Semaphorin 4D treatment is delayed and that the primary action of Semaphorin 4D signaling is presynaptic bouton stabilization, arguing against a triggering mechanism via postsynaptic gephyrin. The increase in VGAT signal reflects recruitment of synaptic vesicles to newly forming synapses (Dobie and Craig 2011, Schuemann *et al.* 2013). Bouton stabilization and gephyrin clustering were also induced by LatB, but LatB failed to induce new inhibitory synapses. This suggests that Semaphorin 4D signaling coordinates pre- and postsynaptic changes at emerging inhibitory synapses. The faster time course for the increase in postsynaptic gephyrin clusters in primary cultures (Kuzirian *et al.* 2013) may reflect an overall difference in neuronal maturation level. In young neurons, new gephyrin clusters can be rapidly induced by local GABA signaling (Oh *et al.* 2016), while in mature neurons prolonged or additional signaling may be required.

It was previously shown that Semaphorin 4D acts as a postsynaptic protein and requires PlexinB1 for promoting inhibitory synapse formation (Kuzirian *et al.* 2013, Raissi *et al.* 2013). Our data shows that this signaling pathway requires co-activation of MET, suggesting that the receptor tyrosine kinase MET acts as a co-receptor of PlexinB1 (Swiercz *et al.* 2008). PlexinB1 and MET receptors can form a complex which, upon Semaphorin 4D stimulation, results in cross-activation of both receptors (Giordano *et al.* 2002). It is currently not known if the PlexinB1 receptors that mediate the Semaphorin 4D signaling are located in the pre- or postsynaptic membrane and our data does not address this issue directly. However, our immunohistochemistry data (Fig. 9) suggest that MET receptors are localized in a subset of inhibitory synapses, in primary hippocampal cultures and organotypic slices. A presynaptic location of MET in inhibitory boutons suggests retrograde signaling of postsynaptic Semaphorin 4D via presynaptic plexinB1 receptors. Retrograde semaphorin signaling was recently demonstrated in *Drosophila* neuromuscular junction (Orr *et al.* 2017). However, cell-specific genetic studies will be needed to rule out a contribution of Semaphorin 4D signaling via postsynaptic receptors in inhibitory synapse formation.

Our data indicates that inhibitory bouton stabilization by activation of the Semaphorin 4D/PlexinB1 signaling pathway is induced through actin remodeling (Swiercz *et al.* 2008, Sun *et al.* 2012). The induced changes in actin are highly specific and not due to a general decrease in actin dynamics since Jasplakinolide did not affect inhibitory boutons. Treatment with the actin depolymerizing drug LatB or the ROCK inhibitor Y-27632 promoted bouton stabilization in a similar way as Semaphorin 4D, presumably by inducing similar changes in presynaptic actin at stabilizing boutons. Given that actin is abundantly present in all cells, it is surprising that bath application of LatB specifically promotes stabilization of immature boutons without affecting other inhibitory boutons. It is important to note that low doses of monomer sequestering drugs, such as LatB, do not lead to the complete disassembly of actin structures and leave postsynaptic spines and synaptic transmission intact (Honkura *et al.* 2008, Rex *et*

*al.* 2009, Bleckert *et al.* 2012). Instead, LatB treatment may result in limited availability of actin monomers in small cellular compartments, which indirectly affects actin-regulating factors resulting in structural changes of the actin cytoskeleton (Ganguly *et al.* 2015, Suarez *et al.* 2015). Our data therefore suggest that the actin cytoskeleton at stabilizing boutons is different from other compartments and specifically sensitive to LatB. However, we stress here that our experiments cannot distinguish between pre- or postsynaptic effects of LatB, but the rapid (boutons are stabilized within 10 minutes) and highly specific effect seems to suggest a local action of LatB. Inhibitory synapses are usually localized directly on the dendritic shaft and not much is known about a possible role of postsynaptic actin structures at these synapses. Within axons, several actin-based structures have been described (Leterrier *et al.* 2017) and presynaptic actin has been implicated in transmission, plasticity, as well as synapse formation (Cingolani and Goda 2008, Chia *et al.* 2013). In *C. elegans* and *Drosophila* it has been demonstrated that presynaptic actin structures undergo important remodeling during synapse formation (Chia *et al.* 2014, Piccioli and Littleton 2014). It is currently not known which actin-regulating factors are involved in presynaptic bouton stabilization, but promising candidates include cortactin (Alicea *et al.* 2017), cofilin (Piccioli and Littleton 2014) and Mical (Orr *et al.* 2017). Future studies will be necessary to unravel precise actin structures in mature and immature boutons and the role of actin-regulating factors during synapse formation.

Changes in inhibitory synapses play an important role in the rewiring of circuits during development and in response to behavioral demands during adulthood (Keck *et al.* 2011, Chen *et al.* 2015, Froemke 2015) and defects in GABAergic synapses are associated with neurodevelopmental diseases (Hensch 2004, Marín 2012). Mutations in the MET gene are an established risk factor for autism spectrum disorder (ASD), as determined by various human imaging and genetic studies (Peng *et al.* 2013). It is a multifunctional receptor involved in many cellular pathways, and its exact role in ASD is not yet understood (Eagleson *et al.* 2017). Previous studies in neurons have implicated MET in regulating postsynaptic strength in excitatory neurons (Qiu *et al.* 2014, Lo *et al.* 2016), excitatory synapse formation (Xie *et al.* 2016) and interneuron migration (Martins *et al.* 2011). Our data demonstrate that activation of MET is also an essential part of the Sema4D signaling pathway promoting activity-dependent inhibitory bouton stabilization, indicating a novel role of MET in the assembly of inhibitory presynapses.



## References

- Alicea, D., Perez, M., Maldonado, C., Dominicci-Cotto, C., and Marie, B., 2017. Cortactin Is a Regulator of Activity-Dependent Synaptic Plasticity Controlled by Wingless. *The Journal of Neuroscience*, 37 (8), 2203–2215.
- Amano, M., Nakayama, M., and Kaibuchi, K., 2010. Rho-kinase/ROCK: A key regulator of the cytoskeleton and cell polarity. *Cytoskeleton*, 67 (9), 545–554.
- Basile, J.R., Holmbeck, K., Bugge, T.H., and Gutkind, J.S., 2007. MT1-MMP Controls Tumor-induced Angiogenesis through the Release of Semaphorin 4D. *Journal of Biological Chemistry*, 282 (9), 6899–6905.
- Bleckert, A., Photowala, H., and Alford, S., 2012. Dual pools of actin at presynaptic terminals. *Journal of Neurophysiology*, 107 (12), 3479–3492.
- Bury, L.A.D. and Sabo, S.L., 2016. Building a Terminal: Mechanisms of Presynaptic Development in the CNS. *Neuroscientist*, 22 (4), 372–391.
- Cagnoni, G. and Tamagnone, L., 2014. Semaphorin receptors meet receptor tyrosine kinases on the way of tumor progression. *Oncogene*, 33 (40), 4795–4802.
- Caroni, P., Donato, F., and Muller, D., 2012. Structural plasticity upon learning: regulation and functions. *Nature Reviews Neuroscience*, 13 (7), 478–490.
- Cellot, G. and Cherubini, E., 2014. GABAergic Signaling as Therapeutic Target for Autism Spectrum Disorders. *Frontiers in Pediatrics*, 2 (July), 1–11.
- Chen, S.X., Kim, A.N., Peters, A.J., and Komiyama, T., 2015. Subtype-specific plasticity of inhibitory circuits in motor cortex during motor learning. *Nature Neuroscience*, 18 (8), 1109–1115.
- Chia, P.H., Chen, B., Li, P., Rosen, M.K., and Shen, K., 2014. Local F-actin network links synapse formation and axon branching. *Cell*, 156 (1–2), 208–220.
- Chia, P.H., Li, P., and Shen, K., 2013. Cellular and molecular mechanisms underlying presynapse formation. *Journal of Cell Biology*, 203 (1), 11–22.
- Christensen, J.G., Schreck, R., Burrows, J., Kuruganti, P., Chan, E., Le, P., Chen, J., Wang, X., Ruslim, L., Blake, R., Lipson, K.E., Ramphal, J., Do, S., Cui, J.J., Cherrington, J.M., and Mendel, D.B., 2003. A selective small molecule inhibitor of c-Met kinase inhibits c-Met-dependent phenotypes in vitro and exhibits cytoreductive antitumor activity in vivo. *Cancer research*, 63 (21), 7345–55.
- Cingolani, L.A. and Goda, Y., 2008. Actin in action: The interplay between the actin cytoskeleton and synaptic efficacy. *Nature Reviews Neuroscience*, 9 (5), 344–356.

- 
- Deguchi, Y., Harada, M., Shinohara, R., Lazarus, M., Cherasse, Y., Urade, Y., Yamada, D., Sekiguchi, M., Watanabe, D., Furuyashiki, T., and Narumiya, S., 2016. mDia and ROCK Mediate Actin-Dependent Presynaptic Remodeling Regulating Synaptic Efficacy and Anxiety. *Cell Reports*, 17 (9), 2405–2417.
- Dobie, F.A. and Craig, A.M., 2011. Inhibitory Synapse Dynamics: Coordinated Presynaptic and Postsynaptic Mobility and the Major Contribution of Recycled Vesicles to New Synapse Formation. *Journal of Neuroscience*, 31 (29), 10481–10493.
- Eagleson, K.L., Milner, T.A., Xie, Z., and Levitt, P., 2013. Synaptic and extrasynaptic location of the receptor tyrosine kinase met during postnatal development in the mouse neocortex and hippocampus. *Journal of Comparative Neurology*, 521 (14), 3241–3259.
- Eagleson, K.L., Xie, Z., and Levitt, P., 2017. The Pleiotropic MET Receptor Network: Circuit Development and the Neural-Medical Interface of Autism. *Biological Psychiatry*, 81 (5), 424–433.
- Esteves da Silva, M., Adrian, M., Schätzle, P., Lipka, J., Watanabe, T., Cho, S., Futai, K., Wierenga, C.J., Kapitein, L.C., and Hoogenraad, C.C., 2015. Positioning of AMPA Receptor-Containing Endosomes Regulates Synapse Architecture. *Cell Reports*, 13 (5), 933–943.
- Flores, C.E., Nikonenko, I., Mendez, P., Fritschy, J.-M., Tyagarajan, S.K., and Muller, D., 2015. Activity-dependent inhibitory synapse remodeling through gephyrin phosphorylation. *Proceedings of the National Academy of Sciences of the United States of America*, 112 (1), E65-72.
- Frias, C.P. and Wierenga, C.J., 2013. Activity-dependent adaptations in inhibitory axons. *Frontiers in Cellular Neuroscience*, 7 (November), 1–16.
- Froemke, R.C., 2015. Plasticity of Cortical Excitatory-Inhibitory Balance. *Annual Review of Neuroscience*, 38 (1), 195–219.
- Fu, Y. and Huang, Z.J., 2010. Differential dynamics and activity-dependent regulation of - and -neurexins at developing GABAergic synapses. *Proceedings of the National Academy of Sciences*, 107 (52), 22699–22704.
- Fu, Y., Wu, X., Lu, J., and Huang, Z.J., 2012. Presynaptic GABA(B) Receptor Regulates Activity-Dependent Maturation and Patterning of Inhibitory Synapses through Dynamic Allocation of Synaptic Vesicles. *Frontiers in cellular neuroscience*, 6 (December), 57.
- Ganguly, A., Tang, Y., Wang, L., Ladit, K., Loi, J., Dargent, B., Leterrier, C., and Roy, S., 2015. A dynamic formin-dependent deep F-actin network in axons. *Journal of Cell Biology*, 210 (3), 401–417.
- Giacobini, P., Messina, A., Morello, F., Ferraris, N., Corso, S., Penachioni, J., Giordano, S., Tamagnone, L., and Fasolo, A., 2008. Semaphorin 4D regulates gonadotropin hormone-releasing hormone-1 neuronal migration through PlexinB1–Met complex. *The Journal of Cell Biology*, 183 (3), 555–566.

- Giordano, S., Corso, S., Conrotto, P., Artigiani, S., Gilestro, G., Barberis, D., Tamagnone, L., and Comoglio, P.M., 2002. The semaphorin 4D receptor controls invasive growth by coupling with Met. *Nature Cell Biology*, 4 (9), 720–724.
- Hensch, T.K., 2004. Critical Period Regulation. *Annual Review of Neuroscience*, 27 (1), 549–579.
- Hensch, T.K., 2005. Critical period plasticity in local cortical circuits. *Nature Reviews Neuroscience*, 6 (11), 877–888.
- Heukers, R., Altintas, I., Raghoenath, S., De Zan, E., Pepermans, R., Roovers, R.C., Haselberg, R., Hennink, W.E., Schifflers, R.M., Kok, R.J., and Van Bergen en Henegouwen, P.M.P., 2014. Targeting hepatocyte growth factor receptor (Met) positive tumor cells using internalizing nanobody-decorated albumin nanoparticles. *Biomaterials*, 35 (1), 601–610.
- Honkura, N., Matsuzaki, M., Noguchi, J., Ellis-Davies, G.C.R., and Kasai, H., 2008. The Subspine Organization of Actin Fibers Regulates the Structure and Plasticity of Dendritic Spines. *Neuron*, 57 (5), 719–729.
- Isaacson, J.S. and Scanziani, M., 2011. How inhibition shapes cortical activity. *Neuron*, 72 (2), 231–243.
- Judson, M.C., Bergman, M.Y., Campbell, D.B., Eagleson, K.L., and Levitt, P., 2009. Dynamic gene and protein expression patterns of the autism-associated met receptor tyrosine kinase in the developing mouse forebrain. *Journal of Comparative Neurology*, 513 (5), 511–531.
- Keck, T., Scheuss, V., Jacobsen, R.I., Wierenga, C.J., Eysel, U.T., Bonhoeffer, T., and Hübener, M., 2011. Loss of sensory input causes rapid structural changes of inhibitory neurons in adult mouse visual cortex. *Neuron*, 71 (5), 869–882.
- Kolodkin, A.L., Matthes, D.J., and Goodman, C.S., 1993. The semaphorin genes encode a family of transmembrane and secreted growth cone guidance molecules. *Cell*, 75 (7), 1389–1399.
- Krueger-Burg, D., Papadopoulos, T., and Brose, N., 2017. Organizers of inhibitory synapses come of age. *Current Opinion in Neurobiology*, 45, 66–77.
- Kuriu, T., Yanagawa, Y., and Konishi, S., 2012. Activity-dependent coordinated mobility of hippocampal inhibitory synapses visualized with presynaptic and postsynaptic tagged-molecular markers. *Molecular and Cellular Neuroscience*, 49 (2), 184–195.
- Kuzirian, M.S., Moore, A.R., Staudenmaier, E.K., Friedel, R.H., and Paradis, S., 2013. The class 4 semaphorin Sema4D promotes the rapid assembly of GABAergic synapses in rodent hippocampus. *The Journal of neuroscience : the official journal of the Society for Neuroscience*, 33 (21), 8961–73.

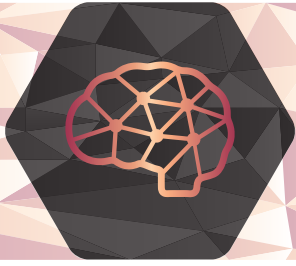


- 
- Leterrier, C., Dubey, P., and Roy, S., 2017. The nano-architecture of the axonal cytoskeleton. *Nature Reviews Neuroscience*, 18 (12), 713–726.
- Lo, F.-S., Erzurumlu, R.S., and Powell, E.M., 2016. Insulin-Independent GABA A Receptor-Mediated Response in the Barrel Cortex of Mice with Impaired Met Activity. *The Journal of Neuroscience*, 36 (13), 3691–3697.
- López-Bendito, G., Sturgess, K., Erdélyi, F., Szabó, G., Molnár, Z., and Paulsen, O., 2004. Preferential origin and layer destination of GAD65-GFP cortical interneurons. *Cerebral Cortex*, 14 (10), 1122–1133.
- Lu, W., Bromley-Coolidge, S., and Li, J., 2017. Regulation of GABAergic synapse development by postsynaptic membrane proteins. *Brain Research Bulletin*, 129 (1), 30–42.
- Marín, O., 2012. Interneuron dysfunction in psychiatric disorders. *Nature Reviews Neuroscience*, 13 (2), 107–120.
- Martins, G.J., Shahrokh, M., and Powell, E.M., 2011. Genetic disruption of Met signaling impairs GABAergic striatal development and cognition. *Neuroscience*, 176, 199–209.
- Müllner, F.E., Wierenga, C.J., and Bonhoeffer, T., 2015. Precision of Inhibition: Dendritic Inhibition by Individual GABAergic Synapses on Hippocampal Pyramidal Cells Is Confined in Space and Time. *Neuron*, 87 (3), 576–589.
- Nelson, S.B. and Valakh, V., 2015. Excitatory/Inhibitory Balance and Circuit Homeostasis in Autism Spectrum Disorders. *Neuron*, 87 (4), 684–698.
- Oh, W.C., Lutzu, S., Castillo, P.E., and Kwon, H.-B., 2016. De novo synaptogenesis induced by GABA in the developing mouse cortex. *Science*, 353 (6303), 1037–1040.
- Oinuma, I., Katoh, H., and Negishi, M., 2006. Semaphorin 4D/Plexin-B1-mediated R-Ras GAP activity inhibits cell migration by regulating  $\beta$  1 integrin activity. *The Journal of Cell Biology*, 173 (4), 601–613.
- Orr, B.O., Fetter, R.D., and Davis, G.W., 2017. Retrograde semaphorin-plexin signalling drives homeostatic synaptic plasticity. *Nature*, 550 (7674), 109–113.
- Paradis, S., Harrar, D.B., Lin, Y., Koon, A.C., Hauser, J.L., Griffith, E.C., Zhu, L., Brass, L.F., Chen, C., and Greenberg, M.E., 2007. An RNAi-based approach identifies molecules required for glutamatergic and GABAergic synapse development. *Neuron*, 53 (2), 217–32.
- Pasterkamp, R.J., 2012. Getting neural circuits into shape with semaphorins. *Nature Reviews Neuroscience*, 13 (9), 605–618.
- Peng, Y., Huentelman, M., Smith, C., and Qiu, S., 2013. MET Receptor Tyrosine Kinase as an Autism Genetic Risk Factor. In: *International Review of Neurobiology*. 135–165.

- Piccioli, Z.D. and Littleton, J.T., 2014. Retrograde BMP Signaling Modulates Rapid Activity-Dependent Synaptic Growth via Presynaptic LIM Kinase Regulation of Cofilin. *Journal of Neuroscience*, 34 (12), 4371–4381.
- Qiu, S., Lu, Z., and Levitt, P., 2014. MET Receptor Tyrosine Kinase Controls Dendritic Complexity, Spine Morphogenesis, and Glutamatergic Synapse Maturation in the Hippocampus. *The Journal of Neuroscience*, 34 (49), 16166–16179.
- Raissi, A.J., Staudenmaier, E.K., David, S., Hu, L., and Paradis, S., 2013. Sema4D localizes to synapses and regulates GABAergic synapse development as a membrane-bound molecule in the mammalian hippocampus. *Molecular and Cellular Neuroscience*, 57 (781), 23–32.
- Rex, C.S., Chen, L.Y., Sharma, A., Liu, J., Babayan, A.H., Gall, C.M., and Lynch, G., 2009. Different Rho GTPase-dependent signaling pathways initiate sequential steps in the consolidation of long-term potentiation. *The Journal of Cell Biology*, 186 (1), 85–97.
- Schuemann, A., Klawiter, A., Bonhoeffer, T., and Wierenga, C.J., 2013. Structural plasticity of GABAergic axons is regulated by network activity and GABAA receptor activation. *Frontiers in neural circuits*, 7 (June), 113.
- Siddiqui, T.J. and Craig, A.M., 2011. Synaptic organizing complexes. *Current Opinion in Neurobiology*, 21 (1), 132–143.
- Sprekeler, H., 2017. Functional consequences of inhibitory plasticity: homeostasis, the excitation-inhibition balance and beyond. *Current Opinion in Neurobiology*, 43, 198–203.
- Staras, K., 2007. Share and share alike: trading of presynaptic elements between central synapses. *Trends in neurosciences*, 30 (6), 292–8.
- Suarez, C., Carroll, R.T., Burke, T.A., Christensen, J.R., Bestul, A.J., Sees, J.A., James, M.L., Sirotkin, V., and Kovar, D.R., 2015. Profilin Regulates F-Actin Network Homeostasis by Favoring Formin over Arp2/3 Complex. *Developmental Cell*, 32 (1), 43–53.
- Sun, T., Krishnan, R., and Swiercz, J.M., 2012. Grb2 mediates semaphorin-4D-dependent RhoA inactivation. *Journal of Cell Science*, 125 (15), 3557–3567.
- Swiercz, J.M., Worzfeld, T., and Offermanns, S., 2008. ErbB-2 and Met Reciprocally Regulate Cellular Signaling via Plexin-B1. *Journal of Biological Chemistry*, 283 (4), 1893–1901.
- Tyndall, S.J. and Walikonis, R.S., 2006. The Receptor Tyrosine Kinase Met and Its Ligand Hepatocyte Growth Factor are Clustered at Excitatory Synapses and Can Enhance Clustering of Synaptic Proteins. *Cell Cycle*, 5 (14), 1560–1568.
- Villa, K.L., Berry, K.P., Subramanian, J., Cha, J.W., Oh, W.C., Kwon, H.B., Kubota, Y., So, P.T.C., and Nedivi, E., 2016. Inhibitory Synapses Are Repeatedly Assembled and Removed at Persistent Sites In Vivo. *Neuron*, 89 (4), 756–769.

- 
- Wierenga, C.J., 2017. Live imaging of inhibitory axons: Synapse formation as a dynamic trial-and-error process. *Brain Research Bulletin*, 129, 43–49.
- Wierenga, C.J., Becker, N., and Bonhoeffer, T., 2008. GABAergic synapses are formed without the involvement of dendritic protrusions. *Nature neuroscience*, 11 (9), 1044–52.
- Wierenga, C.J., Müllner, F.E., Rinke, I., Keck, T., Stein, V., and Bonhoeffer, T., 2010. Molecular and electrophysiological characterization of GFP-expressing CA1 interneurons in GAD65-GFP mice. *PLoS one*, 5 (12), e15915.
- Xie, Z., Eagleson, K.L., Wu, H.-H., and Levitt, P., 2016. Hepatocyte Growth Factor Modulates MET Receptor Tyrosine Kinase and  $\beta$ -Catenin Functional Interactions to Enhance Synapse Formation. *eNeuro*, 3 (4).
- Zhou, Y., Gunput, R.A.F., and Pasterkamp, R.J., 2008. Semaphorin signaling: progress made and promises ahead. *Trends in Biochemical Sciences*, 33 (4), 161–170.





5

## General Discussion

---



Neurons have the ability to shape their synapses in response to the signals they receive. By doing so, our brains can learn and adapt by storing and retrieving new information from neural networks. Uncovering the rules that drive synaptic plasticity is an exciting yet challenging quest. My research focused on synapses formed by inhibitory neurons onto excitatory principal cells. As excitatory activity can recruit additional excitation, a regulatory mechanism is required to prevent run-away activity that disturbs neuronal communication. Inhibition fulfills this regulatory role by determining which signals are allowed to pass. Thus, inhibitory synapses can act as gatekeepers by filtering out unnecessary information. Inhibition is itself subject to tight regulation and too much or too little can lead to neurological complications (Marín 2012). We discovered that excitatory synaptic activity can regulate inhibitory synapses within a dendritic branch as discussed in chapter 2. Here I explore possible underlying mechanisms and discuss the implications of this finding.

### **Inhibitory bouton growth**

Within the axon, synaptic vesicles and active zone proteins are mobile and can be transported between presynaptic terminals (Darcy *et al.* 2006, Staras 2007, Bury and Sabo 2011). In addition to sharing, this allows axons to rapidly form functional neurotransmitter release sites which can be highly mobile (Krueger *et al.* 2003). During our experiments, the inhibitory bouton growth appeared rapidly, yet often the new bouton did not persist for the entire duration of the experiment. The rapid formation of inhibitory boutons suggest that presynaptic vesicles rapidly accumulate from the axon. With the time resolution of our experiments (imaging every 5 minutes), we were not able to fully capture exchange between boutons. However, I did occasionally observe axonal dilations which appeared to move along the axon, which may reflect nascent bouton formation or translocation of presynaptic proteins.

The newly formed boutons often did not persist throughout the experiment, which suggests that there are separate signals for triggering bouton formation and for their maintenance. Indeed, the existence of separate signals is consistent with our Sema4D study (Frias *et al.* 2018), where we found that Sema4D signaling is specifically involved in bouton stabilization (e.g. maintenance), but not in triggering the formation of new boutons. At this point, we do not know what is required to transform the newly formed boutons of chapter 2 into functional inhibitory synapses. It could simply be time, but it may also require specific patterns of activity. For instance, it is plausible that a stronger or longer spine stimulation would promote longer lasting bouton growth. In future studies, it would be interesting to test if this would promote larger growth or longer duration of the inhibitory bouton. There are multiple strategies for increasing the local spine stimulation. For instance, patching the dendrite would provide a better control over the dendritic membrane potential compared to patching the soma, as long neurites distort the ability to clamp the voltage (Bar-Yehuda and Korngreen 2008). Dendritic depolarization would thus not suffer from distance dependent attenuation as in somatic depolarization. Alternatively, the internal potassium concentration could be lowered, depolarizing the resting membrane potential of the patched cell. It is unclear if postsynaptic activity is the decisive factor for stability of the nascent inhibitory

---

bouton, and this would be interesting to investigate further.

Sema4D is not likely to be involved in the inhibitory bouton growth after local spine stimulation as Sema4D signaling does not trigger the formation of *de novo* boutons (Frias *et al.* 2018). However, it would be interesting to test if Sema4D signaling after the first trigger of inhibitory bouton growth would be able to stabilize the new bouton. Of course, as we only took 4 baseline images before we start the uncaging stimulation (~15 minutes), we cannot exclude that the location where we observed bouton formation contained a bouton before.

The formation of a functional synapse requires a concurrent accumulation of both pre- and postsynaptic proteins. The development of the pre- and post-synapse is normally coordinated and the inhibitory presynaptic protein VGAT and the postsynaptic gephyrin both accumulate over several hours (Dobie and Craig 2011, Frias *et al.* 2018). The inhibitory bouton growth we observed after local spine stimulation occurs rapidly, and it is unclear if the postsynaptic proteins already accumulate at this time scale. Unfortunately, we did not follow the new boutons over longer time periods, as has been done before (Wierenga *et al.* 2008). Although in theory possible, in these experiments the numbers would be very low and as the post hoc immunostaining of a single bouton is not trivial, not much statistical power is to be expected from such an endeavor.

Competition between boutons may affect the likelihood of new bouton formation and maturation. In an interesting study, synaptic GABA<sub>A</sub> receptors were disrupted, which lowered the number of dendritic inhibitory synapses on the affected neurons. Unexpectedly, it was accompanied by an increase in dendritic inhibition in unaffected neighboring cells (Frola *et al.* 2013). This indicates that presynaptic axons can distinguish between the two types of dendrites – with and without GABA<sub>A</sub> receptors. It is known that neighboring presynaptic boutons compete with each other for presynaptic vesicles and proteins (Staras *et al.* 2010) and boutons made onto dendrites expressing GABA<sub>A</sub> receptors apparently have an advantage. Within a dendrite, competition may also occur between neighboring GABAergic synapses. As only a subset of inhibitory cells are labeled with GFP in the GAD65-GFP mouse used in our experiments, it is difficult to capture this competition (Wierenga *et al.* 2010).

One aspect that we cannot address in our experiments is if presynaptic activity (i.e. of the inhibitory axon) is required for the formation of the nascent inhibitory boutons after local spine stimulation or its subsequent maturation into a stable inhibitory synapse. It is currently not known how presynaptic activity affects inhibitory bouton lifetime or dynamics. Another interesting option would be that the activity of the inhibitory axon would need to be somehow correlated with the activity of the nearby excitatory inputs. In our experiment, we chose to activate four spines close to the inhibitory axon crossing, but their activity afterwards may be not at all correlated between each other and with the inhibitory axon and therefore the newly formed bouton will disappear quickly. In vivo, when clustered synaptic inputs may often be active together, new inhibitory boutons may be more easily stabilized.

## **E/I coordination through calcium**

The synaptic signal is transmitted from the pre- to the post-synapse, where the electrical component propagates throughout the neuron. Neuronal activity increases the calcium concentration that in turn is responsible for the activity-dependent, synaptic changes in size and number. Proteins activated through calcium signaling can spread from activated synapses to their non-activated neighbors, affecting neighboring synapses in a heterosynaptically manner. In our study, we observed heterosynaptic plasticity in inhibitory synapses induced by the activation of excitatory synapses within a small stretch of dendrite.

Our findings indicate that dendritic inhibition can be coordinated by nearby excitation through NMDA receptor activation. While the mechanisms involved are unknown, potential candidates can be found in CaMKII and calcineurin, prominent calcium sensitive kinase and phosphatase. The role of CaMKII in LTP and calcineurin in LTD has been well studied in excitatory synapses (Zhuo *et al.* 1999, Lisman *et al.* 2012). However, CaMKII and calcineurin also target inhibitory synaptic proteins. For instance, gephyrin, the main inhibitory scaffold protein, is activated by CaMKII $\alpha$ , which can phosphorylate gephyrin on Ser305 (Tyagarajan and Fritschy 2014). This CaMKII $\alpha$ -dependent phosphorylation increases the number of gephyrin clusters that colocalize with presynaptic GAD67 (Flores *et al.* 2015). GABA<sub>A</sub> receptors are another example of inhibitory synaptic proteins that can be phosphorylated by CaMKII $\alpha$ . The CaMKII $\alpha$ -dependent Ser383 phosphorylation of the  $\beta$ 3 subunit of the GABA<sub>A</sub> receptor, recruits gephyrin from the extrasynaptic membrane to the synapse and concomitantly confines GABA<sub>A</sub> receptors at the synapse and mediates inhibitory LTP (Petrini *et al.* 2014). Calcineurin is responsible for the opposite pathway and calcineurin dependent dephosphorylation of the  $\beta$ 3 subunit increases the lateral GABA<sub>A</sub> receptor diffusion and reduces gephyrin clustering (Bannai *et al.* 2009, Muir *et al.* 2010). Together, these studies show that CaMKII and calcineurin are capable of inducing symmetric heterosynaptic plasticity in both excitatory as inhibitory synapses, and thereby regulate dendritic inhibition and excitation in the same direction.

Symmetric heterosynaptic plasticity between excitatory and inhibitory synapses depends on the spatial range of calcium or the activated CaMKII and calcineurin. The CaMKII located at the excitatory synapse seems unlikely to fulfil this role as activated CaMKII remains at the spine by binding NMDA receptor (Strack and Colbran 1998, Penny and Gold 2018).

However, CaMKII is also present in the dendritic shaft and may coordinate excitatory and inhibitory plasticity from there. To activate CaMKII in the shaft, the calcium influx from single excitatory synapse activation may not be sufficient, as the calcium is usually restricted to the spine head (Chen and Sabatini 2012). The required calcium source could instead originate from VGCCs activated by local dendritic spikes or backpropagating action potentials, or calcium can be released from internal stores. By treating neurons with NMDA globally, it was found that moderate NMDA receptor activation induces CaMKII $\alpha$  localization towards inhibitory synapses, while stronger NMDA receptor activation (5-10 times higher NMDA concentrations) favors localization towards excitatory synapses (Marsden *et al.* 2010). It would be interesting for future studies to address in our experiments if localization of



---

CaMKII $\alpha$  towards the crossing of the inhibitory axon promotes inhibitory bouton growth.

What determines if and when CaMKII and calcineurin get activated in the synapse or in the shaft? Both proteins have high affinity to calcium (Teo and Wang 1973, Faas *et al.* 2011). CaMKII and calcineurin can be activated at the same time, and they interact as CaMKII prolongs its own activation through autophosphorylation. Through regulating PP1 activity, calcineurin can terminate this autophosphorylated state (Bradshaw *et al.* 2003, Mansuy 2003). Their relative activation is modulated by frequency, duration, and amplitude of the calcium signals with high frequency calcium activity favoring CaMKII while low frequency activation favors calcineurin (Li *et al.* 2012). Newly developed biosensors based on fluorescence resonance energy transfer (FRET) provide an opportunity to investigate the local activation of CaMKII and calcineurin (Lee *et al.* 2009, Wu *et al.* 2012). FRET between two fluorophores can happen when they are in close proximity and they have an overlapping emission and absorption spectrum. FRET sensors are designed to report the conformational change that occurs after activation as the active and inactive form have separate emission wavelengths. With these new biosensors it is now feasible to study CaMKII and calcineurin simultaneously (Fujii *et al.* 2013). By studying the spread of CaMKII and calcineurin activation together with dendritic inhibition would allow us to directly investigate their potential heterosynaptic action. However, it will require specialized equipment to visualize both sensors and perform glutamate uncaging (Fujii *et al.* 2013).

Asymmetric heterosynaptic plasticity can also occur between neighboring synapses. Dendritic spines are compartmentalized due to their thin spine necks, which form a bi-directional diffusion barrier (Svoboda *et al.* 1996). This causes a divergence between the calcium dynamics in activated synapses, neighboring spines, and the dendritic shaft, which can result in compartment specific activation of CaMKII or calcineurin. Thus, heterosynaptic plasticity can occur asymmetrically, where the activated synapse and neighboring synapses undergo opposite changes. This has been demonstrated in excitatory dendritic synapses, where NMDA receptor-dependent LTP is accompanied by calcineurin-dependent shrinkage in neighboring spines (Oh *et al.* 2015). Synaptic calcineurin is anchored to the postsynaptic density, but this anchoring is disrupted during strong NMDA receptor activation (Wyszynski *et al.* 1998, Sanderson *et al.* 2012). Unlike excitatory synapses, inhibitory synapses are not compartmentalized and located at the dendritic shaft. Inhibitory synapses are therefore not sheltered from the dendritic calcium and perhaps more sensitive to intracellular calcium dynamics. This structural difference may put inhibitory synapses in a favorable position to quickly adapt to changes in activity, which change the calcium dynamics in the dendrite.

The ability of CaMKII and calcineurin to affect both excitatory and inhibitory synapses may make any secondary coordinating signaling obsolete. Through CaMKII, NMDA receptor activation can induce inhibitory LTP by clustering gephyrin (Marsden *et al.* 2007, Petrini and Barberis 2014). However, the NMDA treatment used to activate these receptors also depresses excitation through AMPA receptor endocytosis in a calcineurin dependent manner. In this case excitatory and inhibitory plasticity both serve the same purpose, a decrease of neuronal activity, which both reduces neural activity. Recently, it was shown

that endogenous NMDA activation is also capable of potentiating input specific dendritic inhibition via insertion of GABA<sub>A</sub> receptors at existing synapses (Chiu *et al.* 2018). In our experiments, we found a mechanism for structural growth of nascent inhibitory boutons. In our case, NMDA receptor activation was also required, but it was not sufficient to induce bouton growth in our experiments, as it also requires the activation of the endocannabinoid receptor CB1.

In addition to CaMKII and calcineurin activation, there are other mechanisms that may also link excitation and inhibition. For instance, glutamate can also affect inhibition through metabotropic glutamate receptors (mGluRs). Besides their more established role in excitatory LTD (Jones 2017), mGluR activation can induce GABA<sub>A</sub>R clustering (Bannai *et al.* 2015). The group I mGluR dependent activation of protein kinase C (PKC) results in phosphorylation dependent clustering of GABA<sub>A</sub> receptors, which counteracts calcineurin-dependent dispersion after NMDA receptor activation (Sanderson *et al.* 2012, Bannai *et al.* 2015). Furthermore, ambient levels of glutamate are enough to induce tonic activation of group I mGluRs (Smolders *et al.* 2004). This suggests a role for these mGluRs in the maintenance of GABA<sub>A</sub>Rs clusters.

Through common pathways, postsynaptic calcium signaling affects both excitation and inhibition. Which factor coordinates excitation and inhibition remains to be determined. However, it is likely that CaMKII and calcineurin play an important part in this as they can affect both excitatory and inhibitory synaptic plasticity. To study their involvement, CaMKII or calcineurin can be separately isolated by adding a selective inhibitor in the bath. If CaMKII activity is involved in the activity-dependent inhibitory bouton formation in our experiments, blocking CaMKII should block this formation. Blocking calcineurin may potentiate the observed growth as calcineurin also dephosphorylates CaMKII.

### **Retrograde signaling, from dendrite to axon**

Synapses can only function if both pre- and postsynaptic sides are both functional and opposed to each other. To achieve this, pre- and postsynaptic partners must be able to communicate their presence towards each other. In addition to anterograde signaling such as neurotransmitter release, from axon to dendrite, retrograde signaling from dendrite to axon also plays a large role in synapse plasticity. Our findings show a role for the retrograde messenger endocannabinoid 2-AG. The activity dependent bouton growth we found was dependent on the activation of the CB1 receptor. This bridging role between postsynaptic excitation and presynaptic inhibition may not be unique to 2-AG as other retrograde messengers, such as brain-derived neurotrophic factor (BDNF), and nitric oxide are also released from the dendrite (Fitzsimonds and Poo 1998).

Retrograde signals can only affect the synaptic inhibition if they reach the inhibitory axon. Brain tissue is extremely crowded, which restricts the distance that the retrograde messengers can travel. This spatial restraint is not only due to diffusion but also reactivity. For instance, nitric oxide, a gaseous retrograde messenger, is restricted to the immediate

---

surroundings from the synapse where it is released due to its high consumption rate (Hall and Garthwaite 2009). Thus, the release site of the retrograde messengers is important, and these messengers need to be released from the dendrite in close proximity to their target.

## **BDNF**

BDNF is a prominent neurotrophin that plays a role in a number of synapse related processes such as synaptogenesis, LTP, but also LTD (Gottmann *et al.* 2009). Vesicles carrying BDNF can be secreted from both the dendrite as the axon, after which it binds to the TrkB receptors. These receptors are found on both sides of the synapse and can thus induce retrograde, anterograde, or autocrine signaling (Leßmann and Brigadski 2009, Harward *et al.* 2016). The release BDNF is activity dependent and the amount of activity corresponds to the amount of secretion. At the dendrite, BDNF release may be restricted to single spines during targeted glutamate uncaging (Harward *et al.* 2016, Hedrick *et al.* 2016). However, during backpropagating action potentials, BDNF can be released globally throughout the dendritic tree (Kuczewski *et al.* 2008).

During our experiments, BDNF is likely released from the dendrite, as the stimulation protocol we used combined glutamate uncaging and depolarization. To explore the possible involvement of BDNF in the reported inhibitory synapse growth, we chose to investigate the effects of BDNF signaling on inhibitory bouton dynamics. In our experiments, where BDNF was locally applied, we did not observe a difference in bouton growth compared to the control. This result seems counterintuitive as BDNF signaling is known to modulate inhibitory synapses (Huang *et al.* 1999, Ohba *et al.* 2005, Fiorentino *et al.* 2009), however the outcome of BDNF signaling depends on the duration of BDNF exposure as chronic or transient signaling can have different outcomes.

Chronic application of exogenous BDNF over several days increases the number of excitatory and inhibitory synapses (Bolton *et al.* 2000, Bamji *et al.* 2006). At the pre-synapse, acute application of BDNF over several minutes results in an increased neurotransmitter release probability by increasing the size of readily releasable pool of neurotransmitter vesicles (Jovanovic *et al.* 1996, Simsek-Duran and Lonart 2008). However, this does not seem to translate into a potentiation of inhibition, as recordings of inhibitory postsynaptic currents (IPSCs) were depressed within 10 minutes after applying BDNF (Tanaka *et al.* 1997, Brünig *et al.* 2001). This was mediated through protein phosphatase 2A (PP2A), which dephosphorylates GABA<sub>A</sub> receptors and by doing so mobilizes the receptors and reduces their surface expression. Furthermore, IPSCs were enhanced in neurons of the BDNF knockout mouse, showing a suppressing role for BDNF signaling on inhibition (Henneberger *et al.* 2013). Interestingly, GABAergic depression after BDNF treatment is preceded by BDNF dependent potentiation of inhibition through activating PKC, which phosphorylates and stabilizes the GABA<sub>A</sub> receptors (Jovanovic 2004). Brief BDNF activation, as in our experiments, may thus favor inhibitory potentiation over depression. However, the activation of the TrkB receptor may last for minutes after the BDNF has been secreted, making it difficult to predict the outcome (Hedrick *et al.* 2016).

The ability of BDNF to function as a retrograde messenger and to affect inhibitory synapses lead us to study whether BDNF also influences inhibitory bouton dynamics. Our findings show that brief BDNF application, which was shown to locally trigger fast calcium transients in developing neurons (Lang *et al.* 2007), does not influence inhibitory bouton dynamics. However, this does not exclude a role for BDNF in inhibitory synapse formation as the action of BDNF signaling depends on duration and location. Furthermore, BDNF may play a cooperative role with other messengers such as endocannabinoids (Maison *et al.* 2009). To exclude the role of BDNF in the bouton growth we reported, local stimulation could be repeated while blocking the TrkB receptors.

### **Endocannabinoids**

Endocannabinoids (eCB) are lipid messengers that can modulate synapse function. They are released from the dendrite and act retrogradely on receptors located on the axon where they are mostly known for suppressing neurotransmitter release (Hashimoto *et al.* 2007, Alger and Kim 2011, Castillo *et al.* 2012, Piomelli 2014). The most abundant eCB in the central nervous system, 2-Arachidonoylglycerol (2-AG) is released in an activity dependent manner through either an increase of intracellular calcium or by mGluR activation (Maejima *et al.* 2001, Ohno-Shosaku *et al.* 2001). By activating the CB1 receptor on the axon, eCBs can modulate synaptic plasticity transiently or persistently.

On the short-term, a few seconds of eCB signaling can suppress inhibition after short depolarizations by attenuating presynaptic calcium influx through the VGCCs by G-protein activation (Wilson and Nicoll 2001). Longer eCB signaling, lasting a few minutes, is able to induce long term depression (Llano *et al.* 1991, Chevaleyre and Castillo 2003). eCB dependent LTD is mediated by inhibiting adenylyl cyclase, which downregulates PKA that suppresses neurotransmitter release (Chevaleyre *et al.* 2007). Downregulation of PKA also shifts the kinase and phosphatase activity, as concurrent presynaptic calcineurin activation is shown to be involved in eCB dependent LTD (Heifets *et al.* 2008).

In contrast with the well-established depressing role of eCB, recent studies show eCB signaling can also induce potentiation (Cui *et al.* 2015, Wang *et al.* 2016). The duration and frequency of eCB signaling is important as prolonged and moderate eCB induce LTD, while short and large eCB transients favor LTP at excitatory synapses (Cui *et al.* 2016). This switch seems to depend on the kinase and phosphatase activity as PKA was involved in LTP, while calcineurin mediates LTD. The target for phosphorylation remains to be determined. Our findings suggest that a similar mechanism may occur at inhibitory synapses, as we found that activation of CB1 receptor by 2-AG can trigger inhibitory bouton growth.

If the mechanisms are similar, the activity dependent inhibitory bouton growth is expected to be dependent on PKA. This can be addressed by repeating the experiment and blocking PKA activity. However, local LTD induction on the inhibitory axon does not necessarily contradict inhibitory bouton growth. As presynaptic elements can be shared between synapses, induction of LTD at one synapse may free up resources to form or potentiate a neighboring bouton (Staras 2007).

---

## Retrograde signaling without messengers

Our findings imply an important role for the retrograde messenger endocannabinoid 2-AG, but it is possible that GABAergic synapse growth occurs without the involvement of retrograde messenger signaling. In the scenario where no retrograde messenger is secreted, the dendrite plays the central role, with the post-synapse forming first and the subsequent induction of local bouton formation.

The dendrite must be able to differentiate between the connections it receives in order to target the correct proteins to their destination. Cell adhesion molecules, which bridge the pre- and post-synapse and connect the neurons, can also signal the synaptic partner and induce synapse specific growth. Amongst the neuronal cell adhesion molecules, GABAergic synapse formation can be driven by Neuroligin-2. Neuroligin-2, together with its presynaptic partner  $\beta$ -Neurexin, are known to interact with gephyrin, the postsynaptic inhibitory scaffold protein (Varoqueaux *et al.* 2004). Neuroligins expressed in non-neuronal cells can even induce the formation of presynaptic terminals in contacting axons, demonstrating their synaptogenic potential (Scheiffele *et al.* 2000). Gephyrin interacts with Neuroligin-2, and together with collybistin, which attaches gephyrin to the membrane, they have been shown to induce perisomatic inhibitory synapse formation (Poulopoulos *et al.* 2009). Separate from its interaction with Neuroligin-2, gephyrin is also required for clustering synaptic GABA<sub>A</sub> receptors (Kneussel *et al.* 1999). The number and size of gephyrin clusters, coincide with changes in GABAergic transmission, presumably through synapse formation and GABA<sub>A</sub> receptor recruitment (Tyagarajan *et al.* 2013). Interestingly, gephyrin cluster formation is also dependent on the presence of GABA<sub>A</sub> receptors (Tyagarajan and Fritschy 2014).

During our experiments, it is possible that Neuroligin-2 or gephyrin clusters were localized at the nascent inhibitory bouton. Their involvement can be studied by overexpressing fluorescently labeled proteins. Although, the synaptogenic properties of Neuroligin-2 may affect the chance of inhibitory bouton formation as well, it may also inform us whether Neuroligin-2 is the limiting factor determining the duration of nascent boutons.

## Bi-directional coordination of excitation and inhibition?

In our study, we used a targeted LTP inducing stimulus selectively at several excitatory synapses and observed an inhibitory synapse growing in response. By inducing targeted LTD instead, it could be examined whether excitation and inhibition is also coordinated in the opposite direction. After all, with reduced excitation, the need for inhibitory regulation would also be reduced. Using the same techniques already at our disposal, this could be investigated with a glutamate uncaging based LTD inducing protocol. Despite their opposing roles, the protocol to induce LTP or LTD differs little as both calcineurin and CaMKII can be activated by calcium resulting from glutamate uncaging. LTD can be achieved by using longer uncaging pulses while blocking synaptic transmission and depolarizing the membrane (Kandler *et al.* 1998). Alternatively, applying uncaging pulses at a low frequency also induces LTD, which interestingly occurs through non-ionotropic signaling from the NMDA receptor (Stein *et al.* 2015). Inducing LTD throughout the dendritic branch may result in a global activation of calcineurin that in parallel induces inhibitory LTD, which could be investigated

by studying the inhibitory bouton size.

If inhibitory plasticity can follow changes in excitation, would excitatory plasticity also follow local changes in inhibition? Extrapolating from our results, one might predict that a local increase in inhibition would lead to an excitatory compensatory potentiation. In this case, the coordination between excitation and inhibition would be bi-directional. To investigate this, however, we would have to expand our experimental toolbox as there is currently no selective protocol to induce inhibitory LTP at single synapses. With a different approach using GABA uncaging together with glutamate uncaging we may be able to study this potential bi-directional coupling (Passlick *et al.* 2017). By gradually increasing the amount of uncaged GABA, GABA uncaging can be used as a proxy for inhibitory synapse potentiation. The combination of glutamate uncaging at several excitatory spines with a gradual increased GABA uncaging, the excitatory signal would become increasingly attenuated within the dendrite. If the coupling between excitation and dendritic inhibition is bi-directional, excitation can be expected to potentiate in response to this increased inhibition. After considering the physiological dynamics of the excitatory spines, any additional spine growth would imply a coupling. However, pairing excitation and inhibition is likely result in excitatory depression as both the excitatory signal and the resulting calcium influx are directly attenuated by the inhibition.

### **Clustered plasticity & Impact of local dendritic inhibition**

Dendrites actively shape incoming signals through voltage gated channels, which can result in non-linear dendritic spikes. By preprocessing signals, the dendrite performs the first computational steps by deciding which signals are actively forwarded towards the soma. To drive non-linear summation, synchronized synaptic inputs are required. Perhaps to this end, clusters of neighboring excitatory spines are frequently co-activated (Kleindienst *et al.* 2011, Takahashi *et al.* 2012, Bloss *et al.* 2018). Through a combination of hyperpolarization and shunting, dendritic inhibition is most effective locally, making it the ideal candidate for regulating clustered activity. Besides activity, synaptic plasticity can also spread and affect neighboring synapses heterosynaptically by sharing proteins involved in plasticity. This shared heterosynaptic plasticity may facilitate the formation of co-active clusters of synapses. As inhibition affects activity, so too will it affect activity dependent plasticity.

Cross-talk between spines together with synchronized clustered activity imply that the dendrite operates largely separate from the soma, shaping its own connections and processing incoming activity (Branco and Häusser 2010). Dendritic inhibition is a complementary addition to local computation and is well positioned to regulate activity and calcium dependent processes within the dendrite. By acting on the non-linear summation of incoming inputs, inhibition can effectively fulfill its regulatory role, despite being outnumbered. Interestingly, roughly 30% of dendritic inhibitory synapses connect onto a single excitatory spine rather than the dendritic shaft, resulting in a dually-innervated synapse (Kubota *et al.* 2007). Dual innervation occurs on the largest and most stable spines, and allows for highly local control by inhibition (Chiu *et al.* 2013, Villa *et al.* 2016). Although these dually-innervated synapses are less common, the relationship between dual-innervation with stability and size suggests

---

that inhibition can be locally recruited towards excitation, as synapse size and strength are related. Perhaps underlying the formation of dually-innervated synapses are the same mechanisms responsible for the inhibitory bouton growth after local excitation.

### **Studying local synaptic plasticity**

A limitation of the techniques we used is that while we can quantify inhibitory synapse growth, we cannot measure the responding inhibitory synapse activity. After all it is impossible to trace back the synaptic source of an electrical signal through electrophysiology. As a result, we have not been able to investigate several interesting questions about the implications of inhibitory bouton growth. Here I discuss these questions and propose how they could still be addressed.

Despite being outnumbered by excitatory synapses, inhibitory synapses are capable of regulating excitatory activity, suggesting that inhibitory synapses carry more weight. This raises the question, how tightly are excitation and inhibition balanced? If inhibitory synapses are stronger but less numerous, it is possible that excitation and inhibition within subcellular compartments along the dendrite are not balanced at all. Extrasynaptic GABA<sub>A</sub> receptors also contribute to the inhibition, which makes it necessary to have a functional readout of inhibition. To investigate this question, both excitation and inhibition can be spatially mapped, through sequential glutamate and GABA uncaging. This would allow direct comparison between postsynaptic excitability and inhibition for individual dendrites.

Additional insight may be gained from studying both pre- and postsynaptic sides simultaneously. To achieve this, fluorescent labeled synaptic proteins can be used to study synapse formation in live cells. Although care has to be taken when overexpressing proteins, as the very aspect we are studying may become perturbed, it does grant the ability to localize and quantify the protein of interest. By using fluorescently labeled gephyrin, our study could be extended to study whether axonal inhibitory bouton formation is preceded by postsynaptic gephyrin clustering. Our previous findings suggest that VGAT precedes gephyrin in spontaneous inhibitory synapse formation (Frias *et al.* 2018), though this may differ in activity dependent plasticity.

While we have shown that the mechanism to locally regulate inhibition exists, it remains to be investigated how neuronal activity utilizes it physiologically. Our experiments grant a large degree of spatial control over excitation, but however, they are also time consuming which restricts the number of possible experiments and observations. Perhaps a more global approach is the next step in investigating the relationship between excitation and inhibition. For instance, this can be achieved by recording both the timing and location of neuronal activity together with the number and size of inhibitory synapses. Neuronal activity can be recorded by using calcium sensors such as GCaMP6, which is genetically encoded (Chen *et al.* 2013). Overexpressing GCaMP6 in neuronal cells allows calcium transients to be visualized at subcellular compartments, even in dendritic spines. By recording activity together with inhibitory bouton dynamics, it could be investigated how frequently the activity dependent bouton growth we observed occurs spontaneously, without stimulation.

The mechanisms involved may also be easier to study on a larger scale and frequency at which the inhibitory bouton forms after a spontaneous increase in activity may tell us more about the importance of the bouton formation.

A single neuron can make thousands of synapses, these large numbers makes tracking synapse dynamics over time on a global scale challenging. Ideally, analysis should be quick, easy, reproducible, and flexible as experiments tend to change as we gain more insight. To study large numbers of neurites and synapses, our current semi-automated analysis tools would benefit from more automation. As experimental conditions can vary, and analysis often requires an experienced eye, fully automated analysis will remain less reliable as misclassification will occur. However, for large enough numbers of synapses, fully automated analysis would still be able to capture the dynamics reliably. Even for a small dataset, automated analysis can serve as a starting point, giving the initial estimates, which can still be further fine-tuned.

### **Concluding remarks**

To learn and adapt, information is stored in networks of neurons which are connected by plastic synapses. The fundamental aspects governing synapse dynamics are essential to this. In my thesis, I described our findings on the dendritic coordination between excitation and inhibition. Our work offers new insight in the formation and potentiation of inhibitory synapses. Although we are only starting to understand the cellular mechanisms driving this coordination, the future direction has been set.





## References

- Alger, B.E. and Kim, J., 2011. Supply and demand for endocannabinoids. *Trends in Neurosciences*, 34 (6), 304–315.
- Bamji, S.X., Rico, B., Kimes, N., and Reichardt, L.F., 2006. BDNF mobilizes synaptic vesicles and enhances synapse formation by disrupting cadherin- $\beta$ -catenin interactions. *Journal of Cell Biology*, 174 (2), 289–299.
- Bannai, H., Lévi, S., Schweizer, C., Inoue, T., Launey, T., Racine, V., Sibarita, J.-B., Mikoshiba, K., and Triller, A., 2009. Activity-dependent tuning of inhibitory neurotransmission based on GABAAR diffusion dynamics. *Neuron*, 62 (5), 670–82.
- Bannai, H., Niwa, F., Sherwood, M.W., Le, S., Triller, A., Mikoshiba, K., Bannai, H., Niwa, F., Sherwood, M.W., Shrivastava, A.N., and Arizono, M., 2015. Bidirectional Control of Synaptic GABA A R Clustering by Glutamate and Calcium Article Bidirectional Control of Synaptic GABA A R Clustering by Glutamate and Calcium. *Cell Reports*, 13 (12), 2768–2780.
- Bar-Yehuda, D. and Korngreen, A., 2008. Space-Clamp Problems When Voltage Clamping Neurons Expressing Voltage-Gated Conductances. *Journal of Neurophysiology*, 99 (3), 1127–1136.
- Bloss, E.B., Cembrowski, M.S., Karsh, B., Colonell, J., Fetter, R.D., and Spruston, N., 2018. Single excitatory axons form clustered synapses onto CA1 pyramidal cell dendrites. *Nature Neuroscience*, 21 (3), 353–363.
- Bolton, M.M., Pittman, A.J., and Lo, D.C., 2000. Brain-derived neurotrophic factor differentially regulates excitatory and inhibitory synaptic transmission in hippocampal cultures. *Journal of Neuroscience*, 20 (9), 3221–32.
- Bradshaw, J.M., Kubota, Y., Meyer, T., and Schulman, H., 2003. An ultrasensitive Ca<sup>2+</sup>/calmodulin-dependent protein kinase II-protein phosphatase 1 switch facilitates specificity in postsynaptic calcium signaling. *Proceedings of the National Academy of Sciences*, 100 (18), 10512–10517.
- Branco, T. and Häusser, M., 2010. The single dendritic branch as a fundamental functional unit in the nervous system. *Current opinion in neurobiology*, 20 (4), 494–502.
- Brüning, I., Penschuck, S., Berninger, B., Benson, J., and Fritschy, J.M., 2001. BDNF reduces miniature inhibitory postsynaptic currents by rapid downregulation of GABA<sub>A</sub> receptor surface expression. *European Journal of Neuroscience*, 13 (7), 1320–1328.
- Bury, L.A.D. and Sabo, S.L., 2011. Coordinated trafficking of synaptic vesicle and active zone proteins prior to synapse formation. *Neural development*, 6 (1), 24.
- Castillo, P.E., Younts, T.J., Chávez, A.E., and Hashimoto, Y., 2012. Endocannabinoid Signaling and Synaptic Function. *Neuron*, 76 (1), 70–81.
- Chen, T., Wardill, T.J., Sun, Y., Pulver, S.R., Renninger, S.L., Baohan, A., Schreiter, E.R., Kerr, R.A., Orger, M.B., Jayaraman, V., Looger, L.L., Svoboda, K., and Kim, D.S., 2013. Ultrasensitive fluorescent proteins for imaging neuronal activity. *Nature*, 499 (7458), 295–300.
- Chen, Y. and Sabatini, B.L., 2012. Signaling in dendritic spines and spine microdomains. *Current Opinion in Neurobiology*, 22 (3), 389–396.

- 
- Chevalleyre, V. and Castillo, P.E., 2003. Heterosynaptic LTD of hippocampal GABAergic synapses: A novel role of endocannabinoids in regulating excitability. *Neuron*, 38 (3), 461–472.
- Chevalleyre, V., Heifets, B.D., Kaeser, P.S., Südhof, T.C., Purpura, D.P., and Castillo, P.E., 2007. Endocannabinoid-Mediated Long-Term Plasticity Requires cAMP/PKA Signaling and RIM1 $\alpha$ . *Neuron*, 54 (5), 801–812.
- Chiu, C., Lur, G., and Morse, T., 2013. Compartmentalization of GABAergic inhibition by dendritic spines. *Science*, 340 (May), 759–762.
- Chiu, C.Q., Martenson, J.S., Yamazaki, M., Natsume, R., Sakimura, K., Tomita, S., Tavalin, S.J., and Higley, M.J., 2018. Input-Specific NMDAR-Dependent Potentiation of Dendritic GABAergic Inhibition. *Neuron*, 97 (2), 368–377.e3.
- Cui, Y., Paillé, V., Xu, H., Genet, S., Delord, B., Fino, E., Berry, H., and Venance, L., 2015. Endocannabinoids mediate bidirectional striatal spike-timing-dependent plasticity. *Journal of Physiology*, 593 (13), 2833–2849.
- Cui, Y., Prokin, I., Xu, H., Delord, B., Genet, S., Venance, L., and Berry, H., 2016. Endocannabinoid dynamics gate spike-timing dependent depression and potentiation. *eLife*, 5 (FEBRUARY2016), 1–32.
- Darcy, K.J., Staras, K., Collinson, L.M., and Goda, Y., 2006. Constitutive sharing of recycling synaptic vesicles between presynaptic boutons. *Nature neuroscience*, 9 (3), 315–21.
- Dobie, F.A. and Craig, A.M., 2011. Inhibitory Synapse Dynamics: Coordinated Presynaptic and Postsynaptic Mobility and the Major Contribution of Recycled Vesicles to New Synapse Formation. *Journal of Neuroscience*, 31 (29), 10481–10493.
- Faas, G.C., Raghavachari, S., Lisman, J.E., and Mody, I., 2011. Calmodulin as a direct detector of Ca<sup>2+</sup> signals. *Nature Neuroscience*, 14 (3), 301–304.
- Fiorentino, H., Kuczewski, N., Diabira, D., Ferrand, N., Pangalos, M.N., Porcher, C., and Gaiarsa, J., 2009. GABAB receptor activation triggers BDNF release and promotes the maturation of GABAergic synapses. *Journal of Neuroscience*, 29 (37), 11650–11661.
- Fitzsimonds, R.M. and Poo, M., 1998. Retrograde Signaling in the Development and Modification of Synapses. *Physiological Reviews*, 78 (1), 143 LP-170.
- Flores, C.E., Nikonenko, I., Mendez, P., Fritschy, J.-M., Tyagarajan, S.K., and Muller, D., 2015. Activity-dependent inhibitory synapse remodeling through gephyrin phosphorylation. *Proceedings of the National Academy of Sciences of the United States of America*, 112 (1), E65-72.
- Frias, C.P., Bresser, T., Scheefhals, L., Hu, H.Y., Van Bergen en Henegouwen, P.M.P., Hoogenraad, C.C., and Wierenga, C.J., 2018. Semaphorin4D induces inhibitory synapse formation by rapid stabilization of presynaptic boutons via MET co-activation. *BioRxiv*, 100271, doi: <https://doi.org/10.1101/100271>.
- Frola, E., Patrizi, A., Goetz, T., Medrihan, L., Petrini, E.M., Barberis, A., Wulff, P., Wisden, W., and Sassoè-Pognetto, M., 2013. Synaptic Competition Sculpt the Development of GABAergic Axo-Dendritic but Not Perisomatic Synapses. *PLoS ONE*, 8 (2).

- Fujii, H., Inoue, M., Okuno, H., Sano, Y., Takemoto-Kimura, S., Kitamura, K., Kano, M., and Bito, H., 2013. Nonlinear Decoding and Asymmetric Representation of Neuronal Input Information by CaMKII $\alpha$  and Calcineurin. *Cell Reports*, 3 (4), 978–987.
- Gottmann, K., Mittmann, T., and Lessmann, V., 2009. BDNF signaling in the formation, maturation and plasticity of glutamatergic and GABAergic synapses. *Experimental Brain Research*, 199 (3–4), 203–234.
- Hall, C.N. and Garthwaite, J., 2009. What is the real physiological NO concentration in vivo? *Nitric Oxide - Biology and Chemistry*, 21 (2), 92–103.
- Harward, S.C., Hedrick, N.G., Hall, C.E., Parra-Bueno, P., Milner, T.A., Pan, E., Laviv, T., Hempstead, B.L., Yasuda, R., and McNamara, J.O., 2016. Autocrine BDNF–TrkB signalling within a single dendritic spine. *Nature*, 538 (7623), 99–103.
- Hashimotodani, Y., Ohno-shosaku, T., and Kano, M., 2007. Ca<sup>2+</sup>-assisted receptor-driven endocannabinoid release: mechanisms that associate presynaptic and postsynaptic activities. *Current Opinion in Neurobiology*, 17, 360–365.
- Hedrick, N.G., Harward, S.C., Hall, C.E., Murakoshi, H., McNamara, J.O., and Yasuda, R., 2016. Rho GTPase complementation underlies BDNF-dependent homo- and heterosynaptic plasticity. *Nature*, 538 (7623), 104–108.
- Heifets, B.D., Chevaleyre, V., and Castillo, P.E., 2008. Interneuron activity controls endocannabinoid-mediated presynaptic plasticity through calcineurin. *Proceedings of the National Academy of Sciences*, 105 (29), 10250–10255.
- Henneberger, C., Bard, L., King, C., Jennings, A., and Rusakov, D. a, 2013. NMDA receptor activation: two targets for two co-agonists. *Neurochemical research*, 38 (6), 1156–62.
- Huang, Z.J., Kirkwood, A., Pizzorusso, T., Porciatti, V., Morales, B., Bear, M.F., Maffei, L., and Tonegawa, S., 1999. BDNF regulates the maturation of inhibition and the critical period of plasticity in mouse visual cortex. *Cell*, 98 (6), 739–755.
- Jones, O.D., 2017. Do group I metabotropic glutamate receptors mediate LTD? *Neurobiology of Learning and Memory*, 138, 85–97.
- Jovanovic, J.N., 2004. Brain-Derived Neurotrophic Factor Modulates Fast Synaptic Inhibition by Regulating GABAA Receptor Phosphorylation, Activity, and Cell-Surface Stability. *Journal of Neuroscience*, 24 (2), 522–530.
- Jovanovic, J.N., Benfenati, F., Siowt, Y.L., Sihra, T.S., Sanghera, J.S., Peleht, S.L., Greengard, P., and Czernik, A.J., 1996. Neurotrophins stimulate phosphorylation of synapsin I by MAP kinase and regulate synapsin I-actin interactions. *Neurobiology*, 93 (April), 3679–3683.
- Kandler, K., Katz, L.C., and Kauer, J.A., 1998. Focal photolysis of caged glutamate produces long-term depression of hippocampal glutamate receptors. *Nature Neuroscience*, 1 (2), 119–123.
- Kleindienst, T., Winnubst, J., Roth-Alpermann, C., Bonhoeffer, T., and Lohmann, C., 2011. Activity-dependent clustering of functional synaptic inputs on developing hippocampal dendrites. *Neuron*, 72 (6), 1012–1024.

- 
- Kneussel, M., Brandstätter, J.H., Laube, B., Stahl, S., Müller, U., and Betz, H., 1999. Loss of postsynaptic GABA(A) receptor clustering in gephyrin-deficient mice. *The journal of neuroscience*, 19 (21), 9289–97.
- Krueger, S.R., Kolar, A., and Fitzsimonds, R.M., 2003. The presynaptic release apparatus is functional in the absence of dendritic contact and highly mobile within isolated axons. *Neuron*, 40 (5), 945–57.
- Kubota, Y., Hatada, S., Kondo, S., Karube, F., and Kawaguchi, Y., 2007. Neocortical Inhibitory Terminals Innervate Dendritic Spines Targeted by Thalamocortical Afferents. *Journal of Neuroscience*, 27 (5), 1139–1150.
- Kuczewski, N., Porcher, C., Ferrand, N., Fiorentino, H., Pellegrino, C., Kolarow, R., Lessmann, V., Medina, I., and Gaiarsa, J.-L., 2008. Backpropagating Action Potentials Trigger Dendritic Release of BDNF during Spontaneous Network Activity. *Journal of Neuroscience*, 28 (27), 7013–7023.
- Lang, S.B., Stein, V., Bonhoeffer, T., and Lohmann, C., 2007. Endogenous brain-derived neurotrophic factor triggers fast calcium transients at synapses in developing dendrites. *The Journal of Neuroscience*, 27 (5), 1097–1105.
- Lee, S.-J.R., Escobedo-Lozoya, Y., Szatmari, E.M., and Yasuda, R., 2009. Activation of CaMKII in single dendritic spines during long-term potentiation. *Nature*, 458 (7236), 299–304.
- Leßmann, V. and Brigadski, T., 2009. Mechanisms, locations, and kinetics of synaptic BDNF secretion: An update. *Neuroscience Research*, 65 (1), 11–22.
- Li, L., Stefan, M.I., and Le Novère, N., 2012. Calcium Input Frequency, Duration and Amplitude Differentially Modulate the Relative Activation of Calcineurin and CaMKII. *PLoS ONE*, 7 (9).
- Lisman, J., Yasuda, R., and Raghavachari, S., 2012. Mechanisms of CaMKII action in long-term potentiation. *Nature Reviews Neuroscience*, 13 (3), 169–182.
- Llano, I., Leresche, N., and Marty, A., 1991. Calcium entry increases the sensitivity of cerebellar Purkinje cells to applied GABA and decreases inhibitory synaptic currents. *Neuron*, 6 (4), 565–574.
- Maejima, T., Hashimoto, K., Yoshida, T., Aiba, A., and Kano, M., 2001. Presynaptic Inhibition Caused by Retrograde Signal from Metabotropic Glutamate to Cannabinoid Receptors. *Neuron*, 31 (3), 463–475.
- Maison, P., Walker, D.J., Walsh, F.S., Williams, G., and Doherty, P., 2009. BDNF regulates neuronal sensitivity to endocannabinoids. *Neuroscience Letters*, 467 (2), 90–94.
- Mansuy, I.M., 2003. Calcineurin in memory and bidirectional plasticity. *Biochemical and Biophysical Research Communications*, 311 (4), 1195–1208.
- Marín, O., 2012. Interneuron dysfunction in psychiatric disorders. *Nature Reviews Neuroscience*, 13 (2), 107–120.
- Marsden, K.C., Beattie, J.B., Friedenthal, J., and Carroll, R.C., 2007. NMDA Receptor Activation Potentiates Inhibitory Transmission through GABA Receptor-Associated Protein-Dependent Exocytosis of GABAA Receptors. *Journal of Neuroscience*, 27 (52), 14326–14337.

- Marsden, K.C., Shemesh, A., Bayer, K.U., and Carroll, R.C., 2010. Selective translocation of Ca<sup>2+</sup>/calmodulin protein kinase II (CaMKII) to inhibitory synapses. *Proceedings of the National Academy of Sciences*, 107 (47), 20559–20564.
- Muir, J., Arancibia-Carcamo, I.L., MacAskill, A.F., Smith, K.R., Griffin, L.D., and Kittler, J.T., 2010. NMDA receptors regulate GABAA receptor lateral mobility and clustering at inhibitory synapses through serine 327 on the  $\alpha 2$  subunit. *Proceedings of the National Academy of Sciences*, 107 (38), 16679–16684.
- Oh, W.C., Parajuli, L.K., and Zito, K., 2015. Heterosynaptic Structural Plasticity on Local Dendritic Segments of Hippocampal CA1 Neurons. *Cell Reports*, 10 (2), 162–169.
- Ohba, S., Ikeda, T., Ikegaya, Y., Nishiyama, N., Matsuki, N., and Yamada, M.K., 2005. BDNF locally potentiates GABAergic presynaptic machineries: Target-selective circuit inhibition. *Cerebral Cortex*, 15 (3), 291–298.
- Ohno-Shosaku, T., Maejima, T., and Kano, M., 2001. Endogenous cannabinoids mediate retrograde signals from depolarized postsynaptic neurons to presynaptic terminals. *Neuron*, 29 (3), 729–738.
- Passlick, S., Kramer, P.F., Richers, M.T., Williams, J.T., and Ellis-Davies, G.C.R., 2017. Two-color, one-photon uncaging of glutamate and GABA. *PLoS ONE*, 12 (11), 1–17.
- Penny, C.J. and Gold, M.G., 2018. Mechanisms for localising calcineurin and CaMKII in dendritic spines. *Cellular Signalling*, 49 (May), 46–58.
- Petrini, E.M. and Barberis, A., 2014. Diffusion dynamics of synaptic molecules during inhibitory postsynaptic plasticity. *Frontiers in Cellular Neuroscience*, 8 (September), 1–16.
- Petrini, E.M., Ravasenga, T., Hausrat, T.J., Iurilli, G., Olcese, U., Racine, V., Sibarita, J.-B., Jacob, T.C., Moss, S.J., Benfenati, F., Medini, P., Kneussel, M., and Barberis, A., 2014. Synaptic recruitment of gephyrin regulates surface GABAA receptor dynamics for the expression of inhibitory LTP. *Nature communications*, 5, 3921.
- Piomelli, D., 2014. More surprises lying ahead. The endocannabinoids keep us guessing. *Neuropharmacology*, 76 (PART B), 228–234.
- Poulopoulos, A., Aramuni, G., Meyer, G., Soykan, T., Hoon, M., Papadopoulos, T., Zhang, M., Paarmann, I., Fuchs, C., Harvey, K., Jedlicka, P., Schwarzacher, S.W., Betz, H., Harvey, R.J., Brose, N., Zhang, W., and Varoqueaux, F., 2009. Neurologin 2 Drives Postsynaptic Assembly at Perisomatic Inhibitory Synapses through Gephyrin and Collybistin. *Neuron*, 63 (5), 628–642.
- Sanderson, J.L., Gorski, J.A., Gibson, E.S., Lam, P., Freund, R.K., Chick, W.S., and Dell'Acqua, M.L., 2012. AKAP150-anchored calcineurin regulates synaptic plasticity by limiting synaptic incorporation of Ca<sup>2+</sup>-permeable AMPA receptors. *The Journal of neuroscience: the official journal of the Society for Neuroscience*, 32 (43), 15036–52.
- Scheiffele, P., Fan, J., Choih, J., Fetter, R., and Serafini, T., 2000. Neurologin expressed in nonneuronal cells triggers presynaptic development in contacting axons. *Cell*, 101 (6), 657–669.
- Simsek-Duran, F. and Lonart, G., 2008. The role of RIM1 $\alpha$  in BDNF-enhanced glutamate release. *Neuropharmacology*, 55 (1), 27–34.

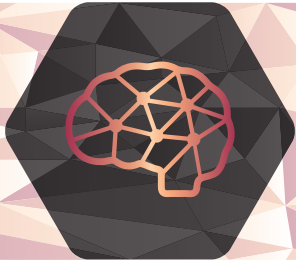
- 
- Smolders, I., Lindekens, H., Clinckers, R., Meurs, A., O'Neill, M.J., Lodge, D., Ebinger, G., and Michotte, Y., 2004. In vivo modulation of extracellular hippocampal glutamate and GABA levels and limbic seizures by group I and II metabotropic glutamate receptor ligands. *Journal of Neurochemistry*, 88 (5), 1068–1077.
- Staras, K., 2007. Share and share alike: trading of presynaptic elements between central synapses. *Trends in neurosciences*, 30 (6), 292–8.
- Staras, K., Branco, T., Burden, J.J., Pozo, K., Darcy, K., Marra, V., Ratnayaka, A., and Goda, Y., 2010. A Vesicle Superpool Spans Multiple Presynaptic Terminals in Hippocampal Neurons. *Neuron*, 66 (1), 37–44.
- Stein, I.S., Gray, J.A., and Zito, K., 2015. Non-Ionotropic NMDA Receptor Signaling Drives Activity-Induced Dendritic Spine Shrinkage. *Journal of Neuroscience*, 35 (35), 12303–12308.
- Strack, S. and Colbran, R.J., 1998. Autophosphorylation-dependent Targeting of Calcium/ Calmodulin-dependent Protein Kinase II by the NR2B Subunit of the N -Methyl- d-aspartate Receptor. *Journal of Biological Chemistry*, 273 (33), 20689–20692.
- Svoboda, K., Tank, D.W., and Denk, W., 1996. Direct Measurement of Coupling Between Dendritic Spines and Shafts. *Science*, 272 (5262), 716–719.
- Takahashi, N., Kitamura, K., Matsuo, N., Mayford, M., Kano, M., Matsuki, N., and Ikegaya, Y., 2012. Locally synchronized synaptic inputs. *Science*, 335 (6066), 353–356.
- Tanaka, T., Saito, H., and Matsuki, N., 1997. Inhibition of GABAA synaptic responses by brain-derived neurotrophic factor (BDNF) in rat hippocampus. *The Journal of neuroscience : the official journal of the Society for Neuroscience*, 17 (9), 2959–66.
- Teo, T.S. and Wang, J.H., 1973. Mechanism of activation of a cyclic adenosine 3':5'-monophosphate phosphodiesterase from bovine heart by calcium ions. Identification of the protein activator as a Ca<sup>2+</sup> binding protein. *The Journal of biological chemistry*, 248 (17), 5950–5.
- Tyagarajan, S.K. and Fritschy, J.-M., 2014. Gephyrin: a master regulator of neuronal function? *Nature Reviews Neuroscience*, 15 (3), 141–156.
- Tyagarajan, S.K., Ghosh, H., Yévenes, G.E., Imanishi, S.Y., Zeilhofer, H.U., Gerrits, B., and Fritschy, J.M., 2013. Extracellular signal-regulated kinase and glycogen synthase kinase 3 $\beta$  regulate gephyrin postsynaptic aggregation and GABAergic synaptic function in a calpain-dependent mechanism. *Journal of Biological Chemistry*, 288 (14), 9634–9647.
- Varoqueaux, F., Jamain, S., and Brose, N., 2004. Neuroligin 2 is exclusively localized to inhibitory synapses. *European journal of cell biology*, 83 (9), 449–56.
- Villa, K.L., Berry, K.P., Subramanian, J., Cha, J.W., Oh, W.C., Kwon, H.B., Kubota, Y., So, P.T.C., and Nedivi, E., 2016. Inhibitory Synapses Are Repeatedly Assembled and Removed at Persistent Sites In Vivo. *Neuron*, 89 (4), 756–769.
- Wang, W., Trieu, B.H., Palmer, L.C., Jia, Y., Pham, D.T., Jung, K.-M., Karsten, C.A., Merrill, C.B., Mackie, K., Gall, C.M., Piomelli, D., and Lynch, G., 2016. A Primary Cortical Input to Hippocampus Expresses a Pathway-Specific and Endocannabinoid-Dependent Form of Long-Term Potentiation. *eNeuro*, 3 (4), 160–16.

- Wierenga, C.J., Becker, N., and Bonhoeffer, T., 2008. GABAergic synapses are formed without the involvement of dendritic protrusions. *Nature neuroscience*, 11 (9), 1044–52.
- Wierenga, C.J., Müllner, F.E., Rinke, I., Keck, T., Stein, V., and Bonhoeffer, T., 2010. Molecular and electrophysiological characterization of GFP-expressing CA1 interneurons in GAD65-GFP mice. *PLoS one*, 5 (12), e15915.
- Wilson, R.I. and Nicoll, R.A., 2001. Endogenous cannabinoids mediate retrograde signalling at hippocampal synapses. *Nature*, 410 (6828), 588–592.
- Wu, H.-Y., Hudry, E., Hashimoto, T., Uemura, K., Fan, Z.-Y., Berezovska, O., Grosskreutz, C.L., Bacskai, B.J., and Hyman, B.T., 2012. Distinct Dendritic Spine and Nuclear Phases of Calcineurin Activation after Exposure to Amyloid- Revealed by a Novel Fluorescence Resonance Energy Transfer Assay. *Journal of Neuroscience*, 32 (15), 5298–5309.
- Wyszynski, M., Kharazia, V., Shangvi, R., Rao, A., Beggs, a H., Craig, a M., Weinberg, R., and Sheng, M., 1998. Differential regional expression and ultrastructural localization of alpha-actinin-2, a putative NMDA receptor-anchoring protein, in rat brain. *The Journal of neuroscience : the official journal of the Society for Neuroscience*, 18 (4), 1383–92.
- Zhuo, M., Zhang, W., Son, H., Mansuy, I., Sobel, R.A., Seidman, J., and Kandel, E.R., 1999. A selective role of calcineurin A in synaptic depotentiation in hippocampus. *Proceedings of the National Academy of Sciences*, 96 (8), 4650–4655.









# Addendum

---

Nederlandse samenvatting

Curriculum vitae

Dankwoord



## Nederlandse samenvatting

Het brein is het meest complexe orgaan in ons lichaam en is opgebouwd uit miljarden neuronen. Deze neuronen vormen onderling duizenden connecties die resulteren in uitgebreide neuronale netwerken. In elk van deze connecties vindt communicatie plaats door middel van signaaloverdracht tussen twee neuronen. Neuronen hebben een karakteristieke morfologie met uitgebreide uitlopers die vertakken vanaf het cellichaam. Deze zijn te onderscheiden op functie: de dendrieten zijn gespecialiseerd in het ontvangen van signalen, terwijl de axonen verantwoordelijk zijn voor het verzenden van signalen. Neuronale signalen worden overgedragen door de afgifte van neurotransmitters. Vervolgens zorgt de specifieke binding van deze neurotransmitters aan receptoren dat dit chemische signaal omgezet wordt in een elektrisch signaal in het neuron. De signalen die gelijktijdig binnenkomen worden geïntegreerd tot één gecombineerd signaal. Als het netto signaal sterk genoeg is, dan reageert het neuron door actief een eigen signaal te generen in de vorm van een actiepotentiaal. Dit signaal propageert door de axon en resulteert in de afgifte van neurotransmitters, zodat het signaal weer verder doorgegeven wordt aan de neuronen die met dit axon verbonden zijn. De intrinsieke eigenschap van neuronen om signalen te interpreteren en daar vervolgens op te reageren geeft het brein de eigenschap om informatie te verwerken.

Informatie is gecodeerd in de temporale en ruimtelijke activiteitspatronen waarin neuronen actiepotentialen genereren. Signalen die een neuron aanzetten tot signaal propagatie worden excitatoir genoemd. Excitatie zonder regulatie is onstabiel. Als ieder ontvangen signaal onbeperkt wordt versterkt, dan gaat de informatie dat het signaal bevat verloren. De tegenhanger van excitatie, inhibitie is dan ook essentieel in het reguleren van activiteit en het bemiddelen van informatieverwerking door selectief signalen te blokkeren of te verzwakken. Het is dan ook niet verassend dat een verstoorde relatie tussen excitatie en inhibitie leidt tot neurologische afwijkingen.

De connecties tussen neuronen waar communicatie plaatsvindt, worden synapsen genoemd. Synapsen bestaan uit een presynaptisch deel, dat gevormd wordt door de axon en verantwoordelijk is voor het sturen van signalen, en een postsynaptisch deel, dat gevormd wordt door de dendriet en signalen ontvangt. De sterkte van een doorgegeven signaal verschilt per synaps en deze variatie is gerelateerd aan de grootte van de synaps. Bovendien is de sterkte van een synaps variabel en kan deze afhankelijk van de neuronale activiteit veranderen. In excitatoire synapsen is aangetoond dat synapsen die veelvuldig bijdragen aan het genereren van actiepotentialen versterkt worden, terwijl synapsen die dat zelden doen worden afgezwakt. Zo kan een neuron zich specialiseren door af te stemmen naar op specifieke inkomende signalen. De activiteit afhankelijke verandering in het gewicht van synapsen vormt de neuronale basis voor het opdoen van nieuwe kennis en vaardigheden.

Inhibitie reguleert welke excitatoire signalen er worden doorgegeven. Om deze regulerende rol in stand te houden, zouden veranderingen in excitatoire signalen ook veranderingen in

---

inhibitie teweeg moeten brengen. Tot op heden is er weinig bekend over de mechanismen die verantwoordelijk zijn voor het coördineren van excitatie met inhibitie en op welke schaal dit voorkomt. Inhibitie kan excitatie lokaal reguleren wanneer beiden arriveren op dezelfde dendriet. Het lokale bereik van inhibitie suggereert dat een eventuele coördinatie tussen excitatie en inhibitie ook lokaal zal plaatsvinden in een dendriet. Deze hypothese wordt ondersteund door de verhouding tussen het aantal inhibitoire en excitatoire synapsen in een dendriet dat constant is, ondanks een variatie in synapsdichtheid. De noodzaak voor lokale dendritische inhibitie wordt duidelijk wanneer er gekeken wordt naar de rol van de dendriet in signaalverwerking. De signalen die door een dendriet richting de soma verplaatsen worden in de dendriet gemoduleerd. Zo kunnen signalen versterkt of verzwakt worden voordat deze kunnen bijdragen aan een potentiële actiepotentiaal. Dendritische inhibitie kan activiteit dicht bij de bron reguleren, voordat deze wordt gemoduleerd.

In hoofdstuk 2 staat onze studie centraal waarin we de lokale coördinatie tussen inhibitie en excitatie onderzoeken. De grote dichtheid aan neuronen maakt het moeilijk om in hersenweefsel neuronen en synapsen te bestuderen met conventionele lichtmicroscopie. Fluorescentie microscopie biedt hier uitkomst, waar uitsluitend de cellen worden gekleurd die een specifieke fluorescente label bevatten. Dit stelt ons in staat om met een micrometer resolutie synapsen te bekijken. In onze studies gebruiken we neuronale celkweek van transgene GAD65-GFP muizen waarin inhibitoire neuronen met groen gekleurd zijn. Door in hetzelfde kweek een excitatoire piramidaal neuron rood te kleuren kunnen we de interactie tussen inhibitie en excitatie visualiseren door te kijken naar het contact tussen een rode dendriet en een groene axon.

Het bestaan van een lokale coördinatie tussen excitatie en inhibitie hebben we onderzocht door selectief excitatoire synapsen te stimuleren en versterken met glutamaat uncaging. Als beiden gecoördineerd zijn, zou de verhoogde excitatie kunnen leiden tot een toename van inhibitie. Dit is ook wat we aantonen, na het stimuleren van excitatie op een dendriet, heeft een inhibitoire axon die met deze dendriet contact maakt een grotere kans om een inhibitoire synaps te vormen. Bij de vorming van deze synaps speelt retrograde signalering van de dendriet naar de axon een belangrijke rol. Zo bleek dat de groei van de inhibitoire synaps namelijk afhankelijk is van de activering van de cannabinoïd 1 receptor. Deze receptoren worden geactiveerd door de afgifte van 2-AG, een bekende retrograde signaleringsmolecuul. Dit betekent dat de dendriet zelf lokaal kan reguleren hoeveel inhibitie het ontvangt op basis van de hoeveelheid excitatie.

De grootte van een synaps is gerelateerd aan de synaptische signaleringssterkte. Door deze synapsgrootte over tijd te meten kan de groei van de synaps worden gekwantificeerd. Het handmatig vergelijken van deze volumes is arbeidsintensief en foutgevoelig. Bij het gebrek aan bestaande analyse tools, heb ik tools ontwikkelt om de analyse te faciliteren. Hierbij ligt de nadruk op aanpasbaarheid, gebruiksvriendelijkheid, en efficiëntie. Deze tools worden beschreven in hoofdstuk 3.

Synapsen zijn dynamisch. Uit onze resultaten blijkt dat lokale activiteit in staat is om een

synaps te laten vormen. Echter of deze synaps zich verder ontwikkelt en een functionele bijdrage levert is niet waarschijnlijk omdat de meeste nieuwe synapsen in onze experimenten na een korte aanwezigheid weer verdwenen. Dit impliceert dat er een ander signaal er nodig is om een tijdelijke synaps te laten door ontwikkelen. Wellicht dat de signaalmolecuul Semaphorin4D (Sema4D) de ontbrekende schakel is. In hoofdstuk 4 bekijken we het effect van Sema4D op inhibitoire synapsen. Sema4D is betrokken bij de vorming van inhibitoire synapsen, maar niet van excitatoire synapsen. We laten zien dat Sema4D niet leidt tot meer nieuwe inhibitoire synapsen, maar specifiek synapsen stabiliseert die in afwezigheid van Sema4D slechts tijdelijk zouden zijn. Door middel van elektrofysiologie, heb ik aangetoond dat deze synapsen na verloop van tijd volwassen worden en bijdragen aan de inhibitie.

Onze resultaten biedt nieuwe inzichten over hoe de dynamiek van inhibitoire synapsen gereguleerd is. Synaptische plasticiteit stelt het brein in staat te leren en zich aan te passen aan de alsmaar veranderende omstandigheden. Om te begrijpen hoe het brein leert, is kennis over de interacties tussen synapsen essentieel.



## Curriculum Vitae

Hai Yin Hu was born on August 18th of 1986 in Helmond, The Netherlands and received his high school diploma in 2004 (Sint-Janscollege, Hoensbroek). Afterwards he enrolled in the Bachelor of Natural Sciences at the Radboud University Nijmegen. During his studies, he spend a year as the treasurer for the study association of natural sciences. As part of his master program, Hai Yin performed two separate research internships, one at the medical biophysiscs department at the Raboud University Nijmegen in the group of prof. dr. A.J. van Opstal. The second internship was completed at the department of physiology at University of Oslo in the group of prof. dr. J.F. Storm. In 2013, Hai Yin received his master diploma with a specialization in biophysics and in the same year he started as a PhD student in the group of dr. Corette J. Wierenga. The results of his PhD project are described in this thesis.





## Dankwoord

Het leven van een PhD student draait voor een groot deel rond zijn of haar onderzoek. Echter onderzoek doe je niet alleen en samen kom je verder. Ik ben dan ook dankbaar dat ik mensen om mij heen had die mijn tijd als promovendus inspirerend, leerzaam, leuk, en gezellig hebben gemaakt. Graag wil ik hier de gelegenheid nemen om iedereen hiervoor te bedanken.

Allereerst wil ik mijn promotoren Casper en Anna en copromotor Corette bedanken. Casper, ondanks je drukke schema en vele taken bleef je altijd makkelijk aanspreekbaar en oprecht geïnteresseerd. Anna, ik ben blij dat mijn tweede promotor wilde zijn. Je weet hoe je iemand stimuleert tot nadenken en scherp houdt door goede, kritische vragen te stellen. Ik ben vereerd dat jullie beiden mijn promotoren zijn.

Correte, ik wil je bedanken voor de kans die me hebt gegeven om als PhD student aan de slag te gaan in jouw groep. Je weet als geen ander hoe je iemand moet enthousiasmeren en motiveren, wat vaak van pas kwam wanneer er experimenten niet volgens plan gingen. Ook was prettig dat bij jou alles bespreekbaar is en je ruimte creëert voor goede discussies. Wat ik ook waardeer is dat je betrokken bent op een persoonlijk vlak. Van begin af aan voelde ik me thuis. Toen ik halverwege mijn promotieonderzoek een ongeval kreeg werden zaken dat eerst vanzelfsprekend waren een stuk lastiger. Bedankt dat je actief meedacht naar praktische oplossingen en je vertrouwen wanneer ik dat goed kon gebruiken. Ook wil ik de leden van het promotiecommissie bedanken. Maarten Kole, Sander van den Heuvel, Elly Hol, Wytse Wadman en Peter Burbach. Bedankt voor het kritisch lezen en beoordelen van mijn proefschrift.

Catia and Dennis, my dear paranymphs. It was a pleasure being your colleague, I always enjoyed our open discussions and your witty humor. Catia, with your warm and energetic nature you never fail to lighten the mood. You were the first of us and with your passion for science and hardworking attitude you set a great example for us all. I admire your exceptional organizational skills, your uncanny memory, and your ability to liven up a party. Dennis, je bent een toffe kerel met een duidelijke mening. Ik vind het knap hoe snel je nieuwe informatie weet op te nemen. Ondanks dat je wel eens intens over kan komen, ben je eigenlijk redelijk relaxed en kan ik met jou altijd wel lachen. Het was een waar genoegen om met je samen te werken. Thank you both for everything!

Uiteraard ben ik ook dankbaar aan mijn overige collega's van het Wierenga lab voor het creëren van een fijne werkomgeving. Ondanks dat de samenstelling flink is veranderd over de jaren, was er altijd een leuke sfeer. René, als jij op vakantie gaat realiseerden we ons allen hoe veel wij op jou bouwden. Elske, het was altijd gezellig om met je te praten. Jian, you are a super nice and humble guy. Carlijn, fijn dat je je altijd vrolijke stemming wilde delen. Lotte, al tijdens je Master stage wist je een sterke indruk te maken met je leergierigheid en doorzettingsvermogen. Marvin, de laatste labgenoot van mijn tijd. Ik hoop dat alles naar wens verloopt. Naast Lotte, wil ik ook Bas, Mirte, en Claudia bedanken. Het was mijn genoegen

---

om zulke talentvolle studenten te begeleiden. Beste Wierengaatjes, bedankt voor een leuke, leerzame, gezellige en mooie tijd!

I would also like to extend my gratitude to my former officemates Riccardo, Ines, Lena, Phil, and Olga. I enjoyed our time together and all the conversations we shared. Riccardo, chances are that by the time you read this I will have to congratulate you first! Ines, your caring personality makes it always easy to talk to you about the good and the bad. Lena, don't forget to take it easy every now and then. Phil, your chaotic yet organized ways were quite impressive, you are always fun to be around. Olga, your happy attitude always brought a smile to the office. Dear office buddies, thank you for making coming to the office enjoyable! I would also like to thank Amélie, Amol, Anaël, Anne, Bart, Bas, Dieudonné, Esther, Eugene, Feline, Harold, Helma, Jinchao, Josta, Joanna, Kah Wai, Laura, Marielle, Marleen, Martha, Marina, Martin, Max, Michael, Mithila, Lukas, Paul, Petra, Phebe, Robin, Roderick, Qinyang, Sam, and Sybren for all the fun times during my stay at the Cell Biology department.

Zo rond het laatste jaar van mijn promotieonderzoek besloot ik om een hond als huisdier te nemen. Iedere dag heb ik plezier aan het gezelschap van mijn kleine, eigenwijze en harige Kaiba. Als leuke bijkomstigheid heb ik tijdens het uitlaten de buurt en de burens beter leren kennen. Van de buurtgenoten wil ik er een paar bedanken. Anne, het is altijd gezellig om met jou te kletsen. Renée, bedankt dat je Kaiba doordeweeks uitlaat. Suzanne, beter een goede buur dan een verre vriend. Door jou voelde ik me al snel thuis na mijn verhuizing. Lieve buurtgenoten, bedankt voor alle gezelligheid!

Lieve vrienden van Nijmegen, wat was het studentenleven toch een lekker zorgeloos bestaan. Martijn, je weet iedere keer wel een levendig verhaal te vertellen. Met jou erbij is het nooit saai. Ramon, jij hebt een gave om met de meeste mensen een klik te maken. Inge, altijd meelevend en bedachtzaam. Het is altijd fijn om met jou te praten. Rik, er zijn er weinig zo aardig en gastvrij zoals jij. Lieve vrienden bedankt voor alle gezelligheid en leuke tijden!

Lieve familie, lieve ouders, Haili, Haixa, Haifen, Caoxia, Luiz, Cheng, en Joshua bedankt dat jullie er altijd voor mij zijn ook als het tegenzit. Zo stonden jullie klaar toen ik jullie steun het meest nodig had, na mijn ongeluk en hielpen jullie mij door deze zware periode vol onzekerheid. Toen het tegenzat, realiseerde ik me echt hoe gelukkig ik mag zijn met jullie. Bedankt voor alle leuke gesprekken, oprechte interesse en carrièreadviezen! Ook bedankt aan mijn neefjes en nichtjes, Evan, Milo, Fae, Tim, Elise, en Dylan voor alle gezelligheid!

